# NAVAL POSTGRADUATE SCHOOL
## MONTEREY, CALIFORNIA

DTIC
S ELECTE
JAN 23 1995
G D

## THESIS

STRUCTURAL DAMAGE DETECTION USING
FREQUENCY DOMAIN ERROR
LOCALIZATION

by

Marvin G. Campbell

December, 1994

Thesis Advisor:                          Joshua H. Gordis

Approved for public release; distribution is unlimited.

DTIC QUALITY INSPECTED 3

19950119 027

# REPORT DOCUMENTATION PAGE

Form Approved OMB No. 0704-0188

| 1. AGENCY USE ONLY *(Leave blank)* | 2. REPORT DATE December 1994. | 3. REPORT TYPE AND DATES COVERED Master's Thesis |
|---|---|---|

| 4. TITLE AND SUBTITLE STRUCTURAL DAMAGE DETECTION USING FREQUENCY DOMAIN ERROR LOCALIZATION | 5. FUNDING NUMBERS |
|---|---|
| 6. AUTHOR(S) Marvin G. Campbell | |

| 7. PERFORMING ORGANIZATION NAME(S) AND ADDRESS(ES) Naval Postgraduate School Monterey CA 93943-5000 | 8. PERFORMING ORGANIZATION REPORT NUMBER |
|---|---|

| 9. SPONSORING/MONITORING AGENCY NAME(S) AND ADDRESS(ES) | 10. SPONSORING/MONITORING AGENCY REPORT NUMBER |
|---|---|

11. SUPPLEMENTARY NOTES The views expressed in this thesis are those of the author and do not reflect the official policy or position of the Department of Defense or the U.S. Government.

| 12a. DISTRIBUTION/AVAILABILITY STATEMENT Approved for public release; distribution is unlimited. | 12b. DISTRIBUTION CODE |
|---|---|

13. ABSTRACT *(maximum 200 words)*

A frequency domain theory for structural dynamic model error localization is applied to the damage detection problem. The localization theory is based on a transformation of the frequency response function matrix, and represents an exact solution for the location of the differences between two frequency response function models, given spatially complete data. The localization is performed at all frequencies in a chosen bandwidth, and therefore implicitly accounts for all modes of interest. Methods for coping with spatially incomplete data are explored analytically and in an experimental study of a composite beam with installed damage of known length.

| 14. SUBJECT TERMS | 15. NUMBER OF PAGES 152 |
|---|---|
| | 16. PRICE CODE |

| 17. SECURITY CLASSIFICATION OF REPORT Unclassified | 18. SECURITY CLASSIFICATION OF THIS PAGE Unclassified | 19. SECURITY CLASSIFICATION OF ABSTRACT Unclassified | 20. LIMITATION OF ABSTRACT UL |
|---|---|---|---|

# STRUCTURAL DAMAGE DETECTION USING FREQUENCY DOMAIN ERROR LOCALIZATION

by

Marvin G. Campbell
Lieutenant, United States Navy
B.S., United States Naval Academy, 1989

Submitted in partial fulfillment
of the requirements for the degree of

## MASTER OF SCIENCE IN MECHANICAL ENGINEERING

from the

## NAVAL POSTGRADUATE SCHOOL
### December 1994

Author: _____
Marvin G. Campbell

Approved by: _____
Joshua H. Gordis, Thesis Advisor

_____
Matthew D. Kelleher, Chairman
Department of Mechanical Engineering

# ABSTRACT

A frequency domain theory for structural dynamic model error localization is applied to the damage detection problem. The localization theory is based on a transformation of the frequency response function matrix, and represents an exact solution for the location of the differences between two frequency response function models, given spatially complete data. The localization is performed at all frequencies in a chosen bandwidth, and therefore implicitly accounts for all modes of interest. Methods for coping with spatially incomplete data are explored analytically and in an experimental study of a composite beam with installed damage of known length.

| Accesion For | | |
|---|---|---|
| NTIS CRA&I | | ☒ |
| DTIC TAB | | ☐ |
| Unannounced | | ☐ |
| Justification | | |
| By | | |
| Distribution / | | |
| Availability Codes | | |
| Dist | Avail and / or Special | |
| A-1 | | |

# TABLE OF CONTENTS

# LIST OF FIGURES

# I. INTRODUCTION

## A. BACKGROUND

Structural damage detection refers to the variety of methods applied in identification of structural damage. The field of damage detection encompasses the qualitative and quantitative determination of structural deficiencies and their locations. Technological advances in material composition and the growing complexity of equipment and machinery in our military provide added challenges to current nondestructive testing procedures. The field of *nondestructive* testing encompasses vastly different methodologies and approaches including radiographic examination, electromagnetic comparator tests, ultrasonic analysis, and dye-penetrant examinations [Ref. 1:p. 79]. While these methods identify near surface defects quite well, internal damage detection is considerably more limited. Nonmetallic structures impose additional limitations on detection method selection.

Structural system identification makes use of measured structural dynamic response data in the detection of damage. The analysis of measured dynamic response information permits subsurface flaw detection by identifying variations in frequency response spectra. Frequency response measurement involves testing components and structures to obtain a quantitative description of their dynamic behavior. More specifically, known harmonic excitation forces are applied and the resulting harmonic response quantified for a given structure. The ratio of excitation forces to response coordinates evaluated at each frequency in a specified bandwidth defines the frequency response function. The frequency response function is a primary component of "modal testing," which generates dynamic system characteristics in the form of modal parameters. Modal parameters include mode

1

shapes, natural frequencies, and damping behavior. These parameters characterize structural response to dynamic loading.

## B. ANALYSIS METHODS

Modal tests are conducted to obtain a mathematical model of a structure. Theoretical models, constructed by finite element methods, are subsequently adjusted to reflect measured modal parameters [Ref. 2:p. 3]. Iterative comparisons between the experimental and theoretical models, followed by appropriate corrections, produce a baseline theoretical model for a structure. Correlation between experimental data of a virgin structure and its corresponding finite element model is the premise which facilitates structural damage assessment. Once a baseline mathematical model is obtained, quantitative discrepancies identified between predicted and measured structural properties reflect errors between the two models. These errors, since absent from initial modeling comparisons, correspond to structural damage. Hence, damage detection is often referred to as error identification. Two approaches to damage detection include modal-based methods and frequency domain methods. Although both methods are presented below, only frequency domain methods for damage detection are employed in this thesis.

### 1. Modal-Based Method

Modal methods for damage detection, hereafter referred to as error identification, are described in references (3) through (5). These methods present an approximate formulation in determining the regions and magnitudes of difference between the test structure mass and stiffness properties and the baseline analytical or finite element mass and stiffness properties. It should be emphasized that actual mass and stiffness matrices are unavailable for the damaged structure. Approximations, using modal parameters calculated from finite

2

element formulations and vibration test estimates, provide experimental impedance information as differential stiffness and mass matrices. The Error Matrix Method [Ref. 3] presents a modal method of error detection. Differences between analytical and experimental models are obtained by constructing experimental stiffness and mass matrices from test structure modal parameters and subtracting analytically derived matrices, respectively. The differences obtained are associated with damage and inform the analyst of the extent and location of structural errors. The formulation of this method and its assumptions are detailed in Chapter II.

## 2. Frequency Domain Method

Frequency domain methods use measured FRF directly to determine impedance error spectra. The frequency domain approach to damage detection entails the compilation of a baseline finite element model or experimentally obtained frequency response function for a structure prior to service. As structural degradation is suspected, or as some type of scheduled preventative maintenance mandates, frequency response tests are performed to obtain new dynamic response data.

In this thesis, frequency domain analysis is employed to process the experimentally obtained FRF. Frequency domain analysis is applied, in lieu of traditional modal methods, to (1) avoid the difficulty in accurately capturing spatial definition of higher mode shapes and (2) to eliminate difficulty in modal parameter estimation in the presence of high modal coupling and non-proportional damping. In order to establish the necessary baseline correlation by which further analysis is conducted, precise descriptions of mode shape data are required [Ref. 2:p. 3]. Hence, greater demands are placed on test data accuracy in reconstructing mode shapes for analysis. When considering minor damage, which potentially

3

affects only higher modes, frequency domain methods of identification conceivably might offer better performance over cumbersome identification of higher mode shapes.

The localization theory [Ref. 6] is based on a transformation of the frequency response function matrix, and provides an exact solution for the location of discrepancies between two FRF models, given spatially complete data. Spatially complete measurement implies that measurement information is available at all possible coordinates of a structure (internal and external), such that data corresponds one to one with the FE coordinate set. Since, it is impossible to measure every possible coordinate within a structure, experimental testing yields spatially incomplete measurements. The difference of an experimentally obtained response function and its corresponding analytic FRF is premultiplied and post-multiplied by the analytic impedance to produce a localization matrix. The localization matrix reflects the errors in the test structure. The theory, detailed in Chapter II, is presented first in a structural damage simulation comprised of two finite element models. Finite element damaged beam models are analyzed under varying combinations of damage, noise, and damping to ascertain preferable reduction methods for spatially incomplete test data, and to evaluate the impact of test frequency range selection. Localization is then performed on composite beams of known damage length, but unknown damage magnitude.

## II. THEORY

## A. ERROR MATRIX METHOD

The Error Matrix Method (EMM), as described in reference (3), provides an approximate formulation for the difference in mass and stiffness matrices. Ideally, the errors could be obtained by simple subtraction of respective matrices as follows:

$$[\Delta M] = [M_x] - [M_a] \qquad (2.1)$$

$$[\Delta K] = [K_x] - [K_a] \qquad (2.2)$$

Subscripts "x" and "a" refer to the experimental model and the analytic model, respectively.

Unfortunately, experimentally-derived mass and stiffness matrices are not available. Moreover, to apply the above equations, both experimental and analytical system matrices must have the same order and rank. These conditions are rarely satisfied, hence an alternative method of determining errors between these matrices must be explored. The EMM constructs ΔK and ΔM using modal parameters as demonstrated in Equations (2.3) through (2.6).

$$[\Delta K] \approx [K_a] \left\lfloor [K_a^*]^{-1} - [K_x^*]^{-1} \right\rfloor [K_a] \qquad (2.3)$$

where,

$$[K_a^*]_{n \times n}^{-1} = [\phi_a]_{n \times m} \, [\omega_a^2]_{m \times m}^{-1} \, [\phi_a]_{m \times n}^T \qquad (2.4a)$$

$$[K_x^*]_{n \times n}^{-1} = [\phi_x]_{n \times m} \, [\omega_x^2]_{m \times m}^{-1} \, [\phi_x]_{m \times n}^T \qquad (2.4b)$$

and,

$$[\Delta M] \approx [M_a] \left\lfloor [M_a^*]^{-1} - [M_x^*]^{-1} \right\rfloor [M_a] \qquad (2.5)$$

5

where,

$$[M_a^*]_{n \times n}^{-1} = [\phi_a]_{n \times m} \, [\phi_a]_{m \times n}^T \qquad (2.6a)$$

$$[M_x^*]_{n \times n}^{-1} = [\phi_x]_{n \times m} \, [\phi_x]_{m \times n}^T \qquad (2.6b)$$

Subscripts "m" and "n" represent the number of experimentally obtained modes and the measured degrees of freedom, respectively. Equations (2.4a) and (2.4b) constitute pseudo-flexibility matrices, while Equations (2.6a) and (2.6b) form pseudo-inertance matrices. These equations develop inverse stiffness and mass matrices using mass normalized mode shapes and natural frequencies of both model and test systems. In order to assure that these matrices are of the same rank, the measured modal parameters in the region of analysis must correspond one-to-one between systems. Consequently, the EMM is extremely sensitive to the measurement accuracy of test mode shapes. Unfortunately, measurement errors caused by noise, nonlinearities, and incompleteness of mode extraction, are inevitable in modal testing. These experimental shortcomings, coupled with the approximate formulation of inverse matrix difference comparisons, complicate physical interpretation of the differences obtained, and often produce widely dispersed errors which impede error location assessment.

## B.  FREQUENCY DOMAIN LOCALIZATION THEORY

### 1.  General Development

The localization theory, developed in reference (6), evolves from a structural synthesis transformation (SST) which provides an analytic relationship between the dynamic systems under analysis. SST uses the concept of an impedance error matrix, which quantifies the discrepancies between two dynamic systems, to develop an exact mathematical relation between experimental and theoretical FRF.

The finite element description for a given structure is defined by the relationship of response to an applied force, e.g.,

$$\begin{Bmatrix} f_i \\ f_c \end{Bmatrix} = \begin{bmatrix} Z_{ii}^a & Z_{ic}^a \\ Z_{ic}^a & Z_{cc}^a \end{bmatrix} \begin{Bmatrix} x_i \\ x_c \end{Bmatrix} \qquad (2.7)$$

The force and response vectors are denoted by "f" and "x", respectively. These vectors, along with the model impedance matrix of Equation (2.7), are complex-valued and frequency dependent. Superscript "a" identifies analytic model impedance matrix values, while subscripts "i" and "c" refer to non-error and error coordinates, respectively. The corresponding relationship for an experimental model, if available, would be labeled with a superscript "x" to identify values as experimental test data, such that,

$$\begin{Bmatrix} f_i \\ f_c \end{Bmatrix} = \begin{bmatrix} Z_{ii}^x & Z_{ic}^x \\ Z_{ic}^x & Z_{cc}^x \end{bmatrix} \begin{Bmatrix} x_i \\ x_c \end{Bmatrix} \qquad (2.8)$$

The error impedance matrix quantifies the difference between impedance matrices of the analytic and experimental models at a specific frequency. If, an experimental impedance matrix were available from test data, the error impedance matrix described would be obtained by the following relation:

$$\begin{bmatrix} 0 & 0 \\ 0 & \Delta Z \end{bmatrix} = \begin{bmatrix} Z_{ii}^x & Z_{ic}^x \\ Z_{ic}^x & Z_{cc}^x \end{bmatrix} - \begin{bmatrix} Z_{ii}^a & Z_{ic}^a \\ Z_{ic}^a & Z_{cc}^a \end{bmatrix} \qquad (2.9)$$

Intentionally, the resultant errors are associated with the error, or "c" coordinates. Ergo, the objective is to determine which physical coordinates correspond to error coordinates.

7

## 2. Structural Synthesis Transformation

Since a measured impedance matrix is unavailable, frequency domain structural synthesis is employed to identify the impedance error matrix using FRF data exclusively. A structural synthesis transformation is constructed from $\Delta Z$ of Equation (2.9) which encompasses the FE model errors. The transformation is then applied to the finite element FRF model to produce a test model FRF.

The frequency response function relates structural response to applied excitation. This transfer function is the inverse of the impedance matrix of Equation (2.7) for a dynamic system and is the flexibility matrix (inverse stiffness matrix) for a static system, namely,

$$\begin{Bmatrix} x_i \\ x_c \end{Bmatrix} = \begin{bmatrix} H_{ii}^a & H_{ic}^a \\ H_{ic}^a & H_{cc}^a \end{bmatrix} \begin{Bmatrix} f_i \\ f_c \end{Bmatrix} \qquad (2.10)$$

Equation (2.10) partitions the finite element model into error coordinates and non-error coordinates. Generally, the "c" response coordinates experience applied forces due to both error impedances and externally applied forces, whereas "i" response coordinates experience only externally applied forces, such that,

$$f_c = f_c^{ext} + f_c^{\Delta z} \qquad (2.11a)$$

$$f_i = f_i^{ext} \qquad (2.11b)$$

Substituting Equation (2.11) into an expanded Equation (2.10) yields the following relationships:

$$x_i = H_{ii}^a f_i^{ext} + H_{ic}^a f_c^{ext} + H_{ic}^a f_c^{\Delta z} \qquad (2.12a)$$

$$x_c = H_{ci}^a f_i^{ext} + H_{cc}^a f_c^{ext} + H_{cc}^a f_c^{\Delta z} \qquad (2.12b)$$

Equation (2.12) in expanded matrix notation reflects the three harmonic excitation terms to be considered, i.e.,

$$
\begin{Bmatrix} x_i \\ x_c \\ x_c \end{Bmatrix} = \begin{bmatrix} H_{ii}^a & H_{ic}^a & H_{ic}^a \\ H_{ci}^a & H_{cc}^a & H_{cc}^a \\ H_{ci}^a & H_{cc}^a & H_{cc}^a \end{bmatrix} \begin{Bmatrix} f_i^{ext} \\ f_c^{ext} \\ f_c^{\Delta z} \end{Bmatrix}
\tag{2.13}
$$

Response coordinates "c" and "i" due to external forces will hereafter be referred to as "e" coordinates, denoting their dependence on external force excitation. Consequently, the three excitation forces are condensed into two under the following identities:

$$
f_e = \left\lfloor \lfloor f_i^{ext} \rfloor \; \lfloor f_c^{ext} \rfloor \right\rfloor^T
\tag{2.14a}
$$

$$
f_c = f_c^{\Delta z}
\tag{2.14b}
$$

Moreover, Equation (2.13) reduces to

$$
\begin{Bmatrix} x_e \\ x_c \end{Bmatrix} = \begin{bmatrix} H_{ee}^a & H_{ec}^a \\ H_{ce}^a & H_{cc}^a \end{bmatrix} \begin{Bmatrix} f_e \\ f_c \end{Bmatrix}
\tag{2.15}
$$

Equation (2.9) demonstrated that the impedance error is defined by the difference between the analytic and experimental impedance models. Hence, a transformation is required which uses the FRF relation of Equation (2.15) and generates a similar relationship for the test system. The impedance error $\Delta Z$ provides the basis by which this transformation is developed.

The impedance error matrix must satisfy the following description:

$$
\{ f_c \} = - \lfloor \Delta Z(\Omega) \rfloor \{ x_c \}
\tag{2.16a}
$$

9

where,

$$\lfloor \Delta z(\Omega) \rfloor = \lfloor [\Delta K] - \Omega^2 [\Delta M] + j\Omega[\Delta c] \rfloor \qquad (2.16b)$$

Here, $[\Delta K]$, $[\Delta M]$, and $[\Delta C]$ represent stiffness, mass, and damping (when available) matrices comparable to those provided by finite element formulation. The forcing frequency is denoted by $\Omega$ and $j = \sqrt{-1}$. The minus sign in Equation (2.16) reflects that reaction forces, imposed by impedance errors on the baseline model, are being considered. The transformation matrix which operates on Equation (2.15) is developed via Equation (2.16) to produce,

$$\begin{Bmatrix} f_e \\ f_c \end{Bmatrix} = \begin{bmatrix} I & 0 \\ 0 & -\Delta Z \end{bmatrix} \begin{Bmatrix} f_e \\ x_c \end{Bmatrix} \qquad (2.17)$$

Substituting this relation into Equation 2.15, yields

$$\begin{Bmatrix} x_e \\ x_c \end{Bmatrix}^* = \begin{bmatrix} H_{ee}^a & H_{ec}^a \\ H_{ce}^a & H_{cc}^a \end{bmatrix} \begin{bmatrix} I & 0 \\ 0 & -\Delta Z \end{bmatrix} \begin{Bmatrix} f_e \\ x_c \end{Bmatrix} \qquad (2.18a)$$

or in simplified form,

$$\begin{Bmatrix} x_e \\ x_c \end{Bmatrix}^* = \begin{bmatrix} H_{ee}^a & -H_{ec}^a \Delta Z \\ H_{ce}^a & -H_{cc}^a \Delta Z \end{bmatrix} \begin{Bmatrix} f_e \\ x_c \end{Bmatrix}^* \qquad (2.18b)$$

The superscript "*" identifies the response coordinates as synthesized, coupled response coordinates. These coordinates represent a synthesized structural response, leading to the development of the transformation equation. In order to concisely present the derivation of this transformation equation, matrices will be identified by capital letters while response coordinates and excitation forces will be represented by lower case letters. Traditional mathematic notation will reappear at the conclusion of the SST derivation. Expansion of Equation (2.18) results in Equations (2.19a) and (2.19b). Simplification of synthesized response coordinates in terms of

10

$$x_c^* = H_{ce}^a \, f_e - H_{cc}^a \Delta Z x_c^* \qquad (2.19a)$$

$$x_e^* = H_{ee}^a \, f_e - H_{ec}^a \Delta Z x_c^* \qquad (2.19b)$$

general coordinates is demonstrated in Equation (2.20) and Equation (2.21). Rearranging Equation (2.19a) produces

$$[ \, I + H_{cc}^a \Delta Z] \, x_c^* = H_{ce}^a \, f_e \qquad (2.20a)$$

yet, from the property of the frequency response function,

$$x_c = H_{ce}^a \, f_e \qquad (2.20b)$$

thus,

$$[ \, I + H_{cc}^a \Delta Z] \, x_c^* = x_c \qquad (2.20c)$$

or,

$$x_c^* = [ \, I + H_{cc}^a \Delta Z]^{-1} \, x_c \qquad (2.20d)$$

Introducing results of Equation (2.20) into Equation (2.19b) leads to the following expression:

$$x_e^* = H_{ee}^a \, f_e - H_{ec}^a \Delta Z \, [ \, I + H_{cc}^a \Delta Z]^{-1} \, x_c \qquad (2.21a)$$

Inserting Equation (2.20b) permits further simplification in

$$x_e^* = H_{ee}^a \, f_e - H_{ec}^a \Delta Z \, [ \, I + H_{cc}^a \Delta Z]^{-1} \, H_{ce}^a \, f_e \qquad (2.21b)$$

Recalling the property of a FRF once again,

$$x_e^* = H_{ee}^* \, f_e \qquad (2.22a)$$

Combining Equations (2.21b) and (2.22a) yields,

$$H_{ee}^* = H_{ee}^a - H_{ec}^a \Delta Z \, [ \, I + H_{cc}^a \Delta Z]^{-1} \, H_{ce}^a \qquad (2.22b)$$

Consolidation of the impedance error matrix $\Delta Z$ for use in the transformation equation, requires further manipulation of the inverse term in Equation (2.22b). Firstly, this term is rewritten as the inverse of a product.

$$[ I + H_{cc}^{a} \Delta Z ]^{-1} = [ (\Delta Z^{-1} + H_{cc}^{a}) \Delta Z ]^{-1} \qquad (2.23a)$$

This form invites application of the matrix property,

$$( [a] \ [b] )^{-1} = [b]^{-1} \ [a]^{-1} \qquad (2.23b)$$

so that,

$$[ I + H_{cc}^{a} \Delta Z ]^{-1} = [\Delta Z]^{-1} [\Delta Z^{-1} + H_{cc}^{a}]^{-1} \qquad (2.23c)$$

Clearly, Equation (2.22) can be rewritten as,

$$H_{ee}^{*} = H_{ee}^{a} - H_{ec}^{a} [ \Delta Z^{-1} + H_{cc}^{a} ]^{-1} H_{ce}^{a} \qquad (2.24a)$$

The superscript "*" which denotes a structure's synthesized coupled response can now be replaced by a superscript "x" to indicate test system response, i.e.,

$$H_{ee}^{x} = H_{ee}^{a} - H_{ec}^{a} [ \Delta Z^{-1} + H_{cc}^{a} ]^{-1} H_{ce}^{a} \qquad (2.24b)$$

or, in its full notation:

$$\begin{bmatrix} H_{ii}^{x} & H_{ic}^{x} \\ H_{ic}^{x} & H_{cc}^{x} \end{bmatrix} = \begin{bmatrix} H_{ii}^{a} & H_{ic}^{a} \\ H_{ic}^{a} & H_{cc}^{a} \end{bmatrix} - \begin{bmatrix} H_{ic}^{a} \\ H_{cc}^{a} \end{bmatrix} [ \Delta Z^{-1} + H_{cc}^{a} ]^{-1} \begin{bmatrix} H_{ic}^{a} \\ H_{cc}^{a} \end{bmatrix}^{T} \qquad (2.24c)$$

Equation (2.24c) is the structural synthesis transformation equation. It provides an exact analytic relationship between two FRF models of a specified dynamic system. The analytic FRF is provided by finite element modeling. An experimental frequency response test generates the true frequency response model as the experimental test FRF model. The SST relationship exists at all frequencies of interest, as defined

by the analysis frequency bandwidth, thereby identifying a frequency-dependent impedance error matrix. The $[\Delta Z(\Omega)]$ obtained accommodates examination of the frequency dependency of localization due to spatially incomplete test measurements. The impedance error spectra generated at each excitation frequency can be further resolved to determine component error contribution, by way of Equation (2.16b).

### 3. Localization Matrix Development

SST enables the analyst to extract frequency-dependent error impedance information from the matrix difference of frequency response data provided by two structural models. The advantage of SST emerges when this transformation is applied to general error detection and localization. The localization theory is cast spatially and in the frequency domain, thus providing the analyst with a physical interpretation of suspected damage quickly and simply. The resultant localization matrix also provides information that ensures unique identification. Returning to condensed mathematic notation, Equation (2.24) can be rewritten as follows:

$$\Delta H_{ee} = H_{ec}^{a}\, D^{-1} H_{ce}^{a} \qquad (2.25a)$$

where,

$$\Delta H_{ee} = H_{ee}^{a} - H_{ee}^{x} \qquad (2.25b)$$

and,

$$D = [\, \Delta Z^{-1} + H_{cc}^{a}\,] \qquad (2.25c)$$

The localization matrix is defined as,

$$L = Z_{ee}^{a} \cdot \Delta H_{ee} \cdot Z_{ee}^{a} \qquad (2.26)$$

13

Substituting Equation (2.25) into (2.26) and expanding yields,

$$L = \begin{bmatrix} Z_{ii}^{a} & Z_{ic}^{a} \\ Z_{ci}^{a} & Z_{cc}^{a} \end{bmatrix} \begin{bmatrix} H_{ic}^{a} \\ H_{cc}^{a} \end{bmatrix} [D^{-1}] [H_{ic}^{a} \ H_{cc}^{a}] \begin{bmatrix} Z_{ii}^{a} & Z_{ic}^{a} \\ Z_{ci}^{a} & Z_{cc}^{a} \end{bmatrix} \qquad (2.27)$$

The frequency response matrix is the inverse of the impedance matrix, i.e.,

$$\begin{bmatrix} Z_{ii}^{a} & Z_{ic}^{a} \\ Z_{ci}^{a} & Z_{cc}^{a} \end{bmatrix} \begin{bmatrix} H_{ii}^{a} & H_{ic}^{a} \\ H_{ci}^{a} & H_{cc}^{a} \end{bmatrix} = \begin{bmatrix} I & 0 \\ 0 & I \end{bmatrix} \qquad (2.28)$$

Equation (2.28) demonstrates that all elements containing mixed product coordinates, i.e., both "i" and "c" coordinates, equal zero. This is a very useful property which lead to the following simplification:

$$L = \begin{bmatrix} 0 \\ I \end{bmatrix} [D^{-1}] [\ 0 \ I\ ] \qquad (2.29)$$

Equation (2.29) reduces to a form comparable to the form exhibited by the left-side of Equation (2.9) in units of Z.

$$L = \begin{bmatrix} 0 & 0 \\ 0 & D^{-1} \end{bmatrix} @ \ \Omega = \Omega_{i} \qquad (2.30)$$

The localization matrix, as designed, identifies errors attributable to "c" coordinates and delivers zero-values at all other coordinates. This calculation is performed at each frequency of interest and provides an exact solution, given spatially complete measurement data. Consider two 48 element FE beam models, where one (the damaged model) has a reduced EI along the center six elements. Figure 2-1 demonstrates the resultant localization matrix for the two systems evaluated at 20 Hz and Figure 2-2 demonstrates the resultant localization matrix evaluated at 230 Hz.

14

Spatially Complete Localization - 20 Hz
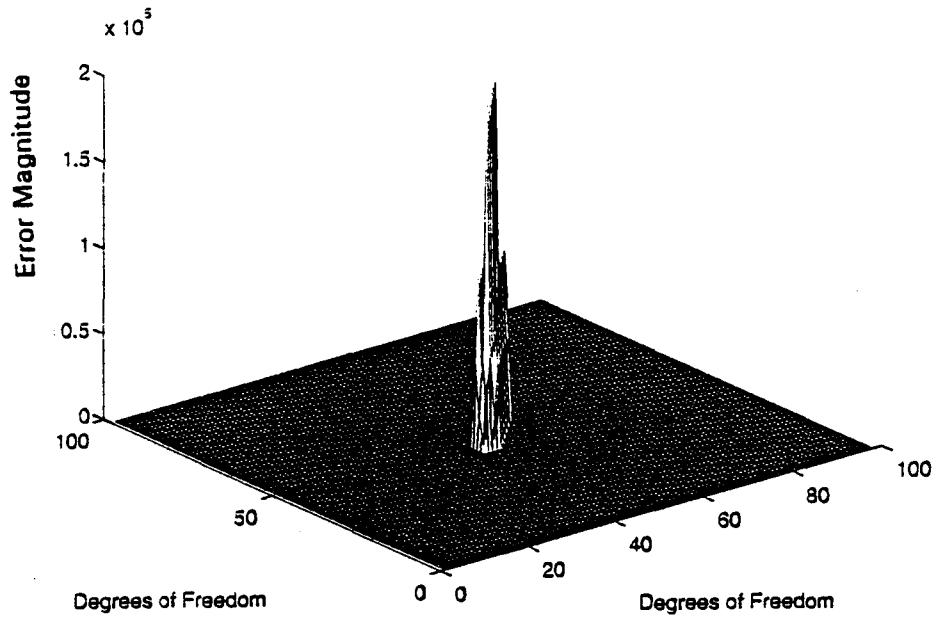


**Figure 2-1** FE single frequency localization.

Spatially Complete Localization - 230 Hz
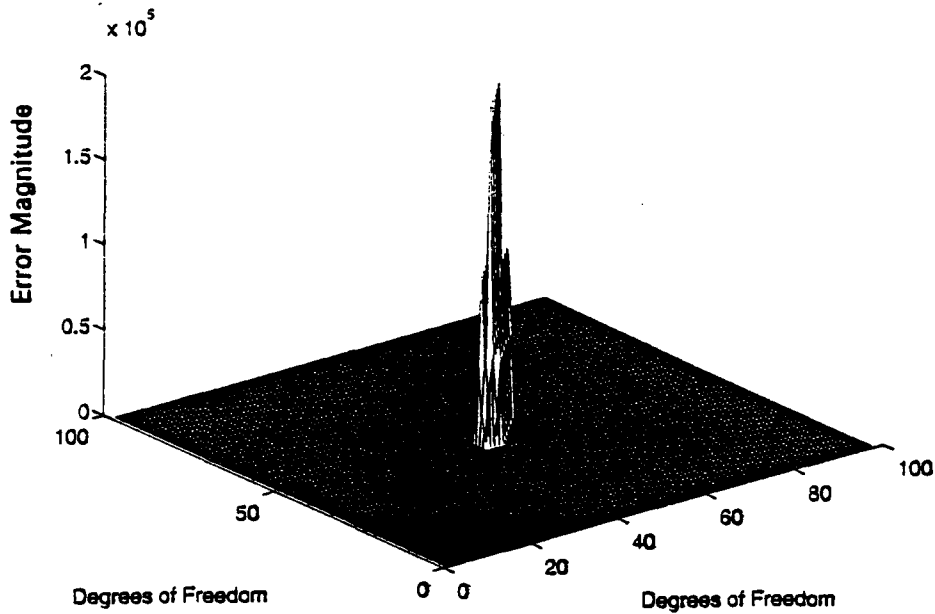


**Figure 2-2** FE single frequency localization.

15

FE Spatially Complete Localization Matrix
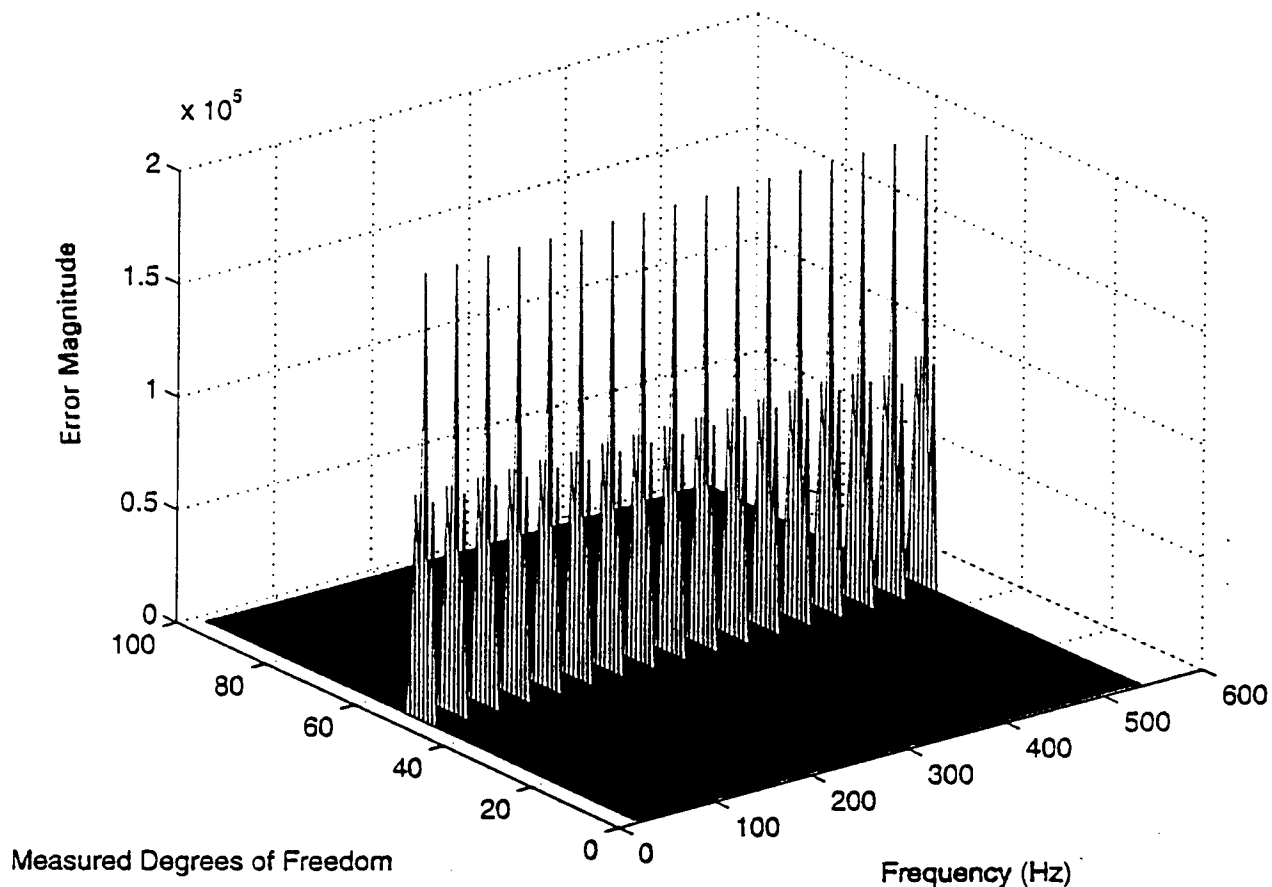


**Figure 2-3**  FE multiple frequency localization.

As Equation (2.30) suggests, and Figures 2-1 and 2-2 demonstrate, all pertinent error identification information can be determined from the main diagonal of the L matrix. By extracting the diagonal of the localization matrix at each frequency of interest, a global localization matrix can be assembled, which provides structural damage assessment at a

16

glance for a given test frequency bandwidth. Figure 2-3 illustrates construction of a global localization matrix by assembling the diagonal information of localization matrices built at specific frequencies. Each column of this matrix reflects localization information by node for a given forcing frequency. Localization units are response per unit excitation, and in our analysis reflect {in/lbf}. The localization matrix identifies the magnitude and location of errors between two systems. Having demonstrated the development of the **L** matrix, reference to localization hereafter will represent a defined frequency bandwidth as opposed to a specific excitation frequency.

The pursuant chapters will demonstrate practical application of this theory. Localization given spatially incomplete data is emphasized, with comparative analyses between model reduction methods provided. Analyses will demonstrate the influence of measurement noise, test frequency bandwidth selection, and damage description, on localization effectiveness and dependability.

# III. SPATIALLY INCOMPLETE IDENTIFICATION

## A. SPATIALLY COMPLETE LOCALIZATION

Chapter II emphasized that the localization theory provides an exact error identification solution given spatially complete data. The formulation of the **L** matrix presented in Equation (2.30) identifies non-zero coordinates as error coordinates which correspond to physical structure coordinates associated with damage. Two finite element free-free beam models provide the simulated test and baseline structures under analysis. One model, the test model, is damped and altered to simulate a potentially damaged test system. The test model FRF, solid line, is constructed by imposing a ten percent EI reduction across the center two elements of a forty-eight element beam. The FRF models, detailed in Appendix A, are shown below in Figure 3-1.
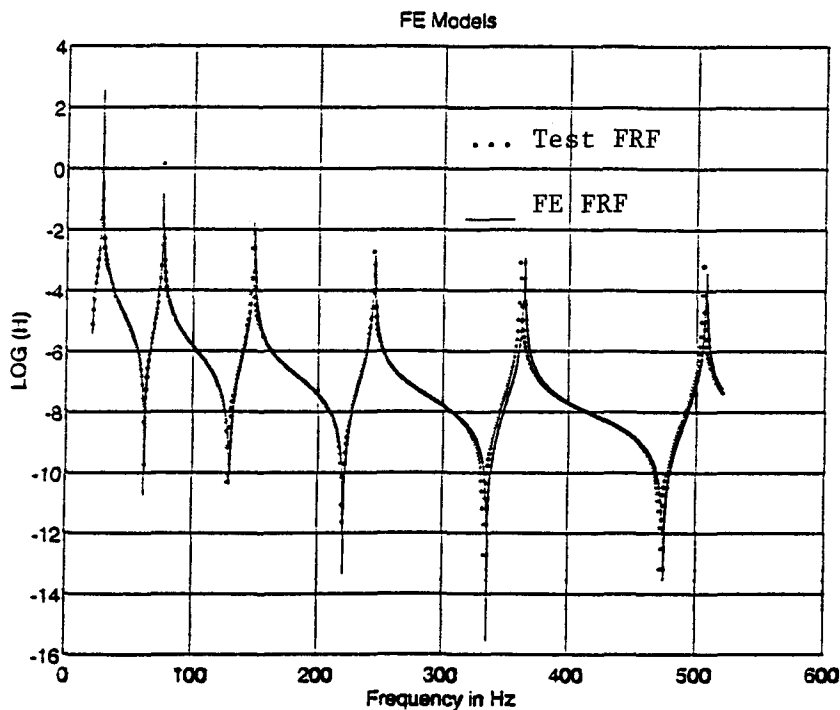


**FE Models**

Figure 3-1  FE simulated test and baseline FRF models.

19

The symmetry requirement of test FRF matrices is ensured by the Bernoulli-Euler beam development of the FE stiffness and mass matrix expressions [Ref. 7:p. 387]. The FRF models of Figure 3-1 overlay one another so closely, that differences are difficult to detect by inspection. Yet, applying Equation (2.26) over the frequency bandwidth of 20-520 Hz, the exact error solution is obtained along with the physical location of damage in Figure 3-2. As the development demonstrated, non-error coordinates appear as zero.
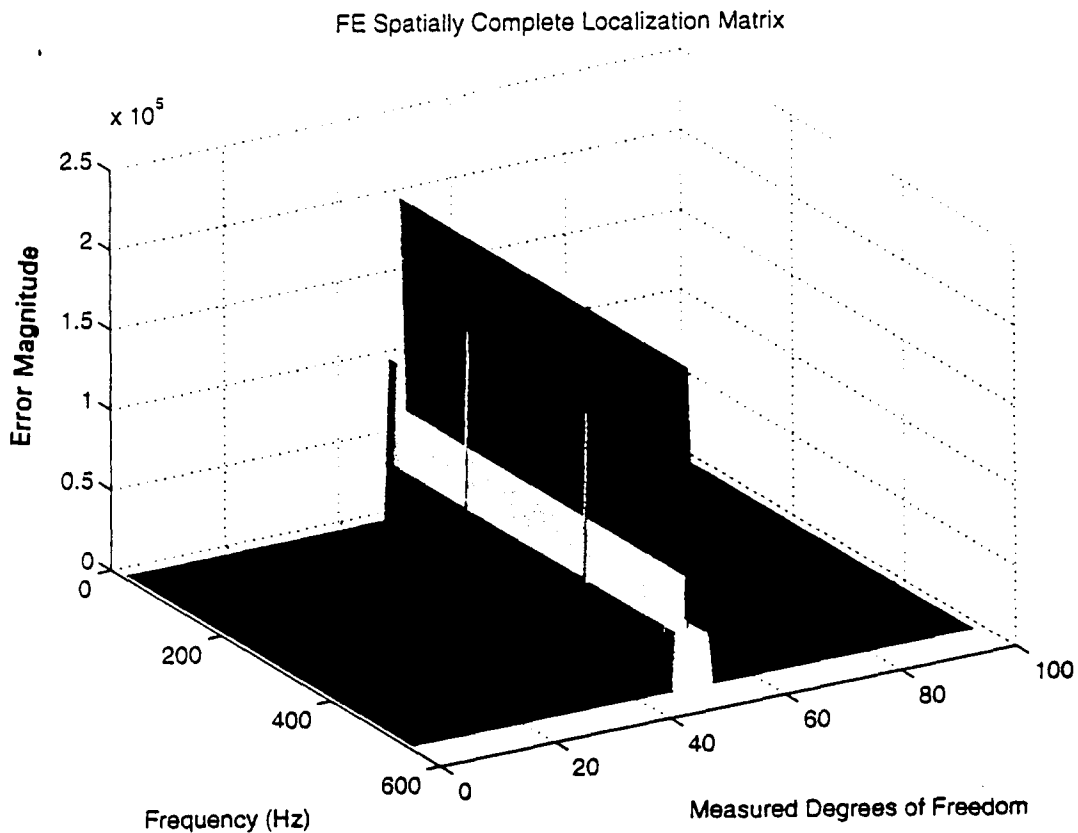


**Figure 3-2** FE model localization, 2" crack at dof 47, frequency bandwidth 20-520 Hz.

20

## B.  SPATIALLY INCOMPLETE LOCALIZATION

Spatially complete data, as demonstrated, provides an exact solution for error identification.  However, for real structures, spatially complete data cannot be practically obtained given a finite supply of response transducers.  The process of analyzing a structure with a finite number of measurement devices defines a reduced order model with a characteristic impedance nonlinearly dependent upon its full order counterpart.  Complete structural system identification over a given frequency range requires that the number of response coordinates and measuring devices equal the number of finite element degrees of freedom (dof).  Since spatially incomplete data is the result of test measurements, either FE model reduction of the analytic system FRF or test model FRF expansion is required.  The reduction methods investigated herein are Extraction reduction [Ref. 10] and Improved Reduction System (IRS) [Ref. 8].  A Fill-In method of expansion is investigated.

### 1.  Extraction Reduction

Extraction reduction refers to a process whereby FE dof corresponding to test measurement dof are extracted from the full order analytic FRF matrix.  The extracted data maps one-to-one the physical coordinates at which test information is available.  The full order FRF matrix is constructed by inverting the impedance matrix obtained from FE model mass, stiffness, and damping (when available) matrices.  The coordinates extracted from the full order system are referred to as retained coordinates, or "aset" coordinates, denoting "analysis set" coordinates.  The omitted coordinates are referred to as "oset" coordinates.  The aset coordinates constitute the reduced FRF matrix.

21

The reduced impedance matrix is then obtained by inverting the reduced FRF matrix. Figures 3-3a and 3-3b demonstrate localization using Extraction reduction, the former being the traditional manner of display for the localization matrix given a frequency bandwidth, while the latter demonstrates error node location superimposing all frequencies. Superposition of localization information at all frequencies simultaneously can reveal misleading information as certain frequencies (such as, natural system frequencies) influence scaling such that valuable detection information is suppressed. Traditional mesh plots reveal localization information provided at each forcing frequency to ascertain a frequency bandwidth in which to concentrate damage detection efforts.

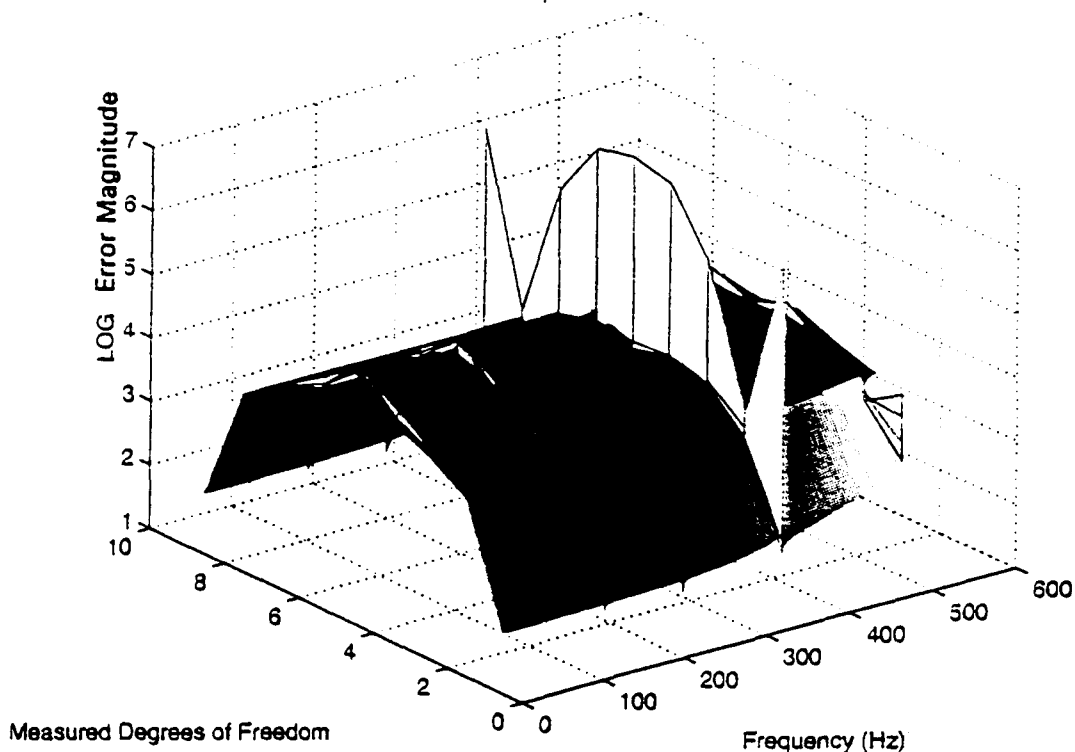FE Spatially Incomplete (9x9) Localization Matrix – Extraction



**Figure 3-3a** FE model localization, 2" crack at node 5, extraction reduction, frequency bandwidth 20-520 Hz.

22
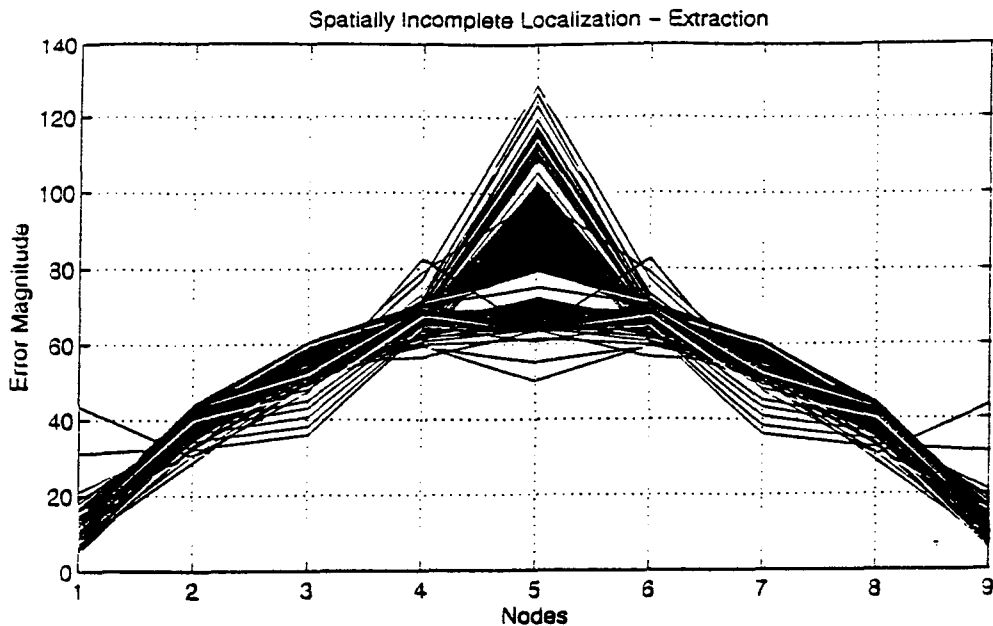
**Figure 3-3b** FE model localization plot, 2" crack centered at node 5, frequency bandwidth 20-520 Hz.

## 2. Improved Reduction System (IRS)

Model reduction introduces the *aset* and *oset* coordinate system. The general impedance relation for a reduced system reflects this new coordinate system, e.g.,

$$\left\{ \begin{matrix} f_a \\ f_o \end{matrix} \right\} = \left[ \begin{matrix} Z_{aa} & Z_{ao} \\ Z_{oa} & Z_{oo} \end{matrix} \right] \left\{ \begin{matrix} x_a \\ x_o \end{matrix} \right\} \tag{3.1}$$

Expanding Equation (3.1) into two equations yields,

$$f_a = Z_{aa}x_a + Z_{ao}x_o \tag{3.2a}$$

$$f_o = Z_{oa}x_a + Z_{oo}x_o \tag{3.2b}$$

The *oset* coordinates, as mentioned previously, correspond to response coordinates not obtained from measurement. Since these coordinates are not associated with dynamic response measurement locations, no information is available at these coordinates. Consequently, the forcing function at these *oset*

23

coordinates can be justifiably set to zero. Making the appropriate substitution in Equation (3.2b), and solving for the generalized structural response coordinates leads to the following simplifications:

$$x_o = -Z_{oo}^{-1} Z_{oa} x_a \qquad (3.3a)$$

$$\begin{Bmatrix} x_a \\ x_o \end{Bmatrix} = \begin{bmatrix} I \\ -Z_{oo}^{-1} Z_{oa} \end{bmatrix} \{x_a\} \qquad (3.3b)$$

Substituting these results into Equation (3.1) yields,

$$\begin{Bmatrix} f_a \\ 0 \end{Bmatrix} = \begin{bmatrix} Z_{aa} & Z_{ao} \\ Z_{oa} & Z_{oo} \end{bmatrix} \begin{bmatrix} I \\ -Z_{oo}^{-1} Z_{oa} \end{bmatrix} \{x_a\} \qquad (3.4a)$$

$$\{f_a\} = \begin{bmatrix} Z_{aa} - Z_{ao} Z_{oo}^{-1} Z_{oa} \end{bmatrix} \{x_a\} \qquad (3.4b)$$

For the static case, where frequency is zero, the impedance relationship of Equation (3.3) reduces to a structural stiffness correlation between retained and omitted coordinates, e.g.,

$$\{x_o\} = \begin{bmatrix} -K_{oo}^{-1} K_{oa} \end{bmatrix} \{x_a\} \qquad (3.5)$$

The IRS reduction method [Ref. 8] provides a frequency independent transformation of Equation (3.5), such that,

$$\{x_o\} = \begin{bmatrix} -K_{oo}^{-1} K_{oa} + T M_{stat}^{-1} K_{stat} \end{bmatrix} \{x_a\} \qquad (3.6a)$$

where,

$$T = K_{oo}^{-1} M_{oa} - K_{oo}^{-1} M_{oo} K_{oo}^{-1} K_{oa} \qquad (3.6b)$$

The subscript "stat" identifies the statically reduced mass and stiffness matrices. The procedure requires full order FE mass and stiffness matrices partitioned into retained and omitted set coordinates as follows:

$$K = \begin{bmatrix} K_{aa} & K_{ao} \\ K_{oa} & K_{oo} \end{bmatrix} \qquad (3.7a)$$

$$M = \begin{bmatrix} M_{aa} & M_{ao} \\ M_{oa} & M_{oo} \end{bmatrix} \qquad (3.7b)$$

The transformation matrix "t", to be defined shortly, has properties such that reduced order stiffness and mass matrices can be constructed as shown in Equation (3.8).

$$\overline{K}^a = t^T K_a t \qquad (3.8a)$$

$$\overline{M}^a = t^T M_a t \qquad (3.8b)$$

Equations (3.8a) and (3.8b) transform full order $n \ x \ n$ finite element model matrices to reduced order $m \ x \ m$ analysis matrices which are subsequently compared to the $"m"$ measured test model degrees of freedom. The transformation matrix applied above is defined as,

$$t = \begin{bmatrix} I_{mxm} \\ T \end{bmatrix} \qquad (3.9)$$

The reduced impedance and FRF matrices can be calculated at each frequency of interest, as shown previously, such that,

$$\overline{Z}^a = \overline{K}^a - \Omega^2 \overline{M}^a \qquad (3.10a)$$

and,

$$\overline{H} = [\overline{Z}^a]^{-1} \qquad (3.10b)$$

where by property of matrix inversion,

$$[\overline{Z}^a]^{-1} = \frac{Adj[\overline{Z}^a]}{Det[\overline{Z}^a]} \qquad (3.10c)$$

Mathematic abbreviations Adj[] and Det[] indicate adjoint and determinant matrices, respectively.  Figures 3-4a and 3-4b demonstrate localization employing IRS reduction.

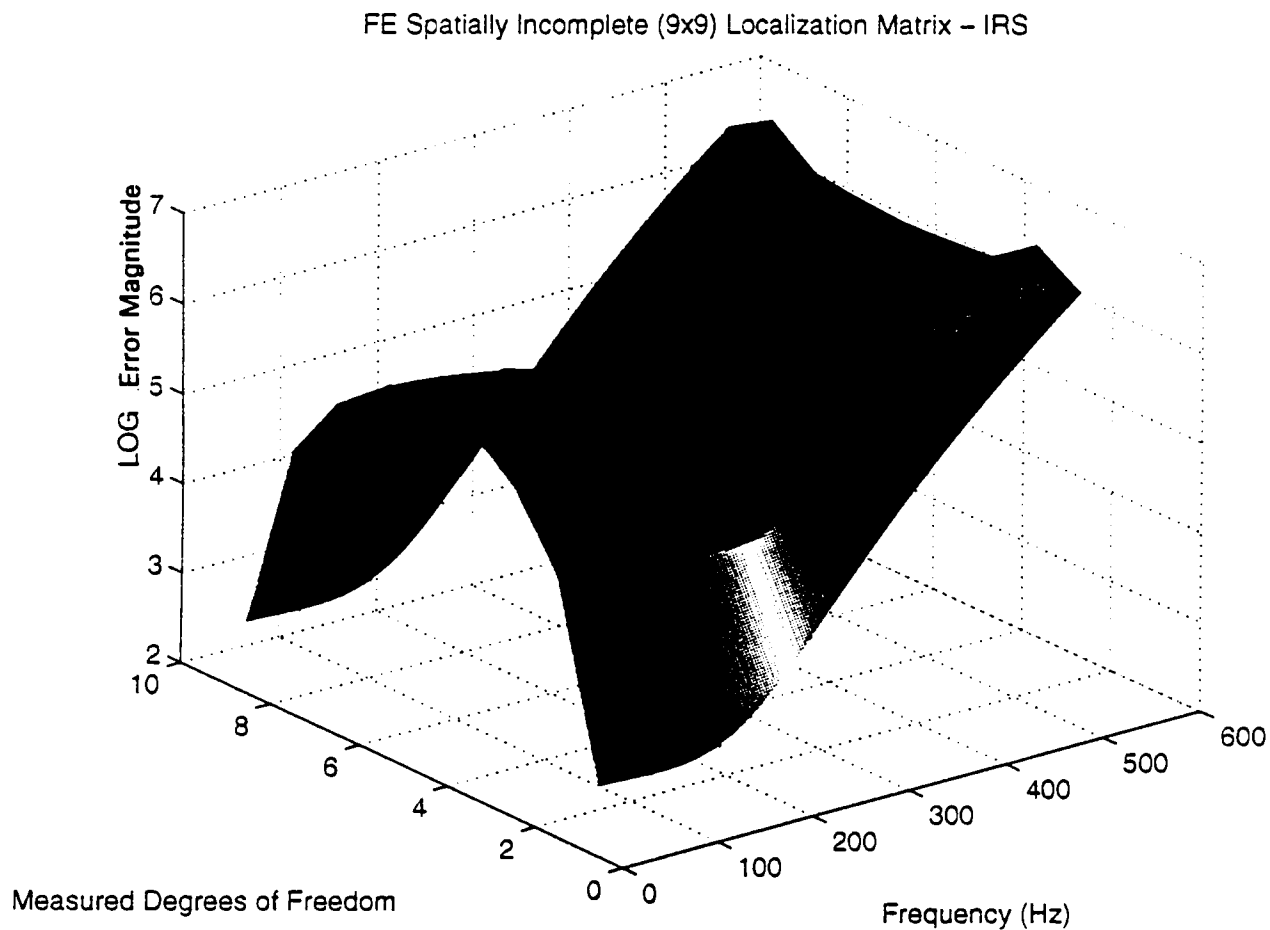FE Spatially Incomplete (9x9) Localization Matrix – IRS



**Figure 3-4a**  FE model localization, 2" crack centrally located, IRS reduction employed, bandwidth 20-520 Hz.
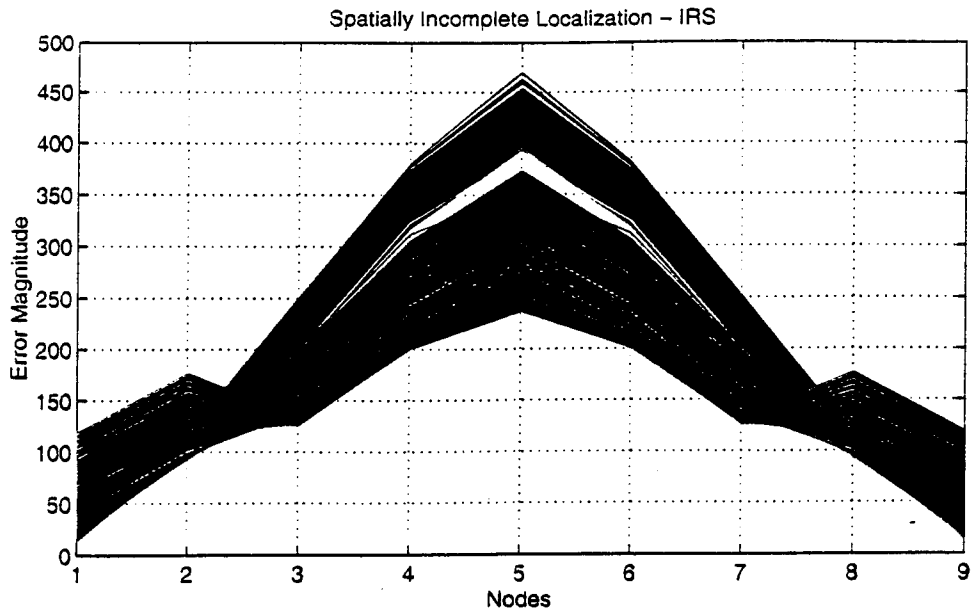
Spatially Incomplete Localization – IRS

**Figure 3-4b**   FE model localization plot, 2" crack located at node 5, IRS reduction employed, bandwidth 20-520 Hz.

### 3.   Fill-in Expansion Method

Model reduction methods constitute one of two techniques for processing spatially incomplete data. The second method, often referred to as matrix expansion, incorporates *aset* measurements into test system matrices of equivalent order to finite element models. One such method, the Fill-in method, superimposes test data from measured dof onto the full order FE model thereof in corresponding coordinate locations. Imposition of test data into a ndof analytic FRF model ensures that the dynamic response of the two systems remain equal at oset coordinates. This phenomenon forces the localization matrix to be zero at oset coordinates, such that identification information is provided solely by *aset* coordinates. The theory potentially will minimize the detrimental effects of test measurement noise by including more noise independent (FE) coordinates in the localization analysis. Figures 3-5a and 3-5b demonstrate Fill-In localization.
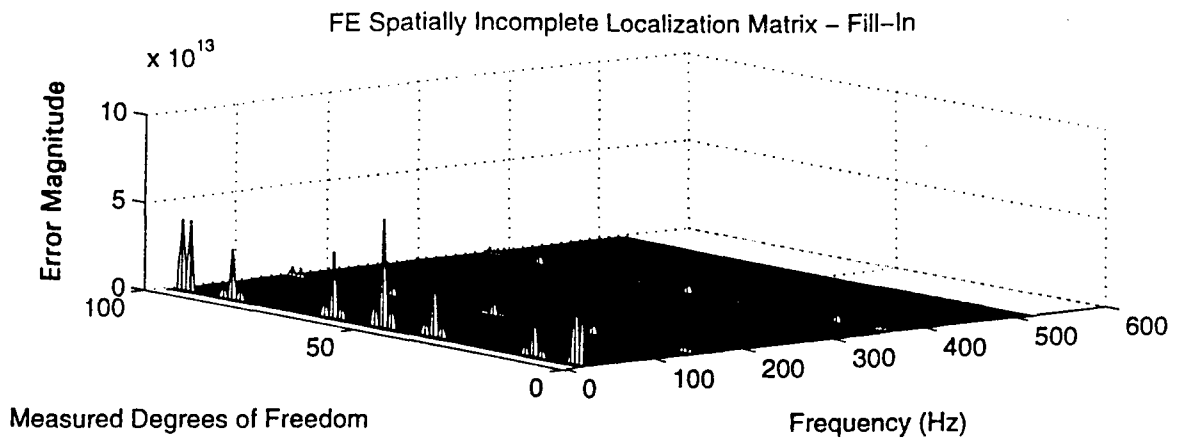
27

FE Spatially Incomplete Localization Matrix – Fill–In

**Figure 3-5a** FE model localization, 2" crack centrally located, Fill-in expansion, bandwidth 20-520 Hz.



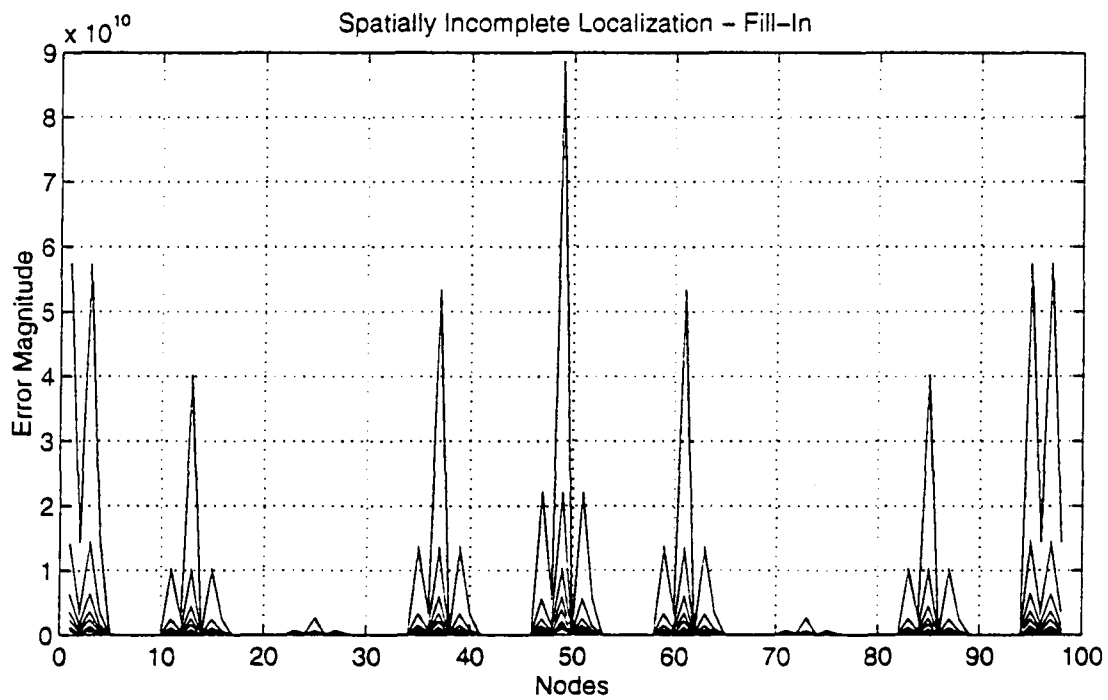Spatially Incomplete Localization – Fill–In

**Figure 3-5b** FE model localization plot, 2" crack located at node 5, IRS reduction employed, bandwidth 20-520 Hz.

# IV. LOCALIZATION SIMULATION

Frequency bandwidth selection, measurement noise, and damage size, all contribute to the success of damage detection by spatially incomplete frequency domain analysis. These factors impact reliability and accuracy of localization applications independently and cooperatively. Ramifications of each factor on identification methods are assessed from finite element model simulation. IRS reduction is employed instead of extraction reduction in this thesis because extraction reduction introduces FE model oset natural frequencies into the analysis, imposing nonlinearity through a secondary dynamic system.

## A. FREQUENCY BANDWIDTH SELECTION

The primary consideration in selecting a test frequency bandwidth is capturing sufficient resonant frequency information to assess experimental-theoretical correlation. Once an accurate finite element model has been constructed, efforts are channeled in selection of an experimental frequency range which yields the most useful error identification information. The advantage of high or low frequency ranges in the presence of minor damage is investigated. Performing FE simulations with our case models, i.e., the virgin FE beam model and the 2-inch crack FE beam model, the impact of frequency bandwidth selection is revealed. Test cases include frequency spans of 20-200 Hz, 20-520 Hz, 20-1000 Hz, and 500-2000 Hz. These cases are plotted in Figures 4-1 through 4-4, respectively. The test cases suggest that there is no clear localization advantage associated with higher frequency modes. This assessment is consistent with the experimental findings of Chapter V. Lower frequencies (the first several modes) exhibited a greater propensity to unveil structural damage.

29

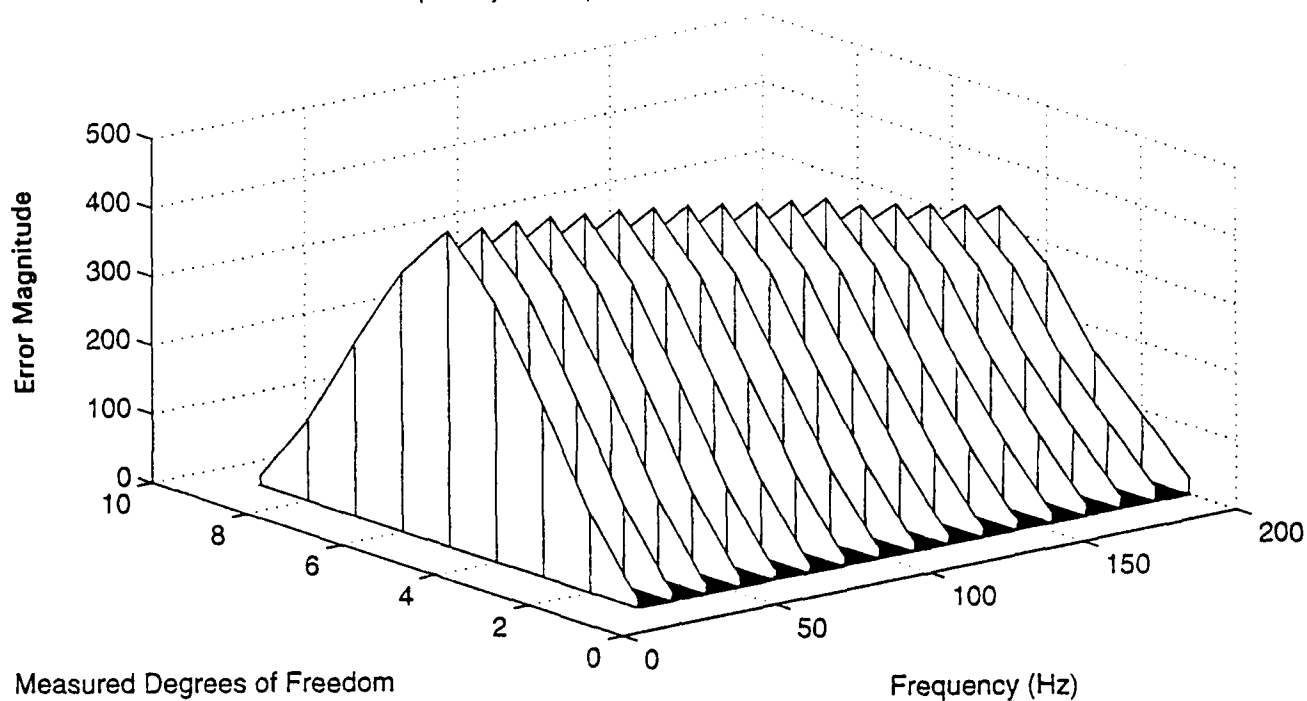FE Spatially Incomplete (9x9) Localization Matrix – IRS

**Figure 4-1** FE localization, 2" crack at node 5, 20-200 Hz.



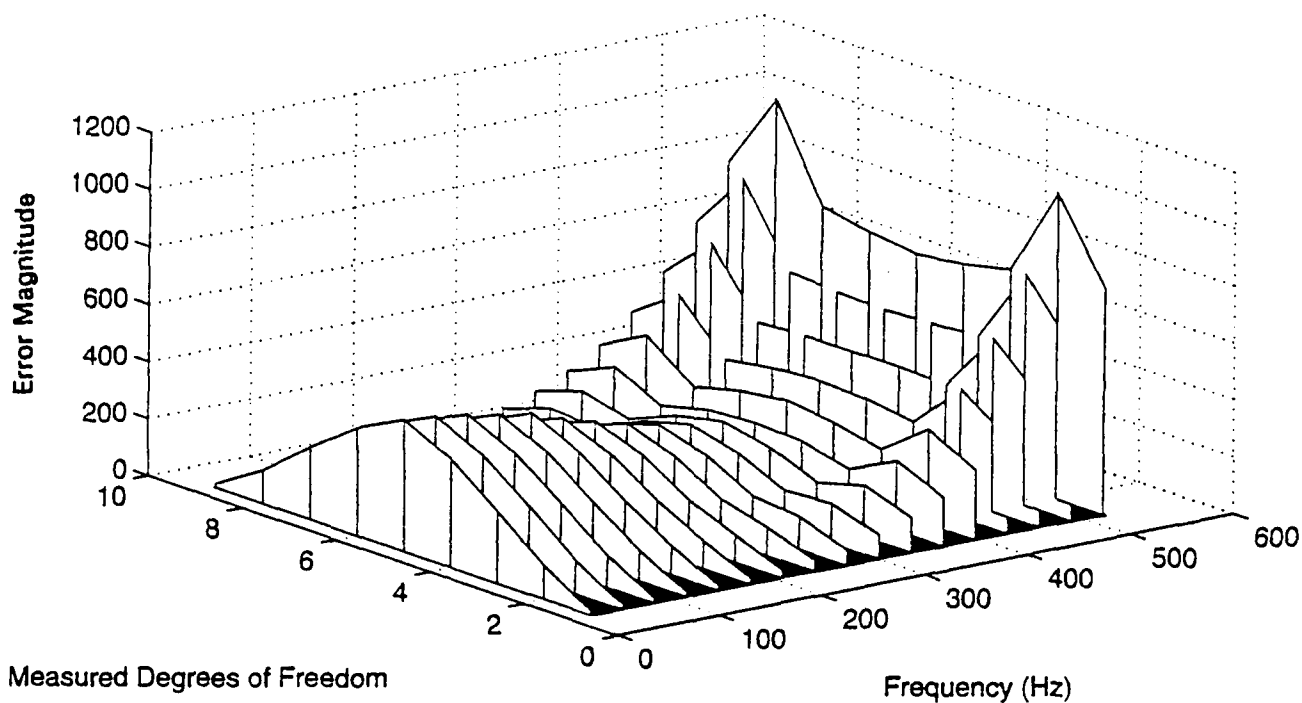FE Spatially Incomplete (9x9) Localization Matrix – IRS

**Figure 4-2**  FE localization, 2" crack at node 5, 20-520 Hz.

FE Spatially Incomplete (9x9) Localization Matrix – IRS
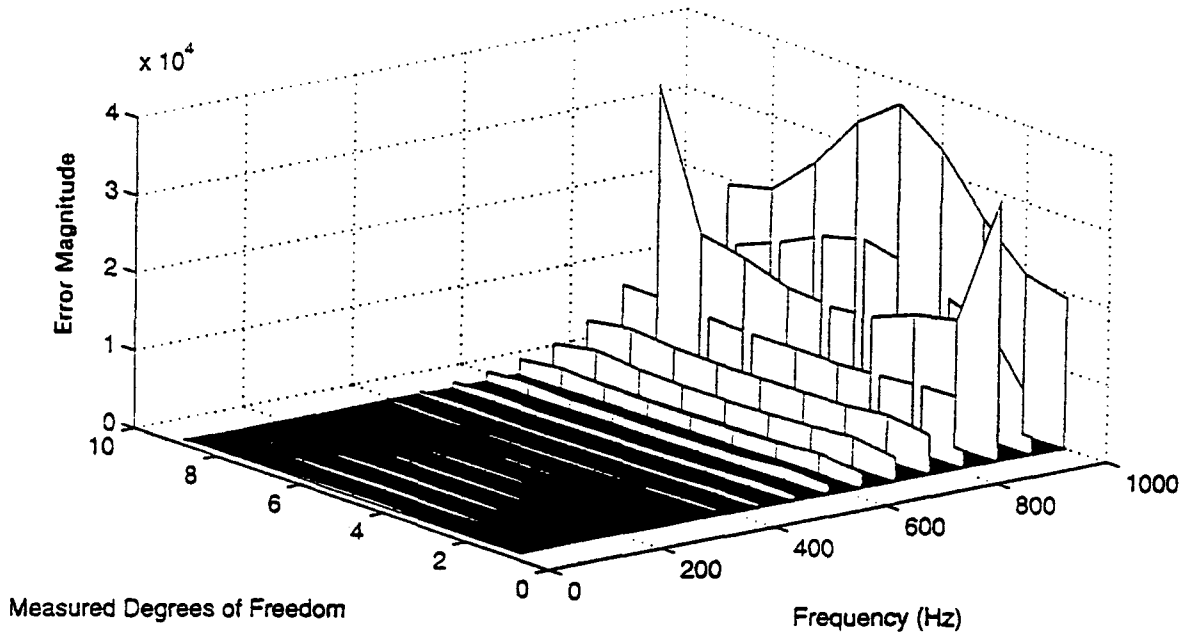
**Figure 4-3** FE localization, 2" crack at node 5, 20-1000 Hz.

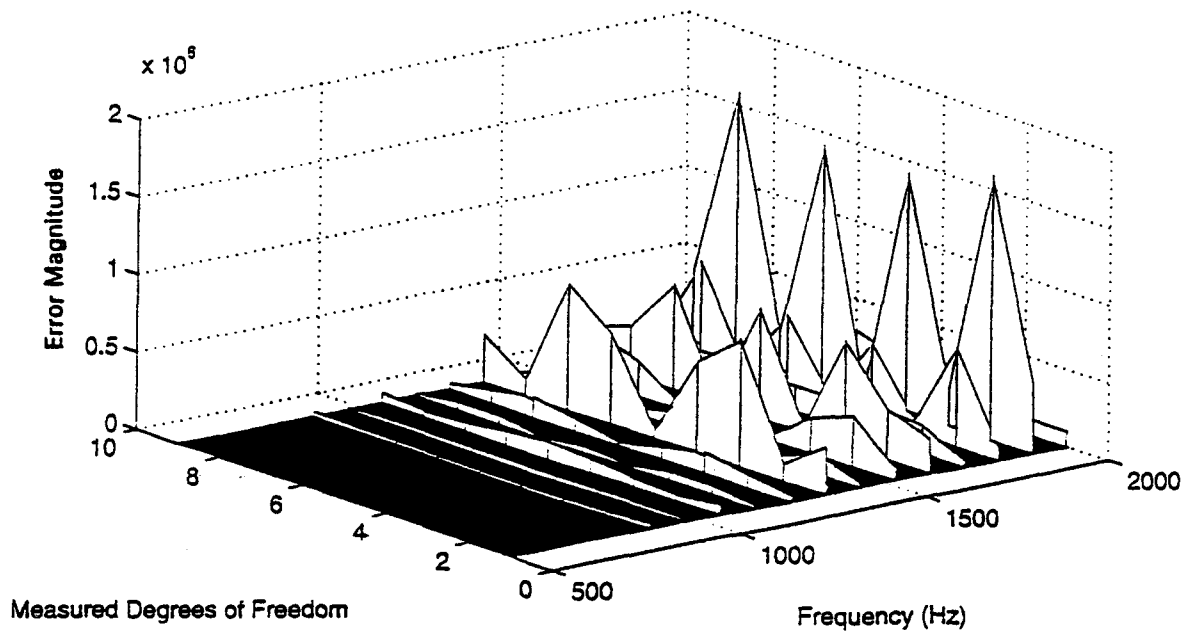

FE Spatially Incomplete (9x9) Localization Matrix – IRS

**Figure 4-4** FE localization, 2" crack at node 5, 500-2000 Hz.

31

## B. NOISE

Two elements inherent in experimental test data are incompleteness and noise. The effects of spatially incomplete data were demonstrated in Chapter III. The following discussion addresses the effects of noise on damage detection. Measurement noise exacerbates the difficulty in ascertaining error differences between spatially incomplete test FRF data and reduced model FRF, by introducing spurious information in the localization equation. False signals, when scaled in regions near natural frequencies, conceal true damage coordinates by amplifying false error coordinates. Consequently, incorrect assessment of damage location may result.

Recall the two FE models of Figure 3-1 with 2-inch central damage across a 48 inch, 48 element beam. Varying degrees of damage is imposed across the central 2 inches by reducing stiffness or mass density of the corresponding beam elements incrementally by 5%, 10%, and 50%. Beam localization is conducted with 1%, 2%, and 5% noise, respectively. FE noise simulation is accomplished by applying a scale factor to each column of the experimental FRF matrix, determined from:

$$\frac{noisevalue}{100} = \frac{scale\ factor \times \|rand(H_{exp}(:,i))\|}{\|H_{exp}^{i}\|} \quad (4.1)$$

By generating new random noise for each column corresponding to an excitation frequency, measurement noise is imposed analytically. To reduce the influence of resonant frequency scaling in our analysis, the inter-resonant regions of model FRF's are considered. Inter-resonant regions exclude resonant regions of the FRF where response is unbounded. Since lower mode frequencies have proven valuable in localization, as demonstrated in the previous section, we investigate the effect of noise in these regions. Nine

translational dof are considered, simulating measurement. Figures 4-5 through 4-8 exhibit both mesh plots and node plots in the first inter-resonant region for the various noise conditions and 5% EI reduction. Figures 4-9, 4-10, and 4-11 display the effects of noise on localization for the same structure but in other inter-resonant regions. Figures 4-12 through 4-15 demonstrate the effects of noise on a structure with 5% nominal reduction in mass density. Figures 4-16 through 4-19 reflect analysis for a beam with 10% EI reduction. Figures 4-20 through 4-23 reflect a structure with 10% nominal reduction in mass density. Figures 4-24 through 4-27 reflect analysis for a beam with 50% EI reduction. Figures 4-28 through 4-31 display localization results for a beam structure with 50% nominal reduction in mass density.

The localization trends exhibited in these plots suggest that measurement noise, as expected, greatly complicate error identification. The general assumption when undertaking error detection by theoretical-experimental correlation methods is that errors are present in the analytical model and not in the measurements [Ref. 3]. The simulation reveals that this is not necessarily the case. The localization matrix identifies discrepancies between the test structure and its corresponding analytical model, regardless of their source. In simulation, we can arbitrarily impose damage in the form of a EI reduction or a mass density reduction. A reduction in aggregate EI in an element corresponds to the real world condition of a reduction in structural stiffness.

Reference (3) discusses the impact of noise in Error Matrix Methods and simulates measurement noise (1) by altering eigenvalues on the order of .01% and (2) by significant digit truncation to reflect accuracy limitations of test measurements. The discussion concludes from FE simulation that both conditions significantly impact error identification information accuracy.

33

FE Spatially Incomplete (9x9) Localization Matrix – No Noise
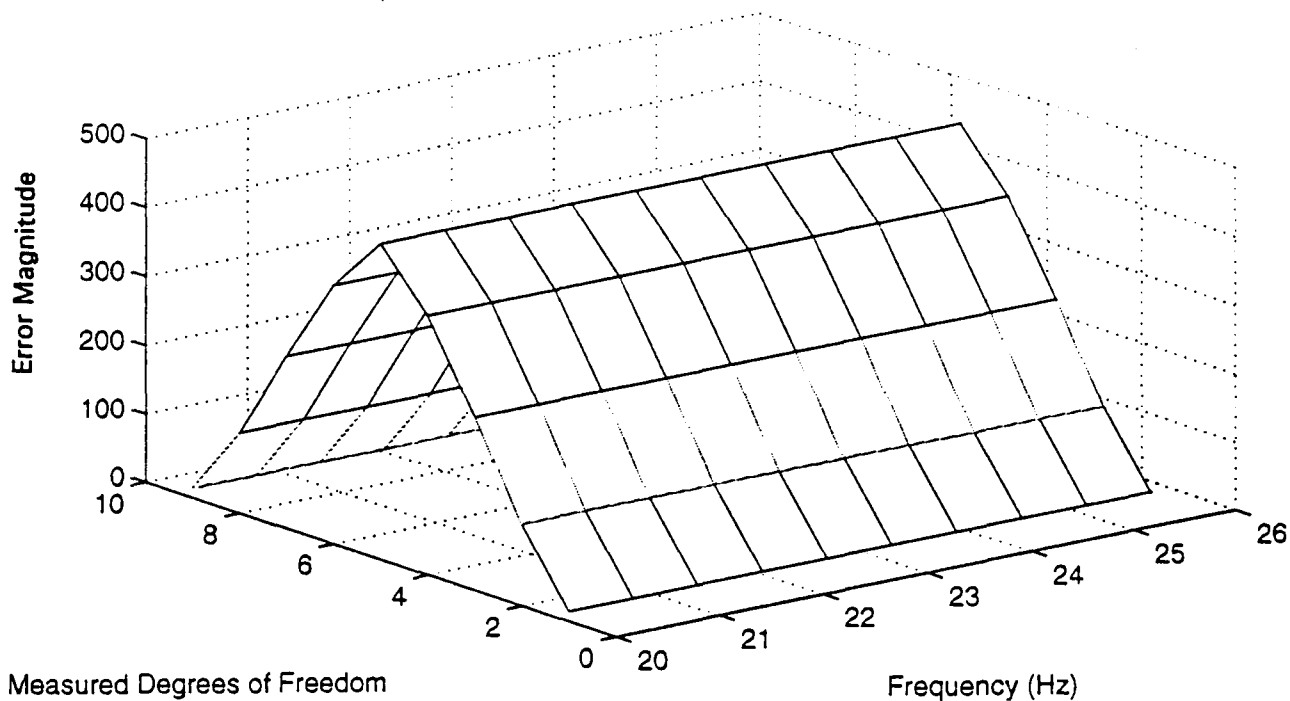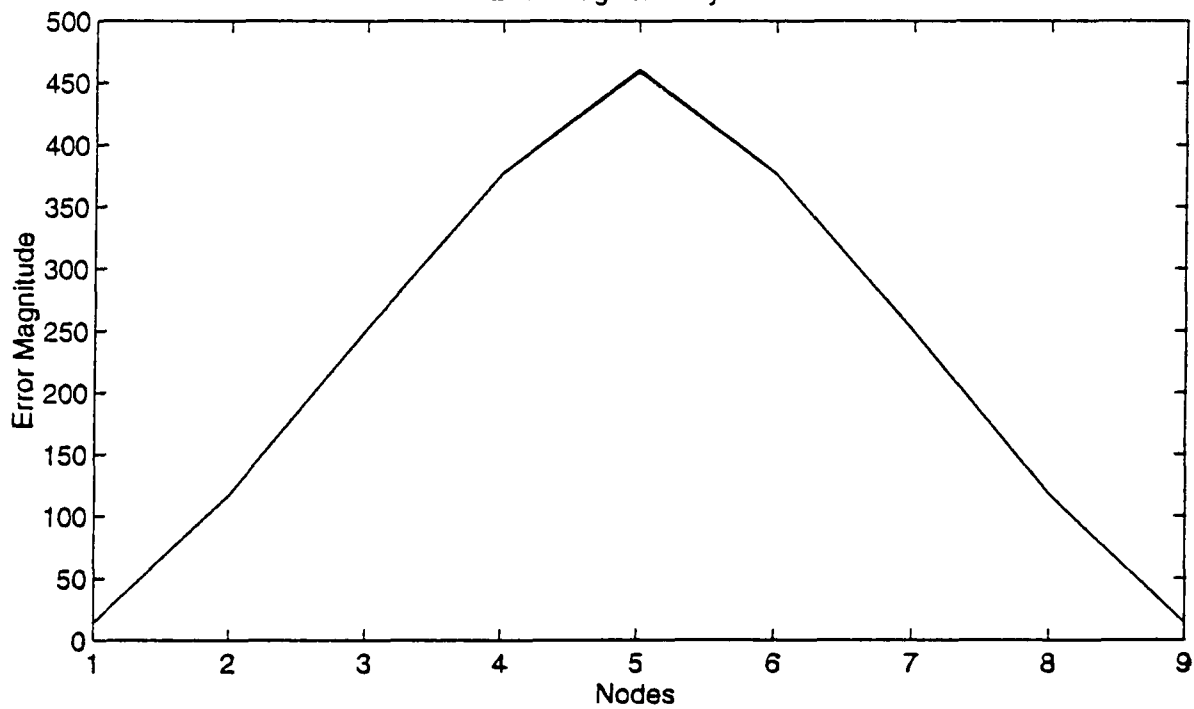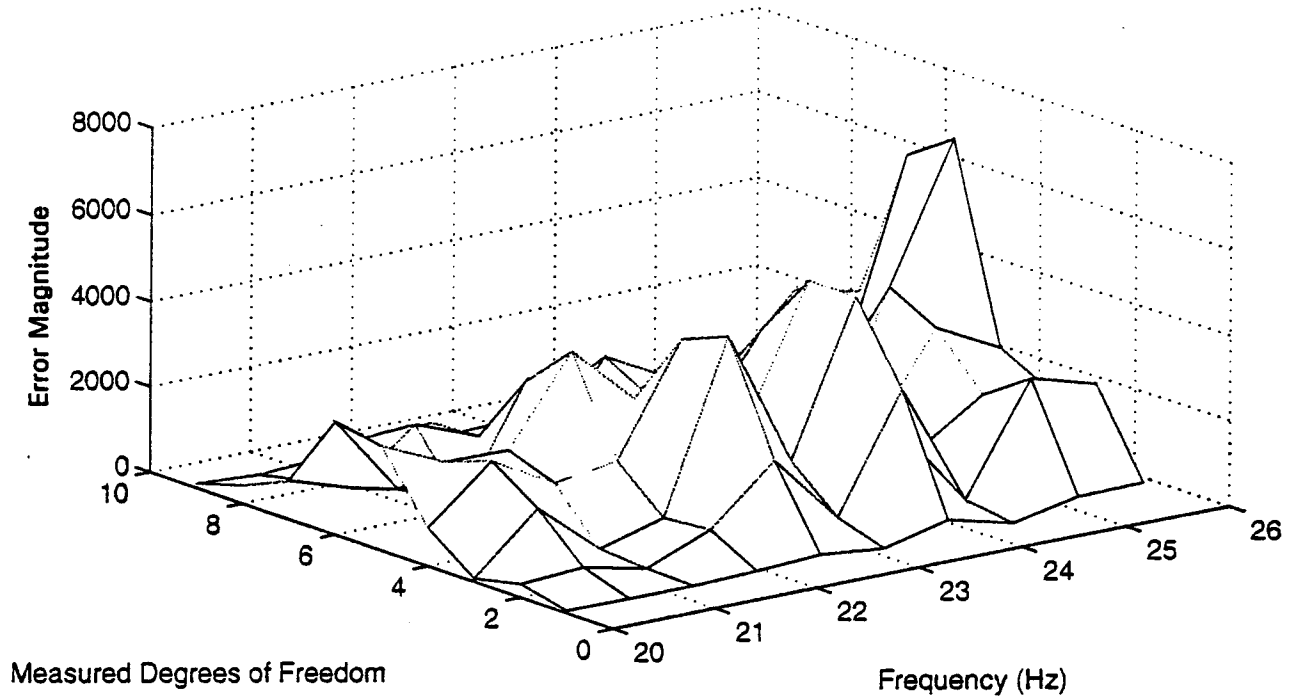
Error Magnitude by Node

**Figure 4-5** FE noise simulation, 5% EI reduction (mdof or node 5), no noise, inter-resonant region 20-26 Hz.

FE Spatially Incomplete (9x9) Localization Matrix – 1% Noise
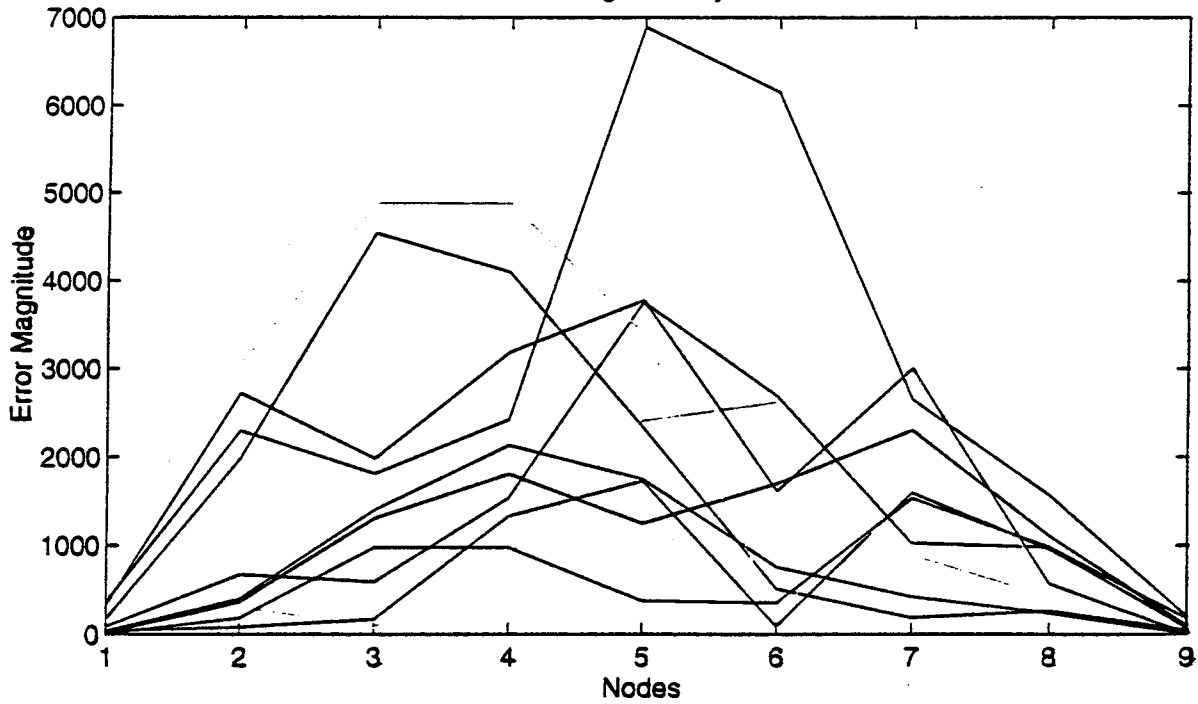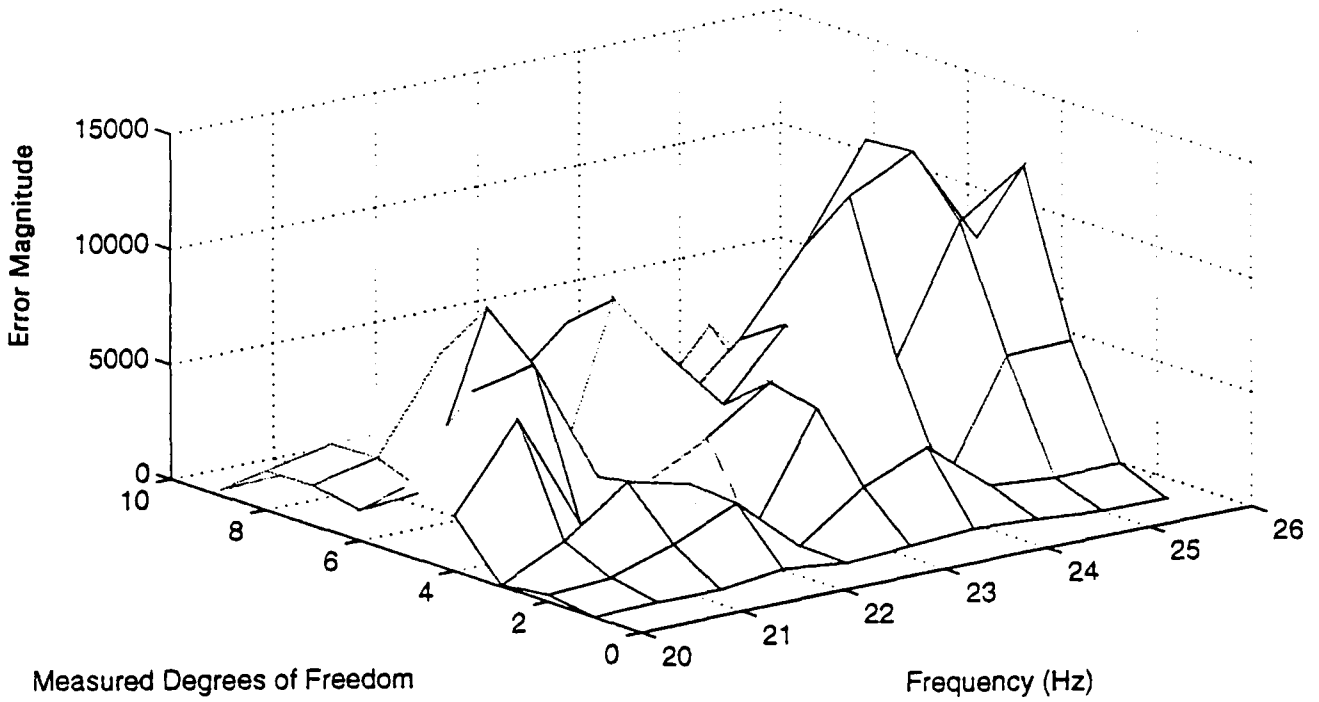
Error Magnitude by Node

**Figure 4-6** FE noise simulation, 5% EI reduction (mdof or node 5), 1% noise, inter-resonant region 20-26 Hz.

FE Spatially Incomplete (9x9) Localization Matrix – 2% Noise



Error Magnitude by Node

**Figure 4-7** FE noise simulation, 5% EI reduction (mdof or node 5), 2% noise, inter-resonant region 20-26 Hz.

FE Spatially Incomplete (9x9) Localization Matrix – 5% Noise
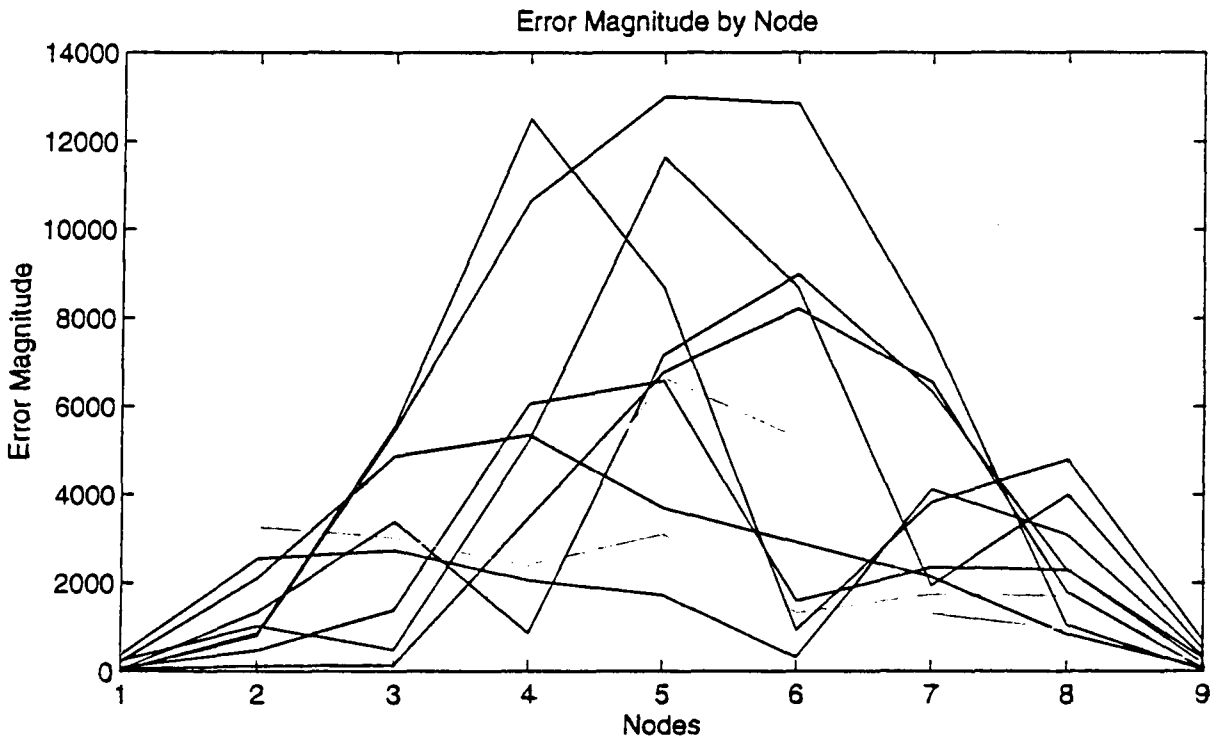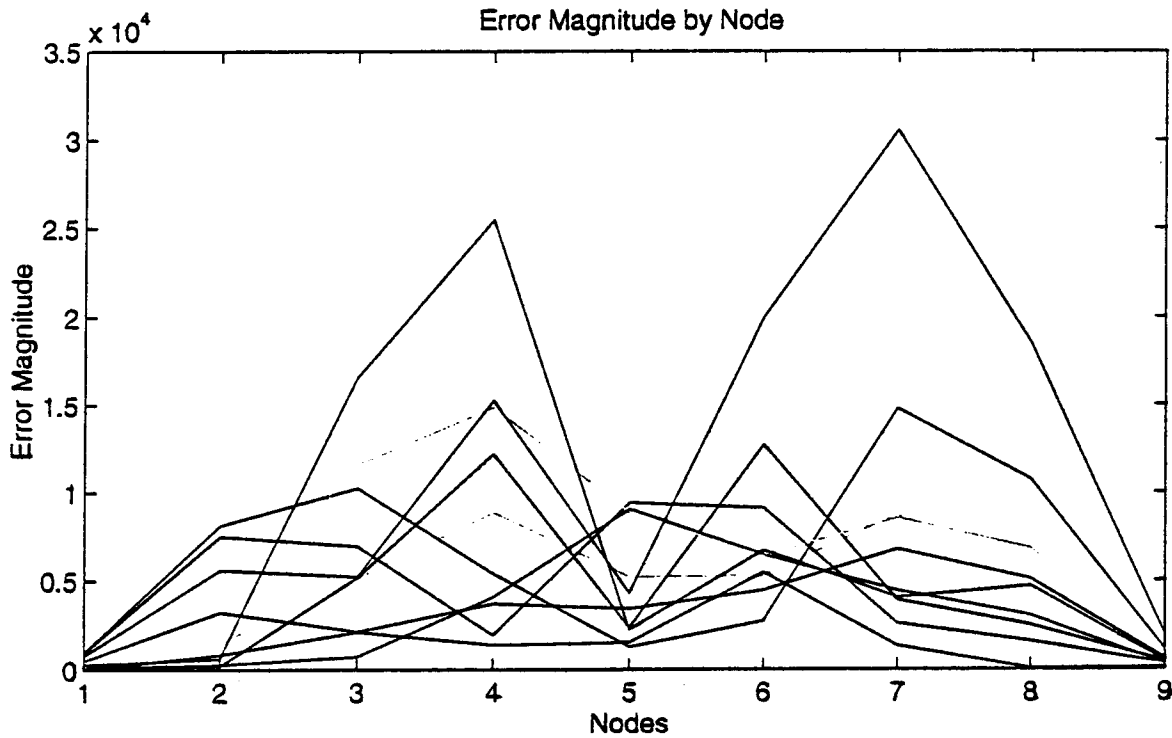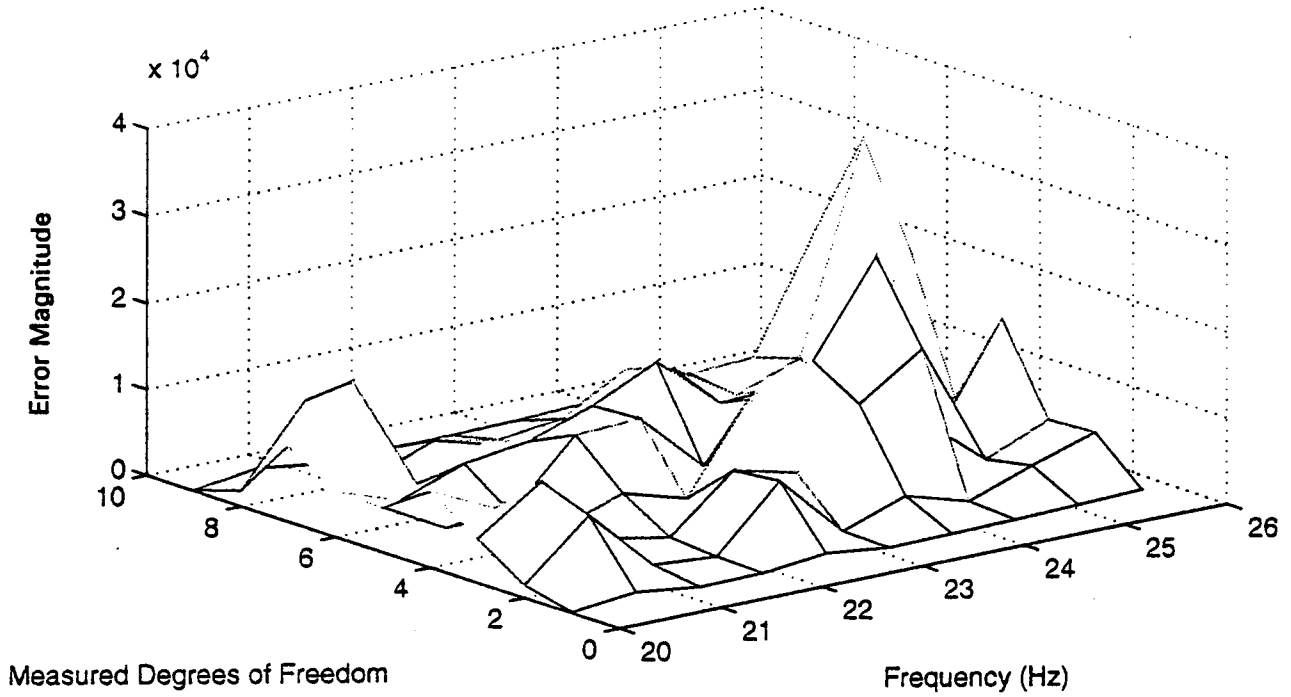


Error Magnitude by Node

**Figure 4-8** FE noise simulation, 5% EI reduction (mdof or node 5), 5% noise, inter-resonant region 20-26 Hz.

FE Spatially Incomplete (9x9) Localization Matrix – No Noise

Error Magnitude

500

0

Measured Degrees of Freedom

Frequency (Hz)

FE Spatially Incomplete (9x9) Localization Matrix – 1% Noise

5000

0

Measured Degrees of Freedom

Frequency (Hz)

FE Spatially Incomplete (9x9) Localization Matrix – 2% Noise

10000

5000

0

Measured Degrees of Freedom

Frequency (Hz)

x 10⁴   FE Spatially Incomplete (9x9) Localization Matrix – 5% Noise

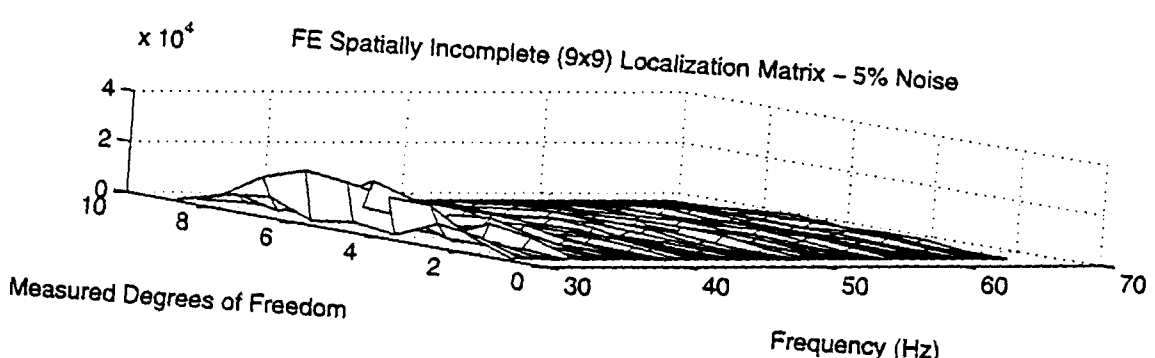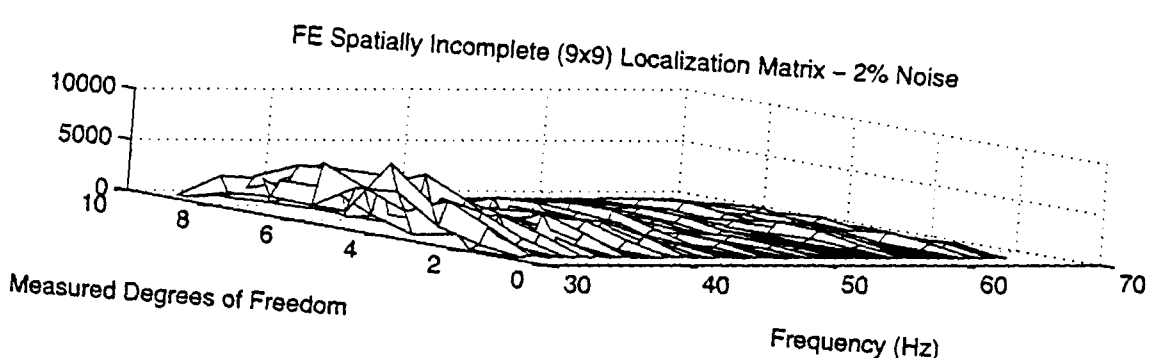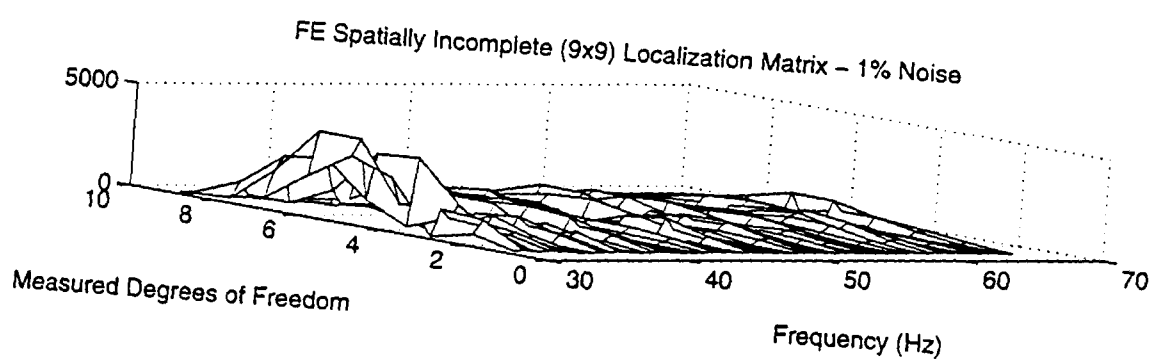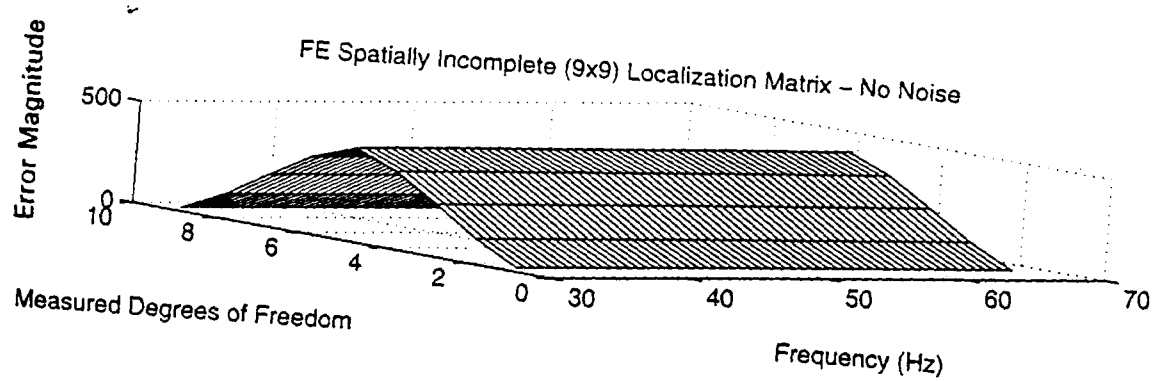4

2

0

Measured Degrees of Freedom

Frequency (Hz)

**Figure 4-9**  FE noise simulation, 5% EI reduction (mdof 5),
various noise conditions, 30-68 Hz.

38

FE Spatially Incomplete (9x9) Localization Matrix – No Noise



FE Spatially Incomplete (9x9) Localization Matrix – 1% Noise



FE Spatially Incomplete (9x9) Localization Matrix – 2% Noise



FE Spatially Incomplete (9x9) Localization Matrix – 5% Noise



**Figure 4-10**  FE noise simulation, 5% EI reduction (mdof 5), various noise conditions, 82-133 Hz.

FE Spatially Incomplete (9x9) Localization Matrix – No Noise

FE Spatially Incomplete (9x9) Localization Matrix – 1% Noise

FE Spatially Incomplete (9x9) Localization Matrix – 2% Noise

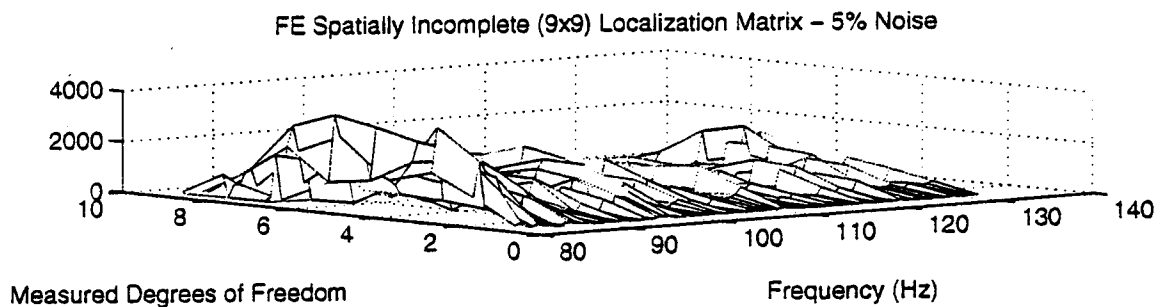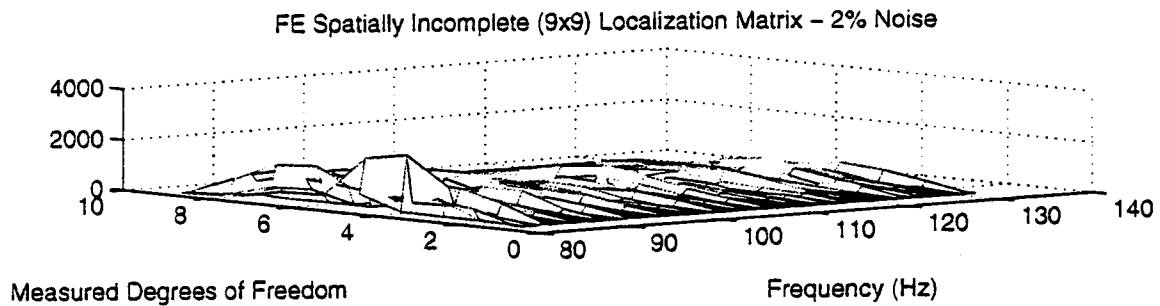FE Spatially Incomplete (9x9) Localization Matrix – 5% Noise

**Figure 4-11** FE noise simulation, 5% EI reduction (mdof 5), various noise conditions, 158-233 Hz.

FE Spatially Incomplete (9x9) Localization Matrix – No Noise

FE Spatially Incomplete (9x9) Localization Matrix – 1% Noise

FE Spatially Incomplete (9x9) Localization Matrix – 2% Noise

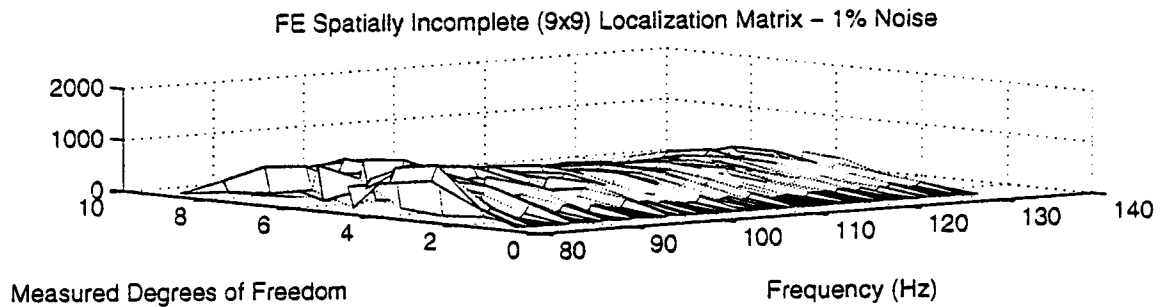FE Spatially Incomplete (9x9) Localization Matrix – 5% Noise

**Figure 4-12**  FE noise simulation, 5% rho reduction (mdof 5), various noise conditions, 20-26 Hz.
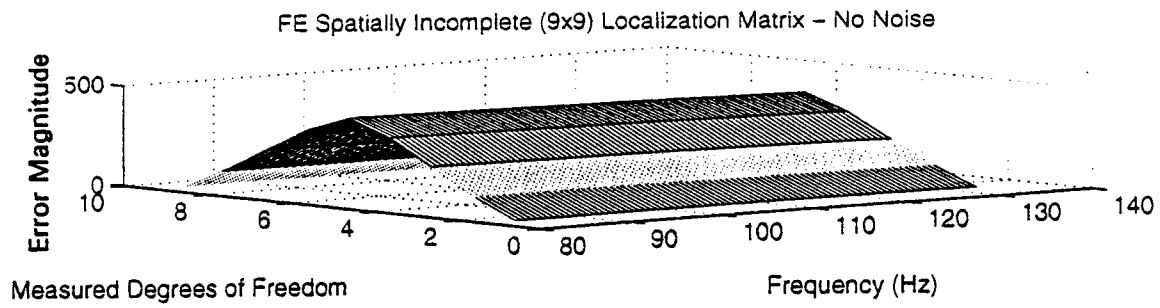
41

FE Spatially Incomplete (9x9) Localization Matrix – No Noise

FE Spatially Incomplete (9x9) Localization Matrix – 1% Noise

FE Spatially Incomplete (9x9) Localization Matrix – 2% Noise

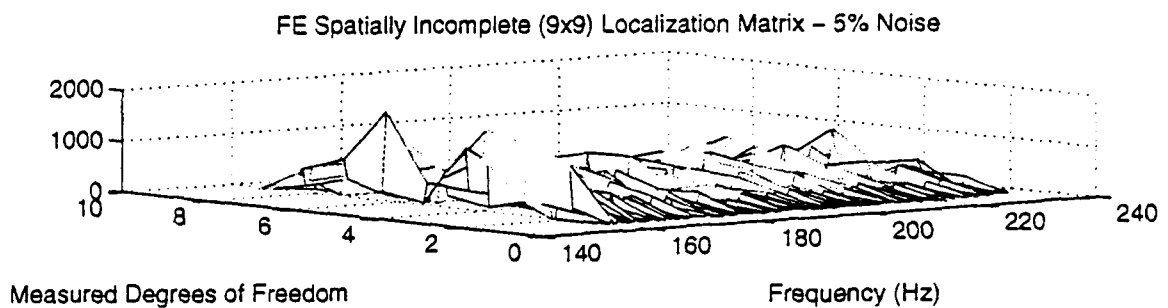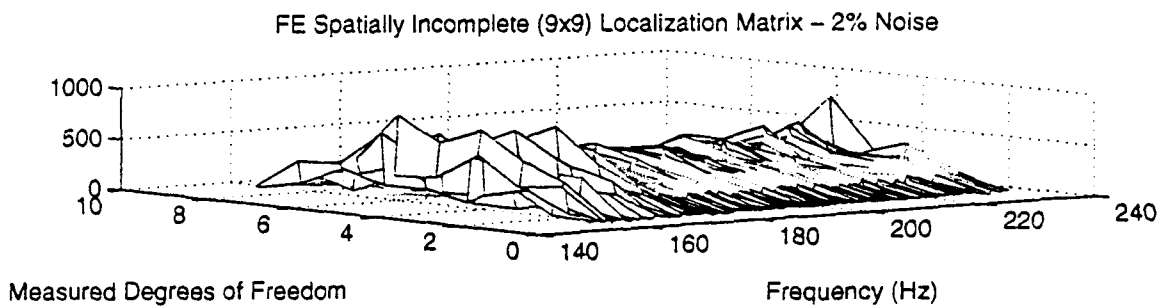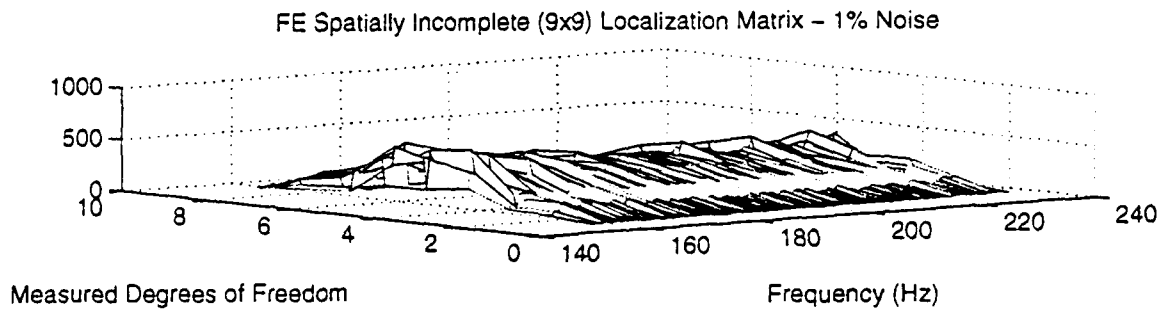FE Spatially Incomplete (9x9) Localization Matrix – 5% Noise

**Figure 4-13** FE noise simulation, 5% rho reduction (mdof 5), various noise conditions, 30-68 Hz.

FE Spatially Incomplete (9x9) Localization Matrix – No Noise

FE Spatially Incomplete (9x9) Localization Matrix – 1% Noise

FE Spatially Incomplete (9x9) Localization Matrix – 2% Noise

FE Spatially Incomplete (9x9) Localization Matrix – 5% Noise

**Figure 4-14** FE noise simulation, 5% rho reduction (mdof 5), various noise conditions, 82-133 Hz.
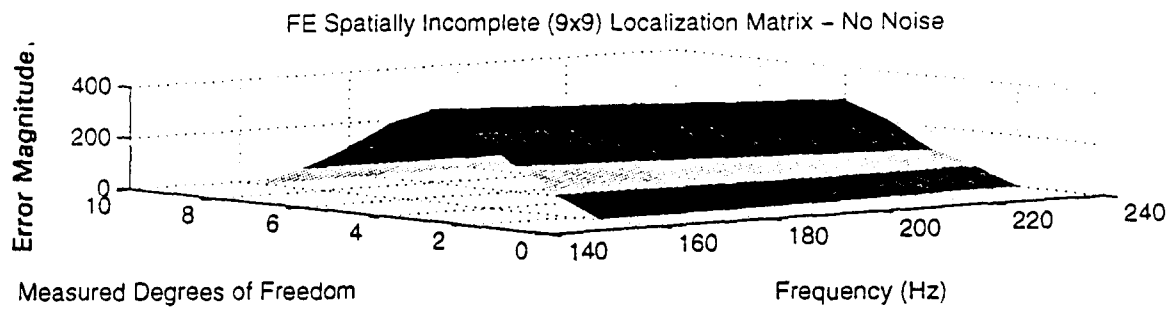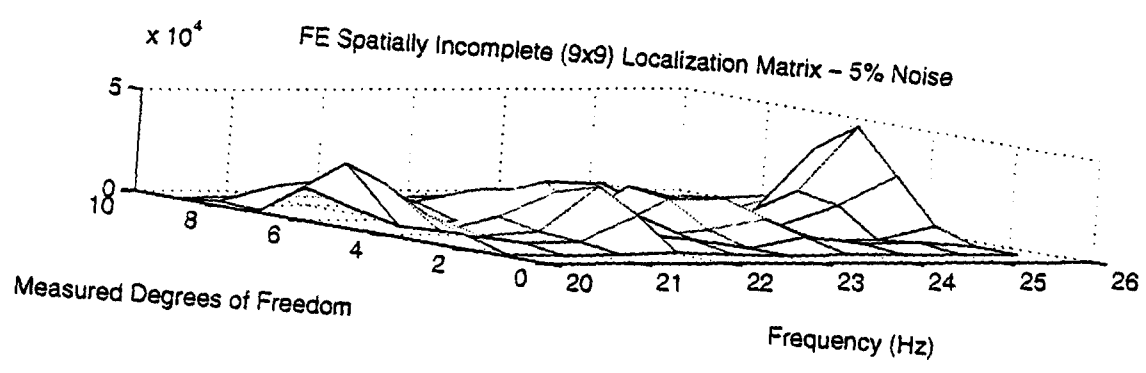
FE Spatially Incomplete (9x9) Localization Matrix – No Noise

FE Spatially Incomplete (9x9) Localization Matrix – 1% Noise

FE Spatially Incomplete (9x9) Localization Matrix – 2% Noise

FE Spatially Incomplete (9x9) Localization Matrix – 5% Noise

**Figure 4-15** FE noise simulation, 5% rho reduction (mdof 5), various noise conditions, 158-233 Hz.
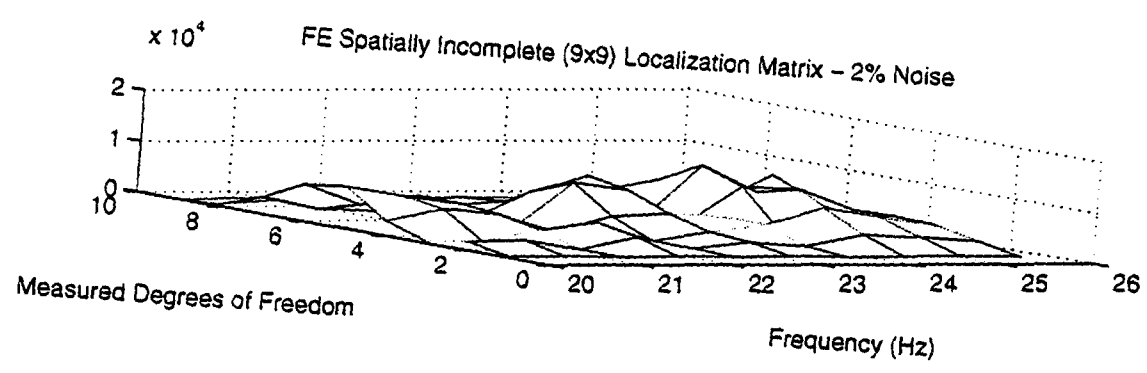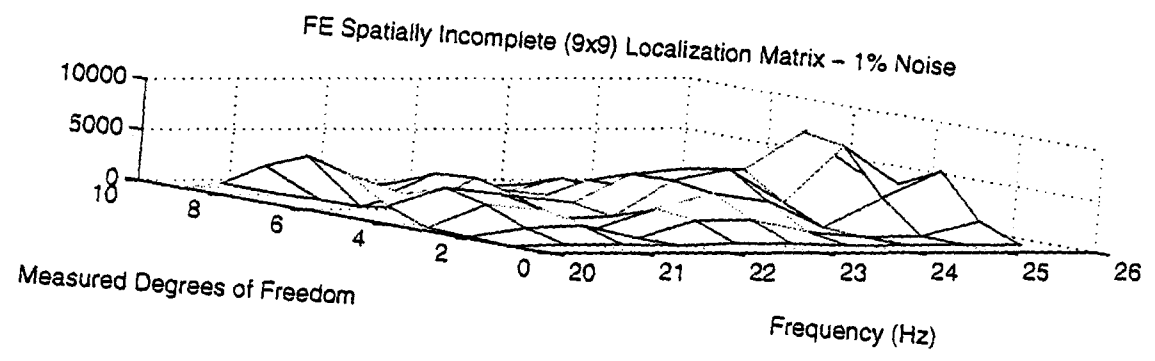
**Figure 4-16**   FE noise simulation, 10% EI reduction (mdof 5), various noise conditions, 20-26 Hz.

**Figure 4-17** FE noise simulation, 10% EI reduction (mdof 5), various noise conditions, 30-68 Hz.

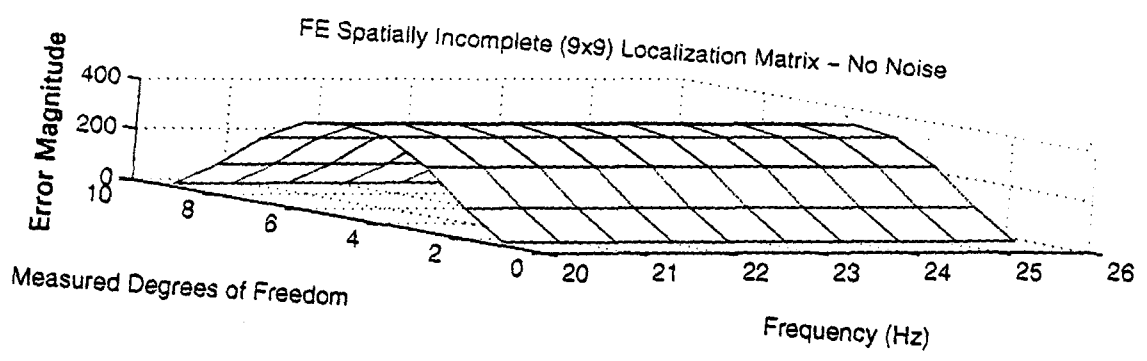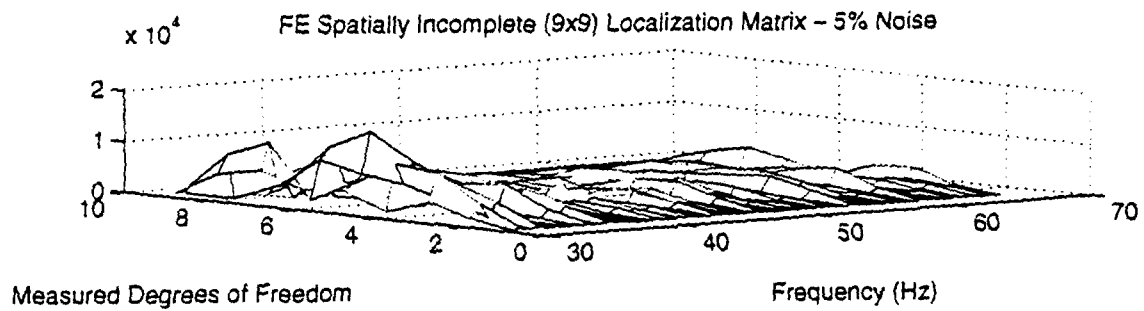**Figure 4-18**  FE noise simulation, 10% EI reduction (mdof 5), various noise conditions, 82-133 Hz.

47

FE Spatially Incomplete (9x9) Localization Matrix – No Noise

FE Spatially Incomplete (9x9) Localization Matrix – 1% Noise

FE Spatially Incomplete (9x9) Localization Matrix – 2% Noise

FE Spatially Incomplete (9x9) Localization Matrix – 5% Noise

**Figure 4-19** FE noise simulation, 10% EI reduction (mdof 5), various noise conditions, 158-233 Hz.

**Figure 4-20** FE noise simulation, 10% rho reduction (mdof 5), various noise conditions, 20-26 Hz.
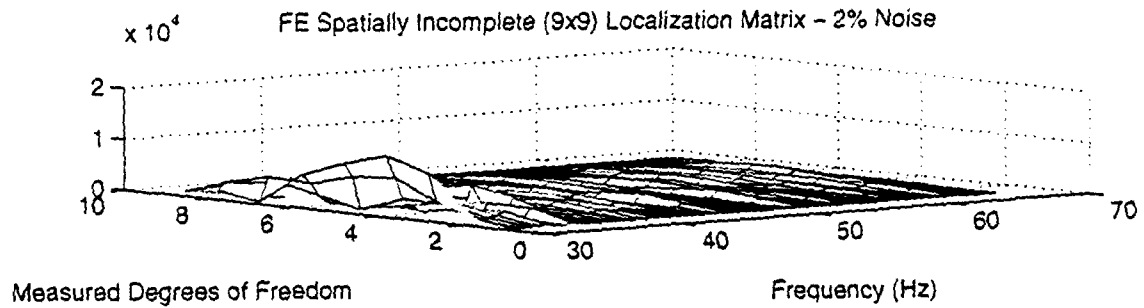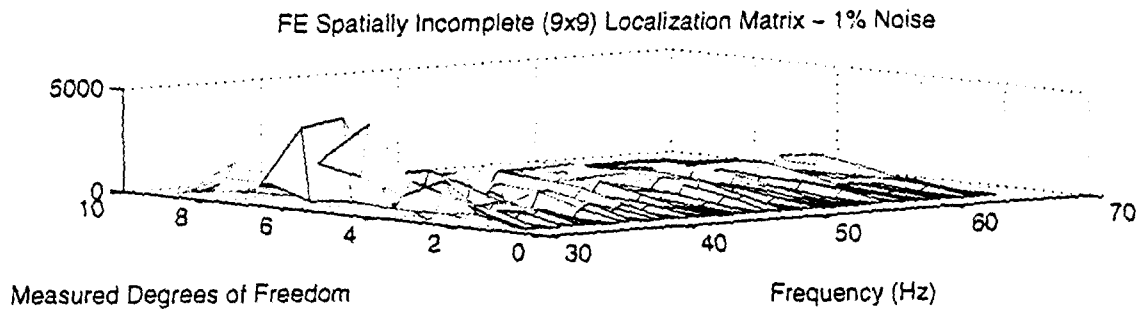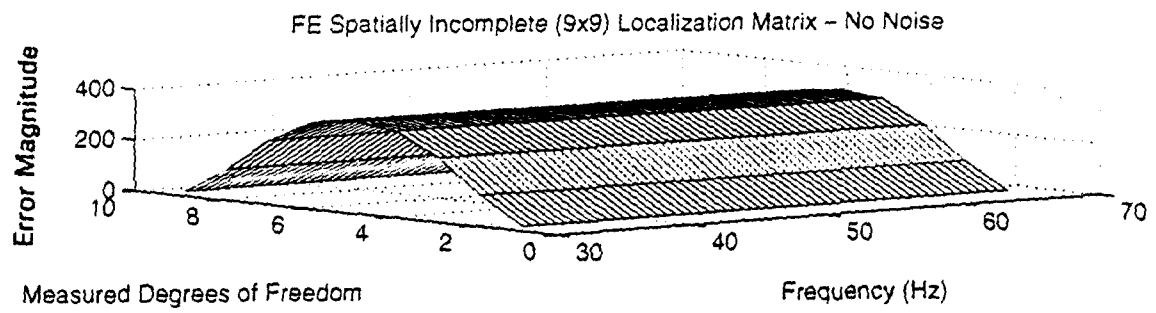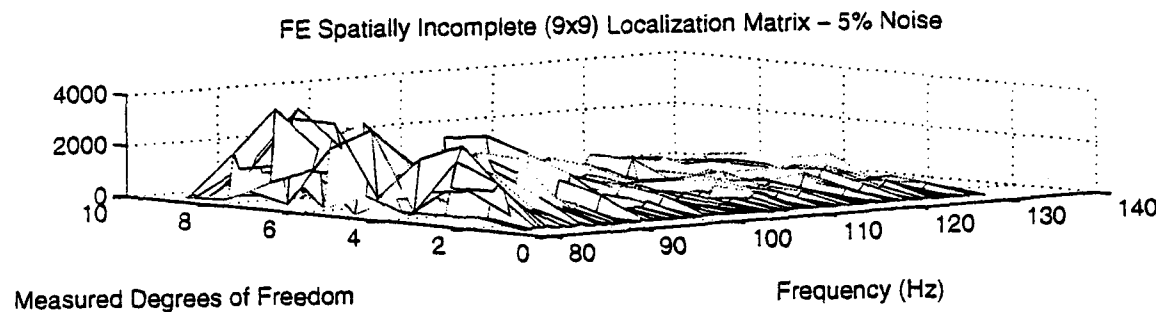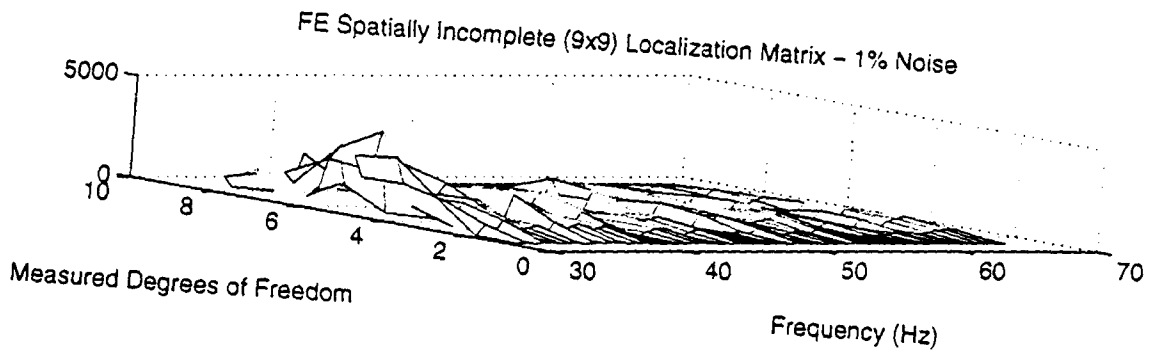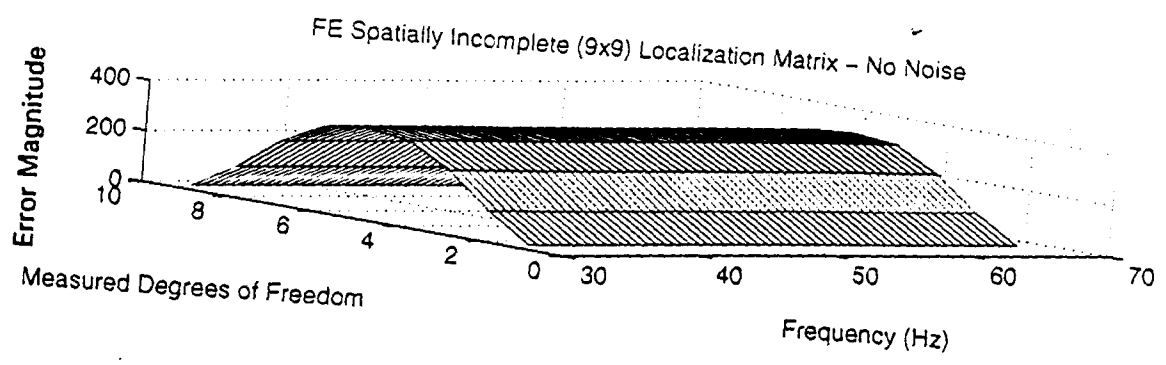
**Figure 4-21** FE noise simulation, 10% rho reduction (mdof 5), various noise conditions, 30-68 Hz.

FE Spatially Incomplete (9x9) Localization Matrix – No Noise

FE Spatially Incomplete (9x9) Localization Matrix – 1% Noise

FE Spatially Incomplete (9x9) Localization Matrix – 2% Noise

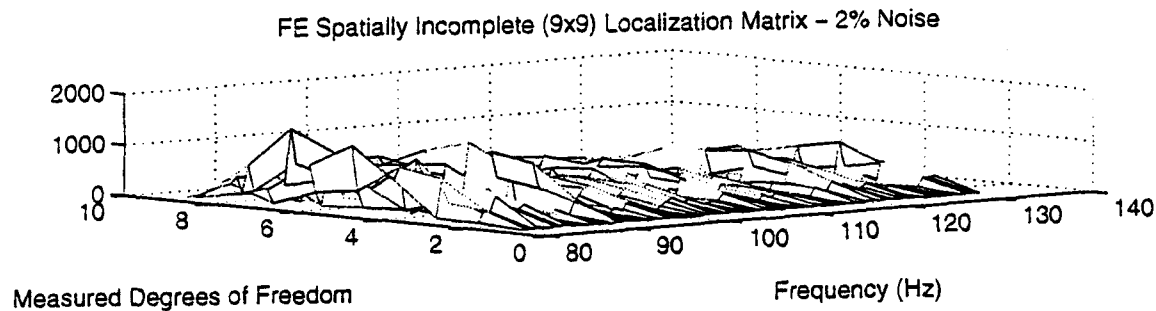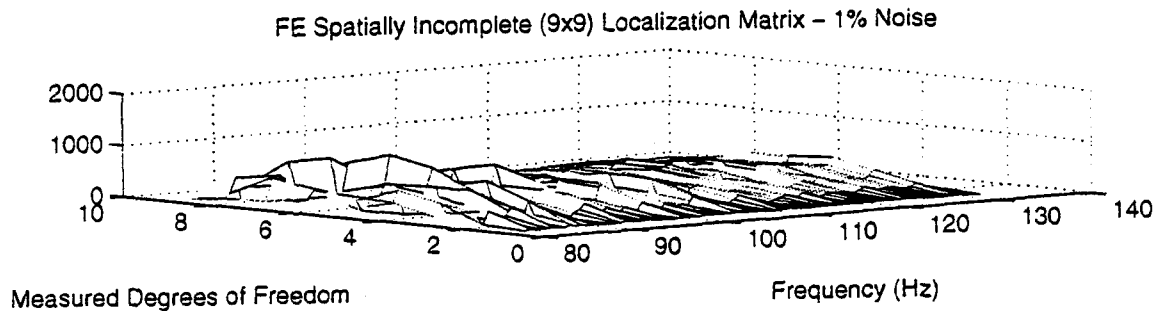FE Spatially Incomplete (9x9) Localization Matrix – 5% Noise
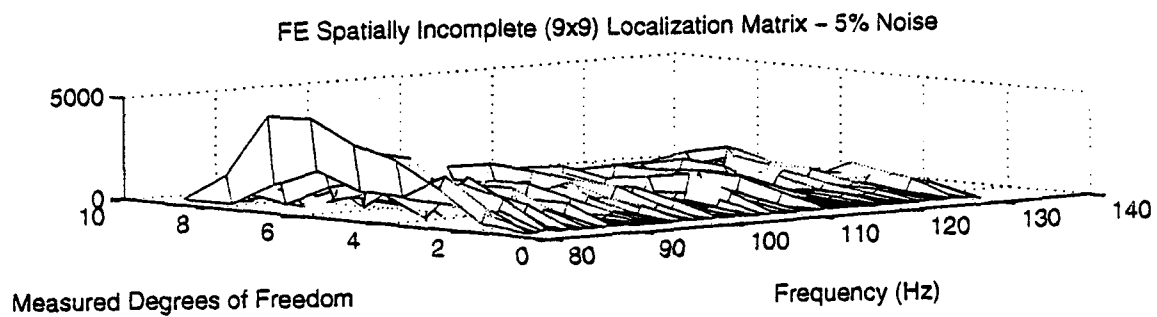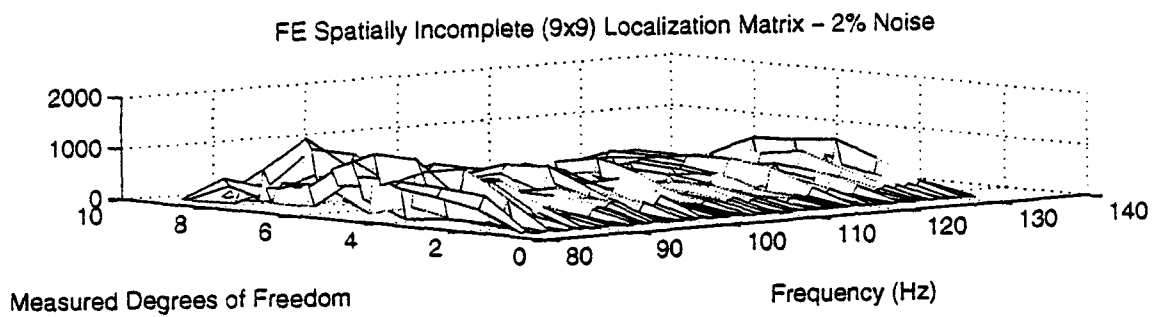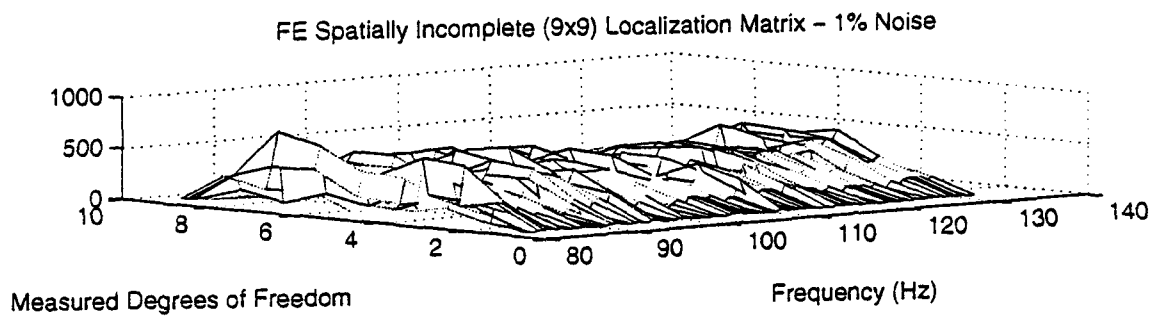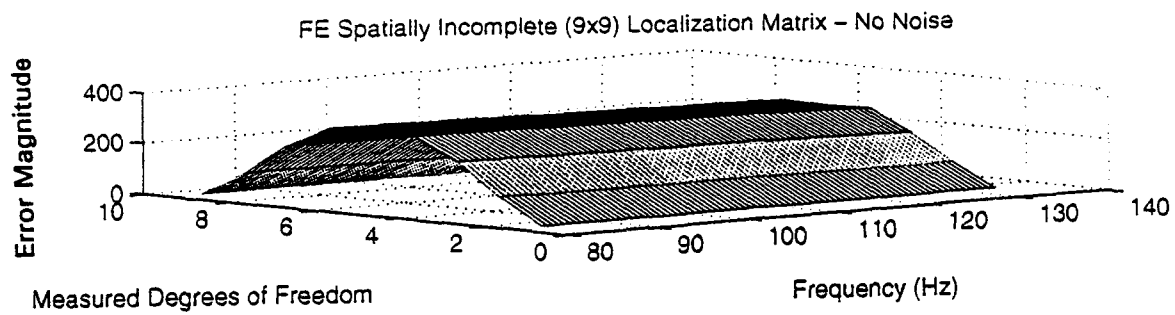
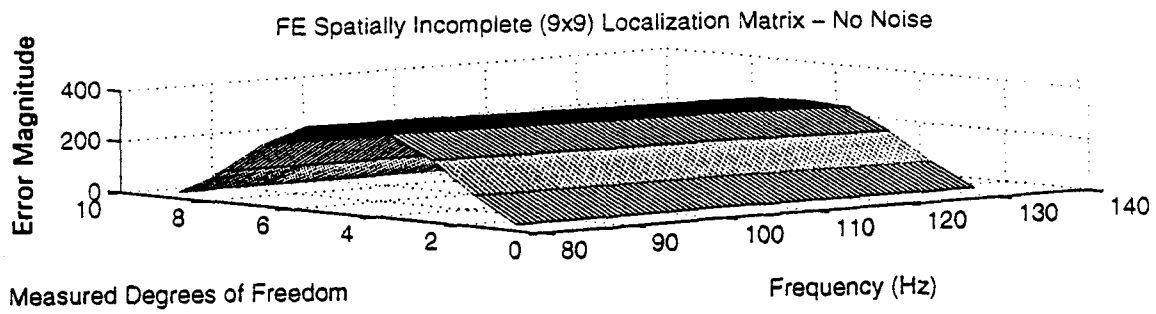**Figure 4-22** FE noise simulation, 10% rho reduction (mdof 5), various noise conditions, 82-133 Hz.

FE Spatially Incomplete (9x9) Localization Matrix – No Noise



FE Spatially Incomplete (9x9) Localization Matrix – 1% Noise



FE Spatially Incomplete (9x9) Localization Matrix – 2% Noise



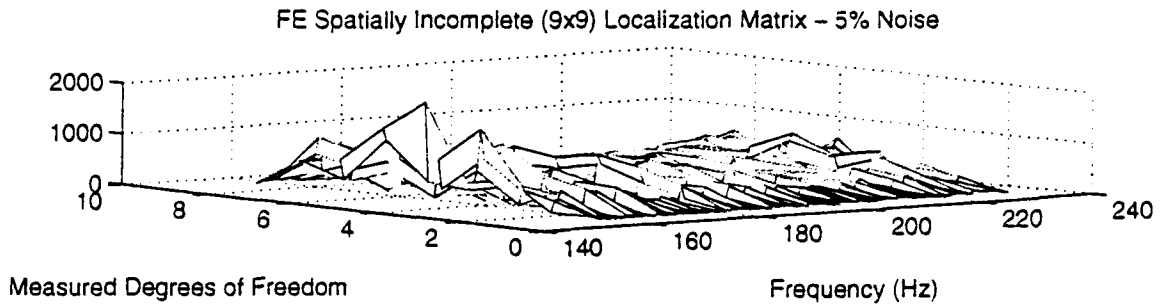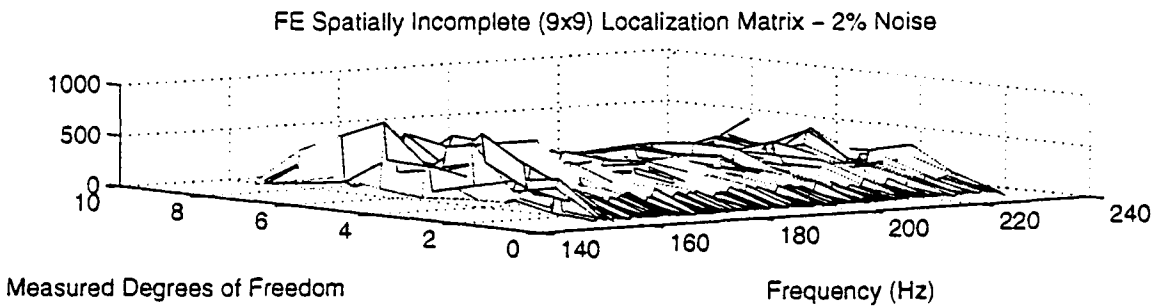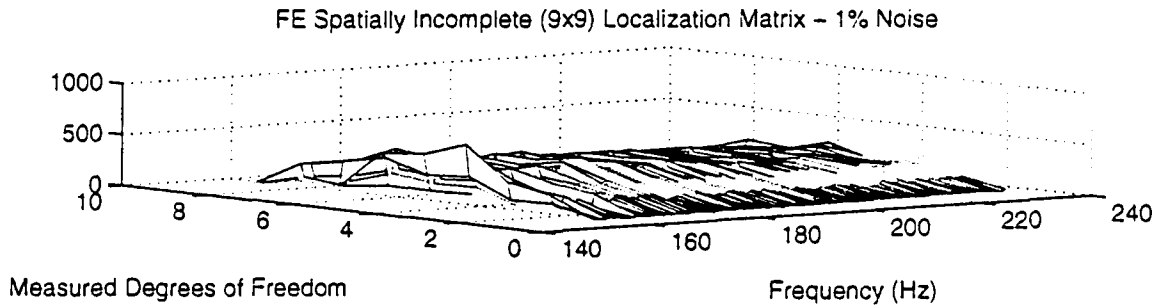FE Spatially Incomplete (9x9) Localization Matrix – 5% Noise
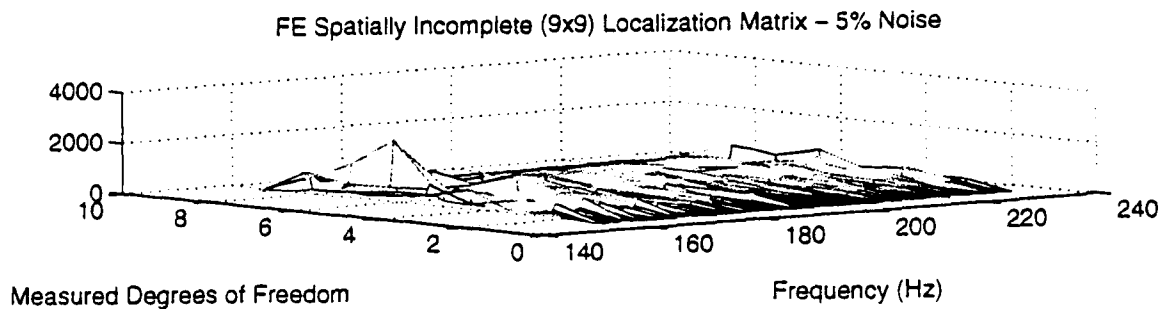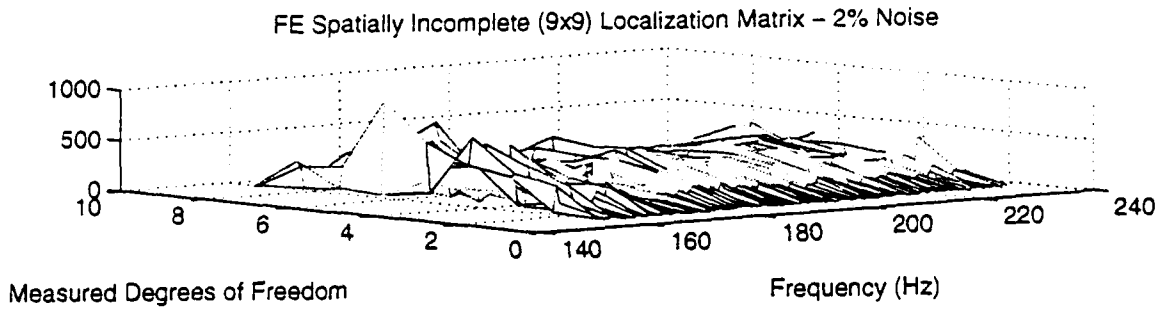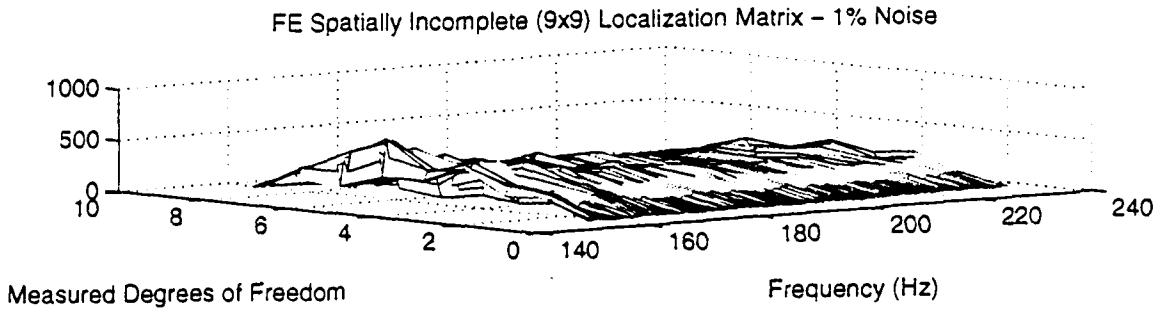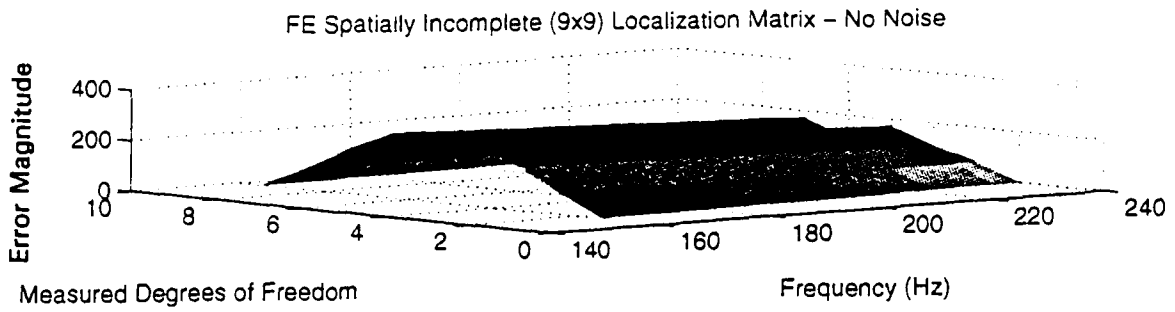
**Figure 4-23** FE noise simulation, 10% rho reduction (mdof 5), various noise conditions, 158-233 Hz.

52

FE Spatially Incomplete (9x9) Localization Matrix – No Noise

FE Spatially Incomplete (9x9) Localization Matrix – 1% Noise

FE Spatially Incomplete (9x9) Localization Matrix – 2% Noise

FE Spatially Incomplete (9x9) Localization Matrix – 5% Noise
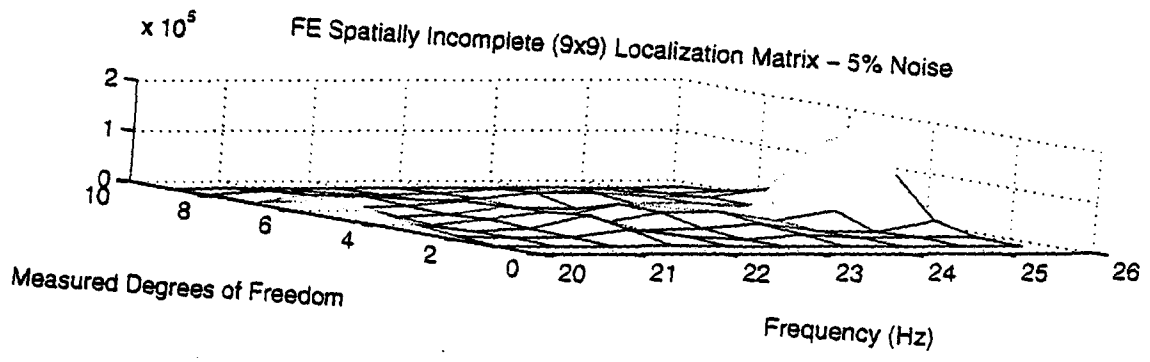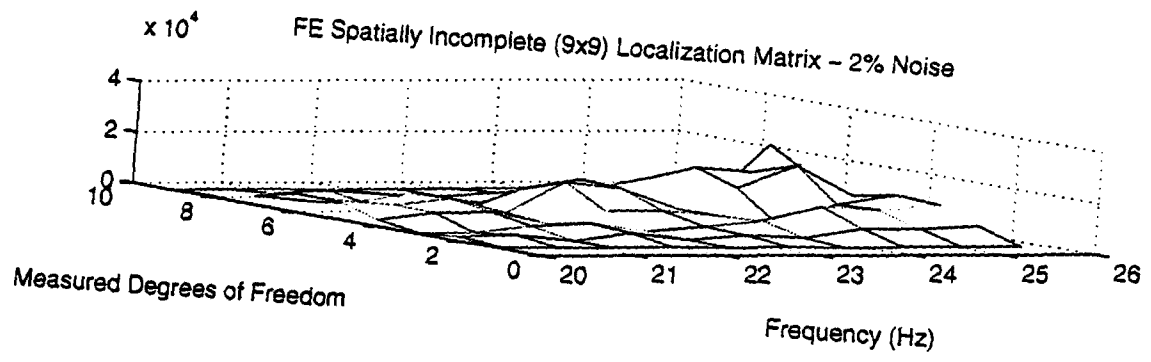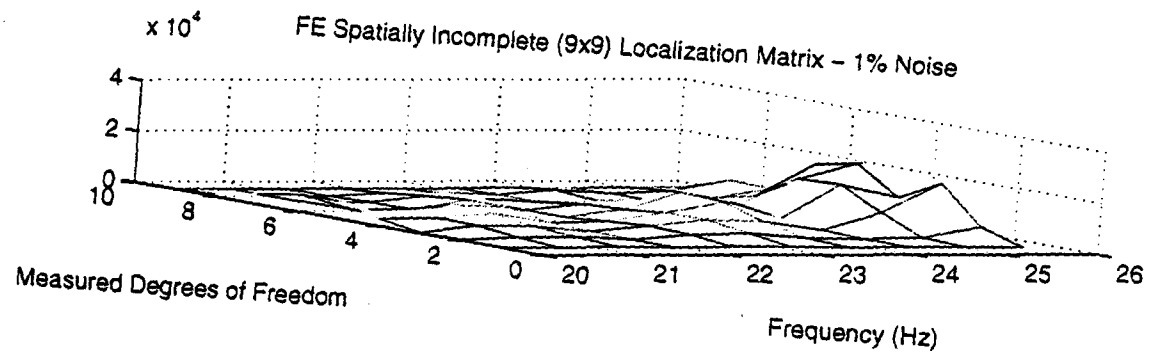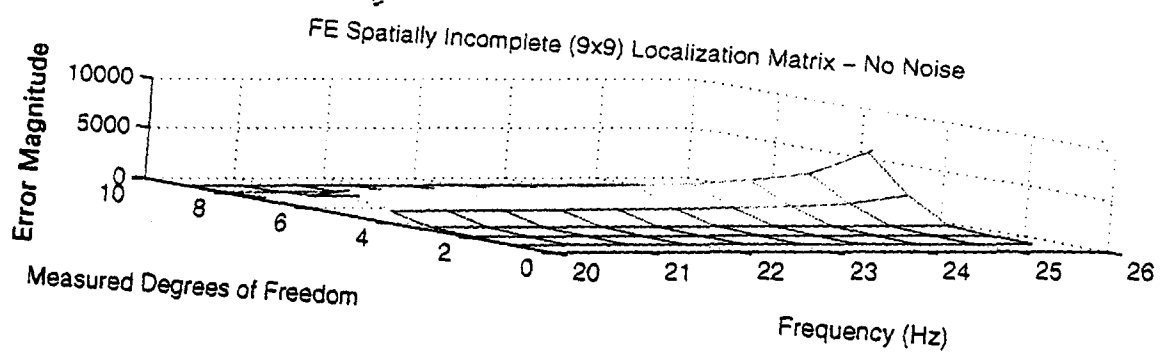
**Figure 4-24**  FE noise simulation, 50% EI reduction (mdof 5), various noise conditions, 20-26 Hz.

53

FE Spatially Incomplete (9x9) Localization Matrix – No Noise

FE Spatially Incomplete (9x9) Localization Matrix – 1% Noise

FE Spatially Incomplete (9x9) Localization Matrix – 2% Noise

FE Spatially Incomplete (9x9) Localization Matrix – 5% Noise
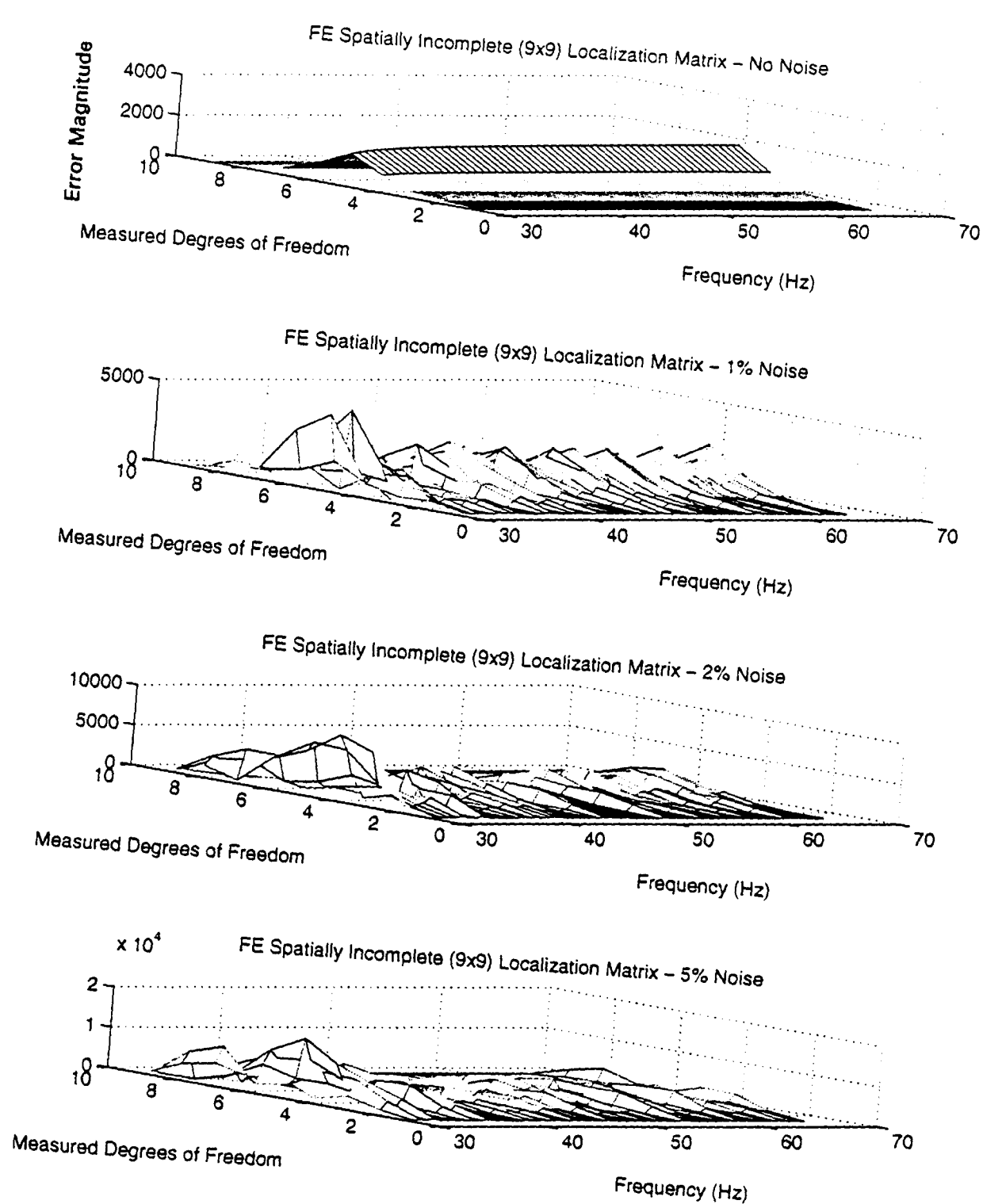
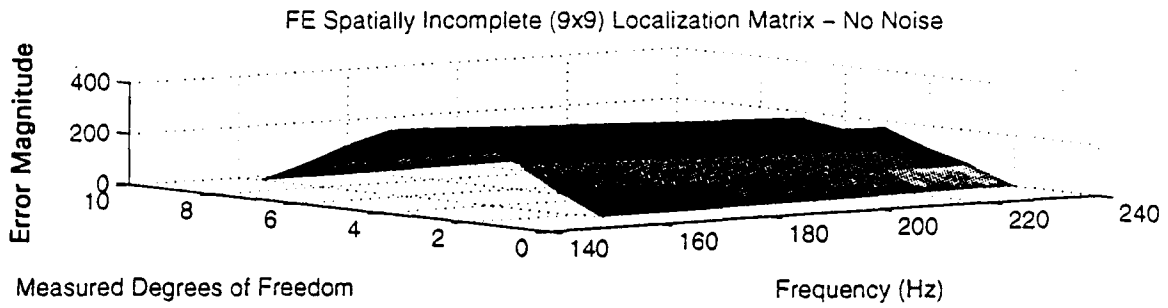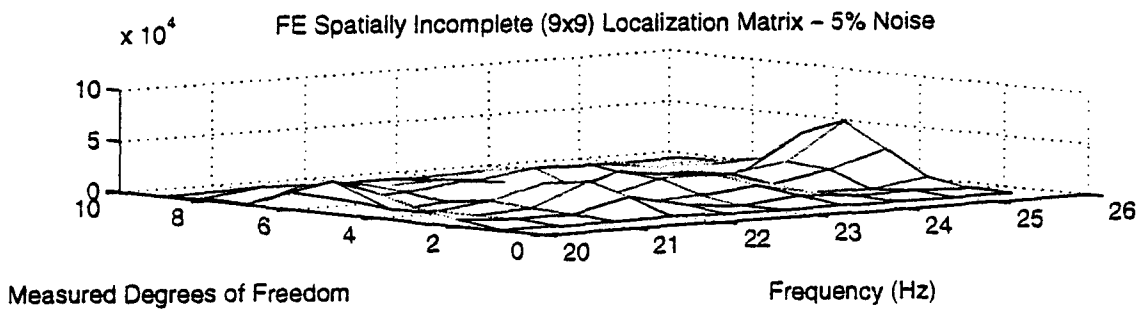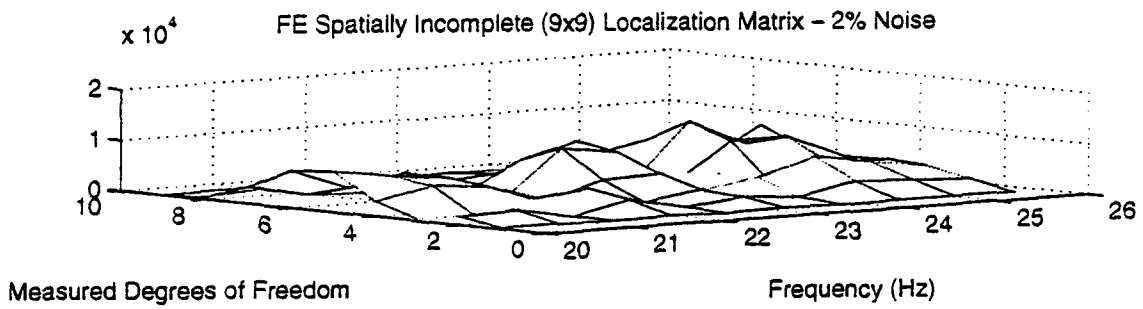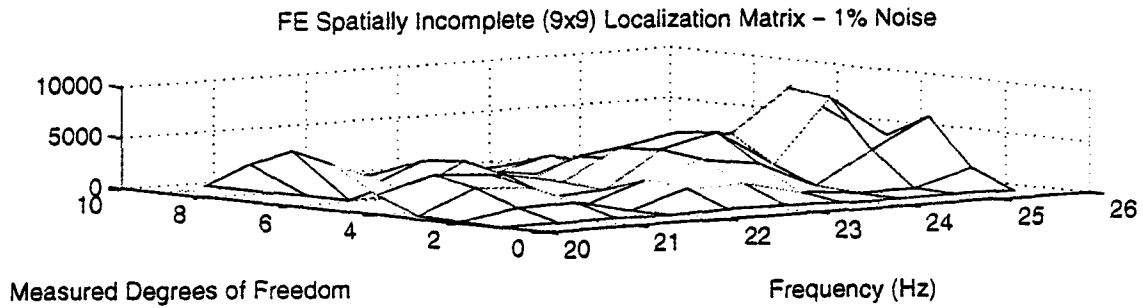**Figure 4-25** FE noise simulation, 50% EI reduction (mdof 5), various noise conditions, 30-68 Hz.

54
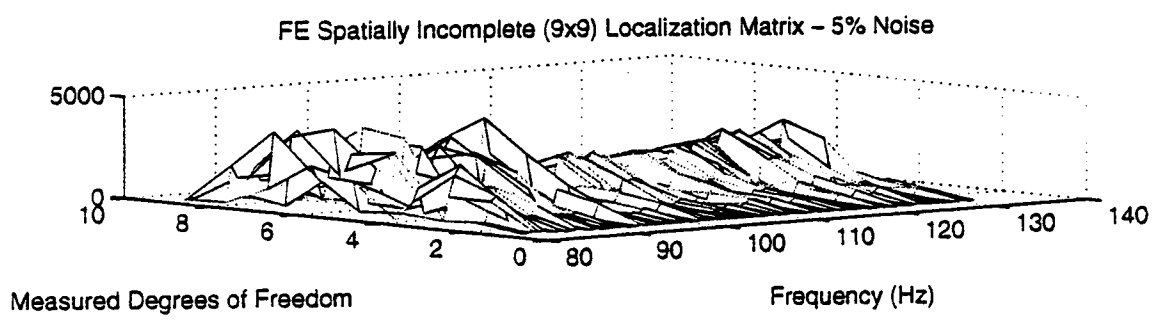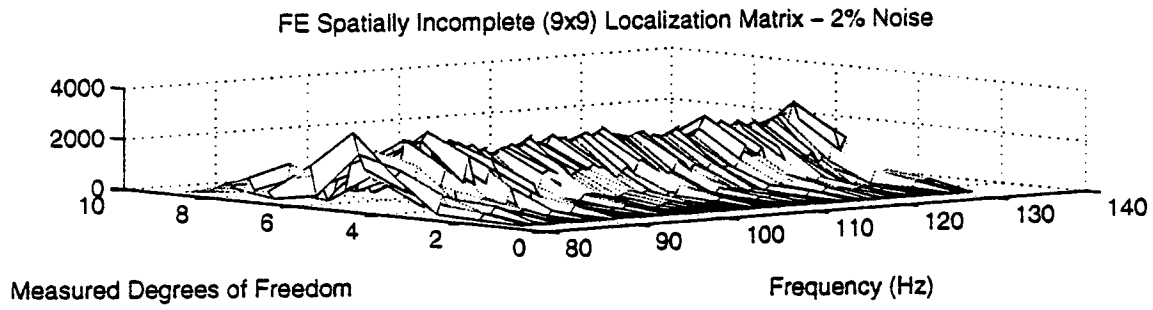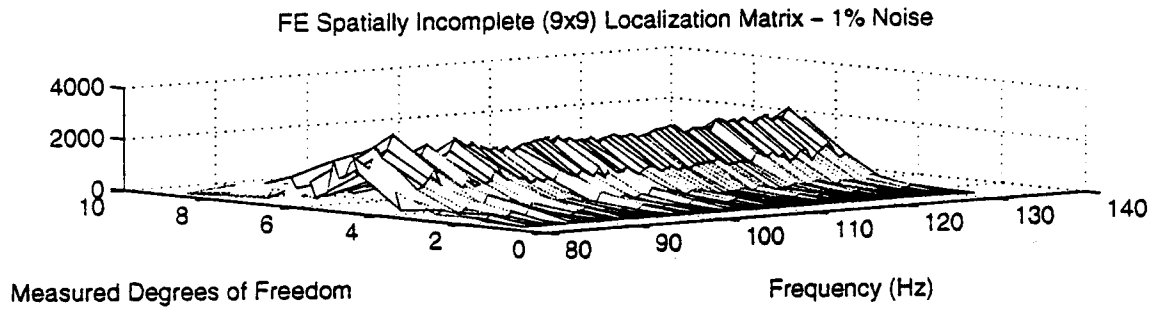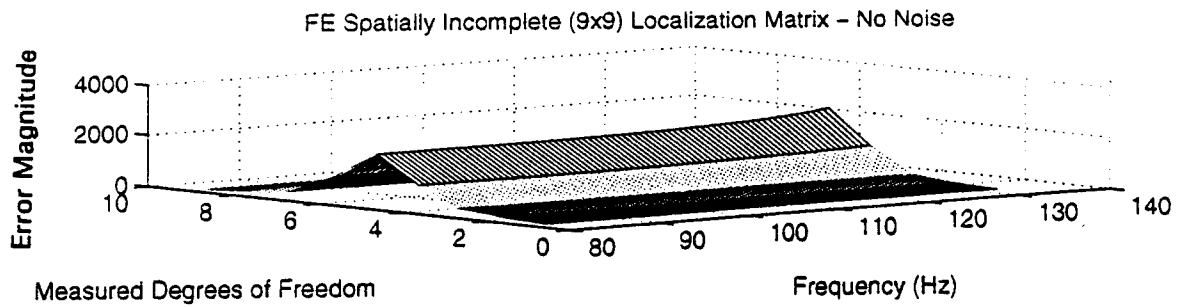
**Figure 4-26** FE noise simulation, 50% EI reduction (mdof 5), various noise conditions, 82-133 Hz.

55

FE Spatially Incomplete (9x9) Localization Matrix – No Noise

FE Spatially Incomplete (9x9) Localization Matrix – 1% Noise

FE Spatially Incomplete (9x9) Localization Matrix – 2% Noise

FE Spatially Incomplete (9x9) Localization Matrix – 5% Noise
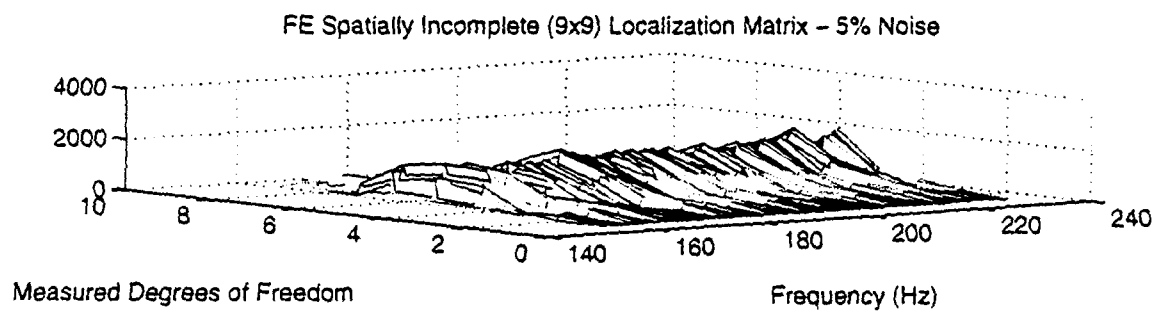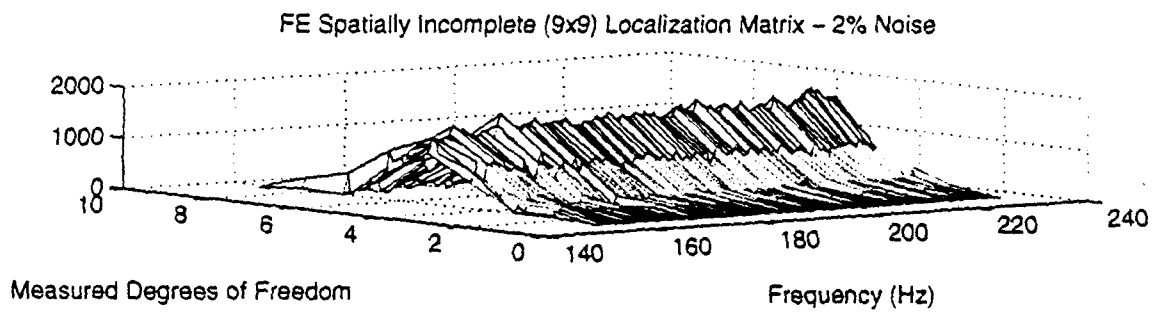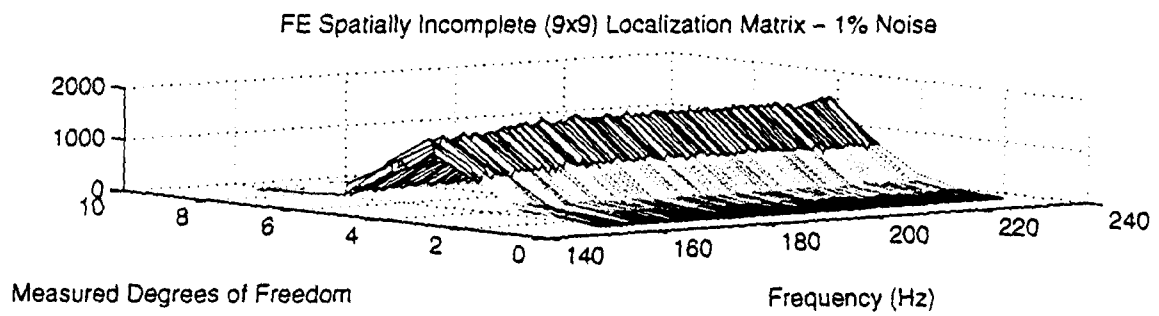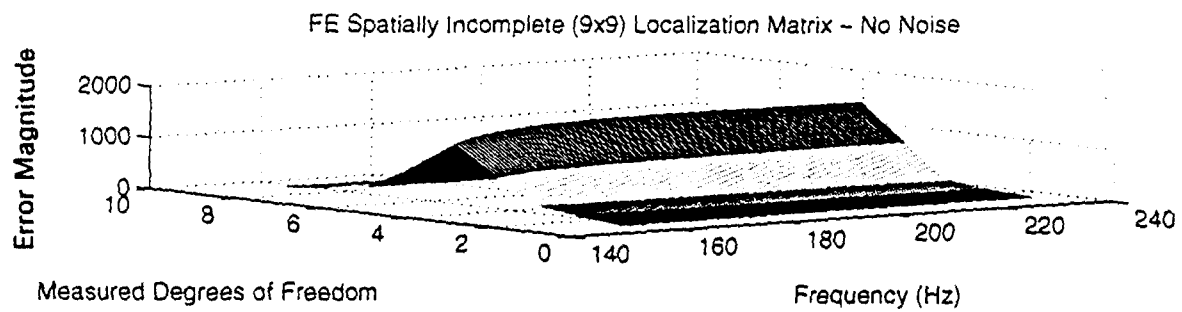
**Figure 4-27**  FE noise simulation, 50% EI reduction (mdof 5), various noise conditions, 158-233 Hz.
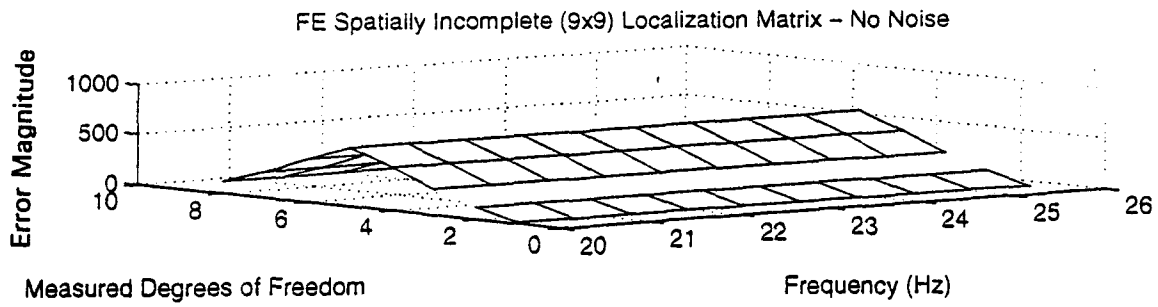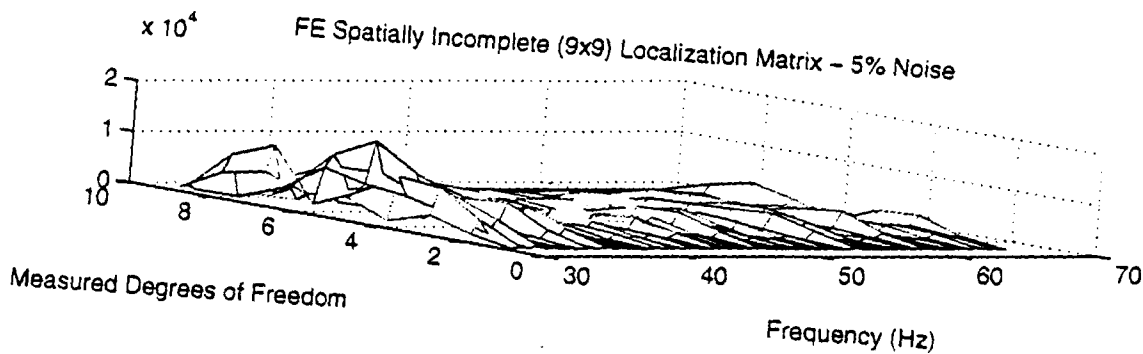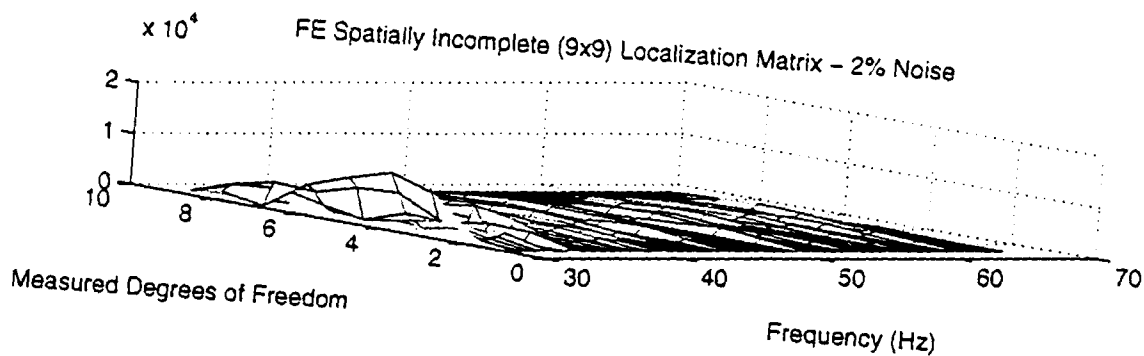
56
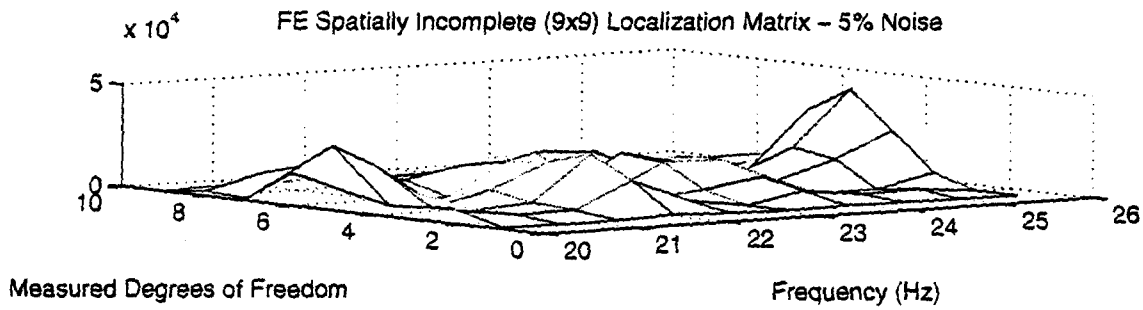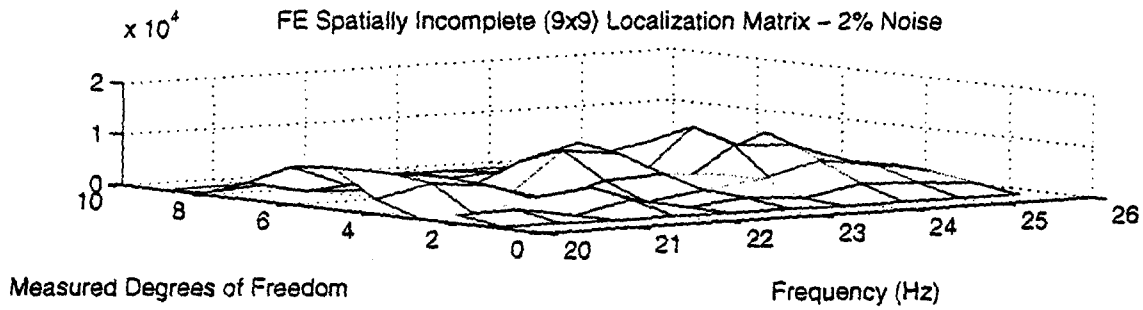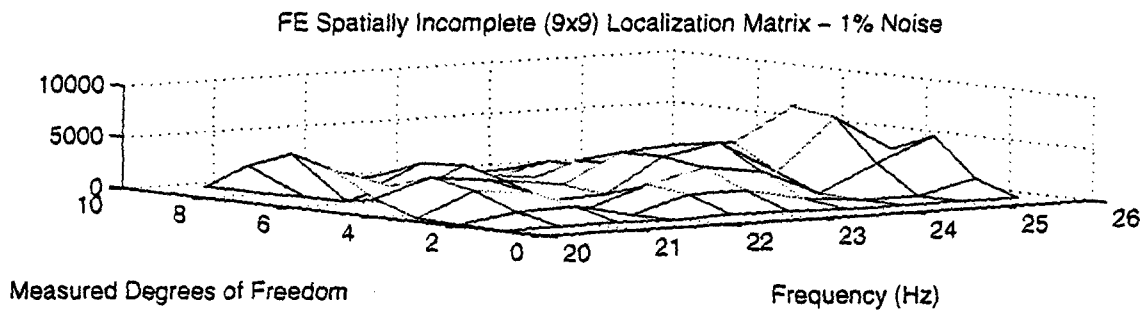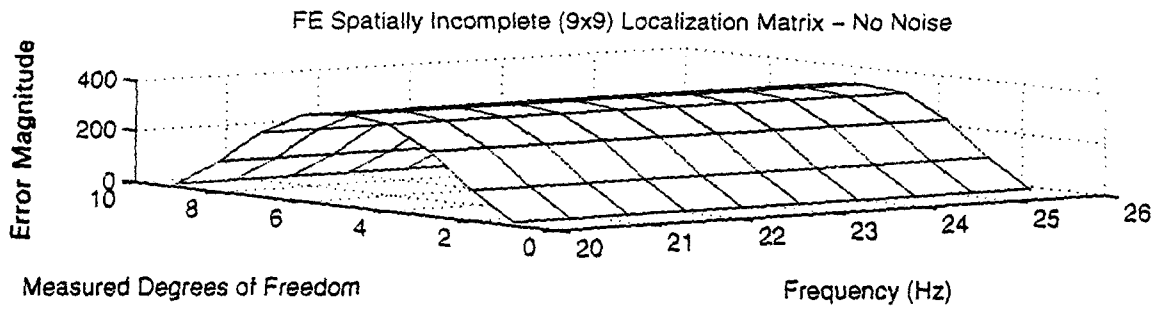
Figure 4-28 FE noise simulation, 50% rho reduction (mdof 5),
various noise conditions, 20-26 Hz.

57
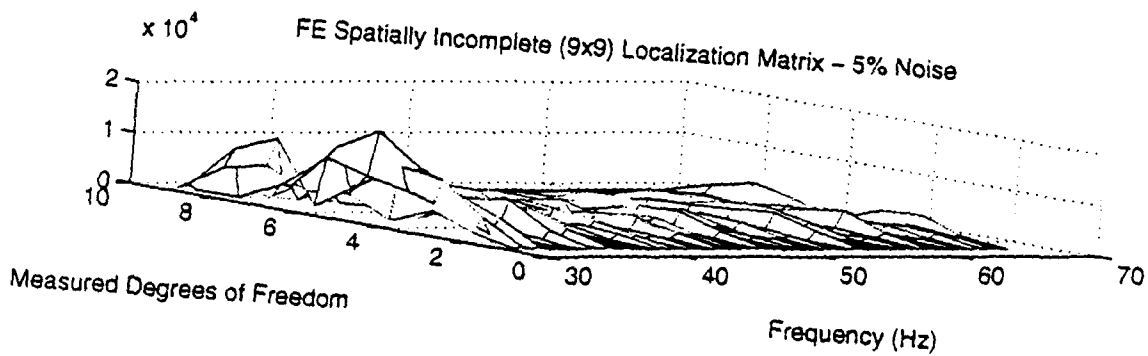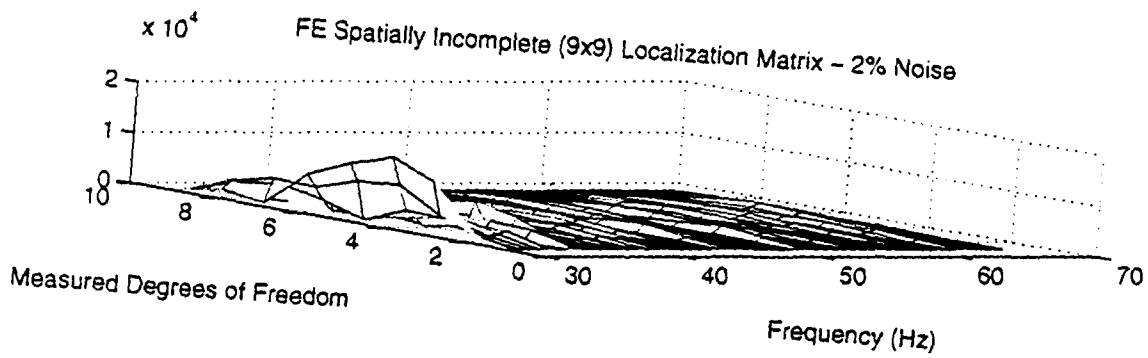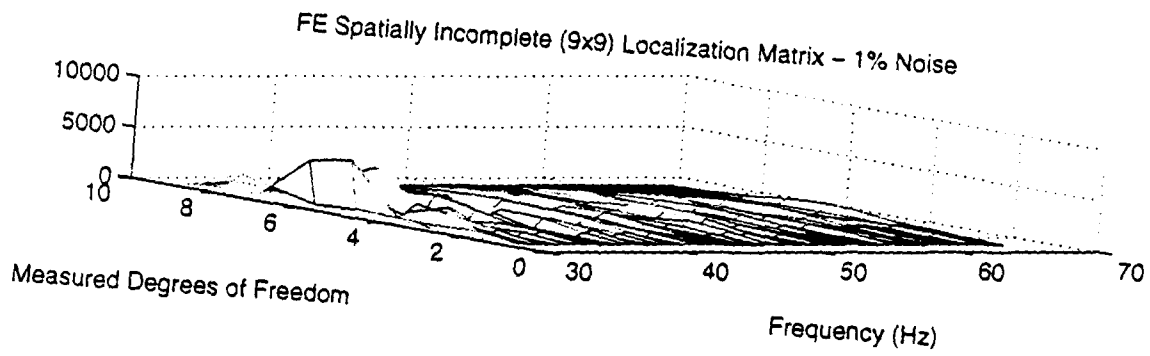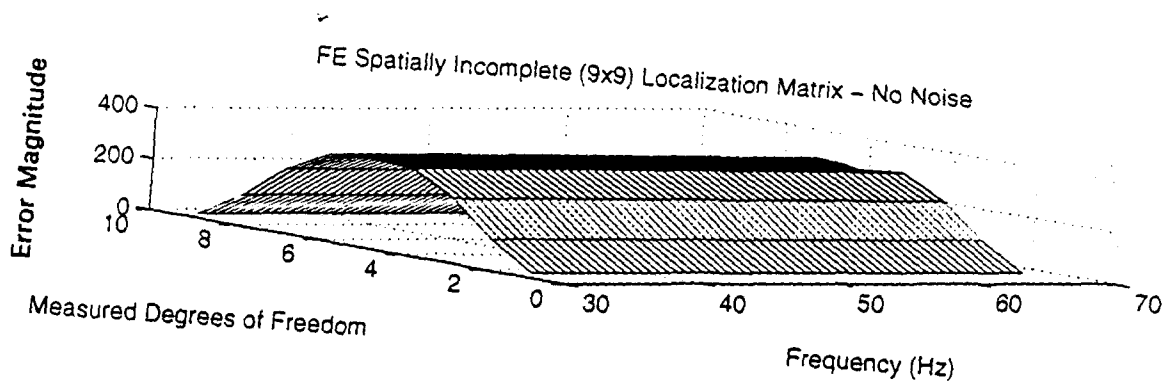
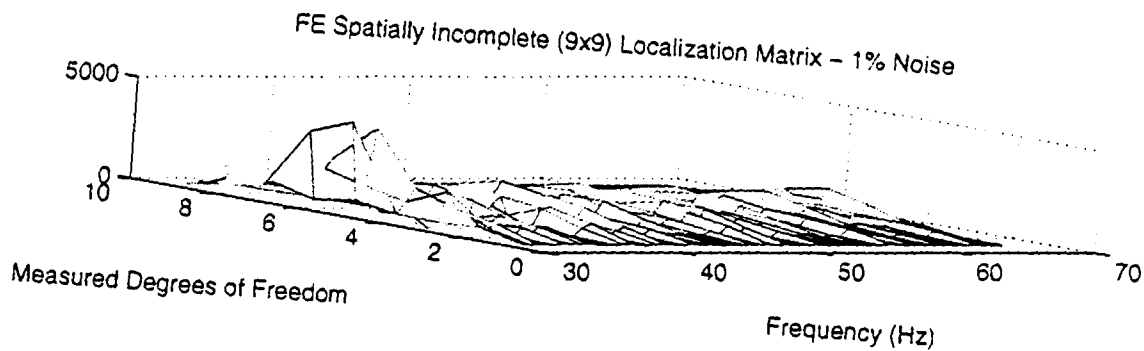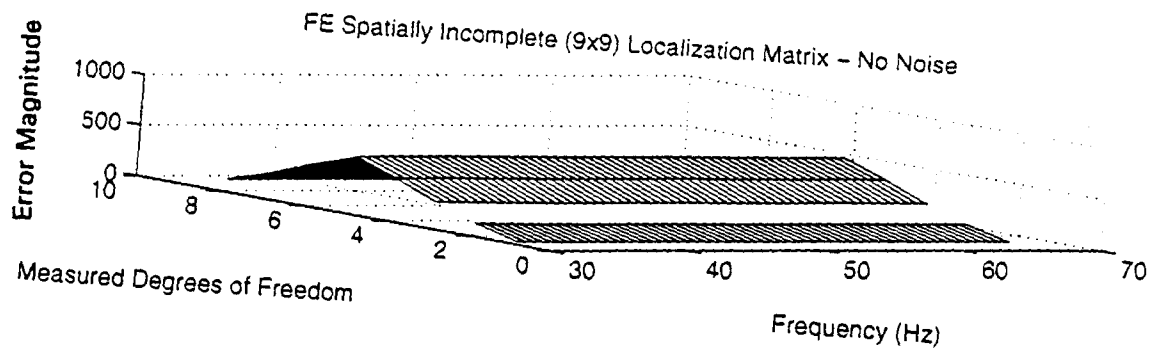**Figure 4-29** FE noise simulation, 50% rho reduction (mdof 5), various noise conditions, 30-68 Hz.
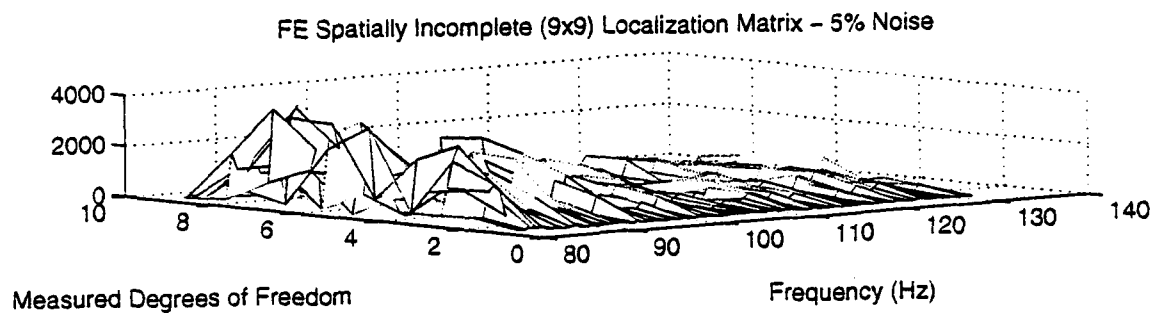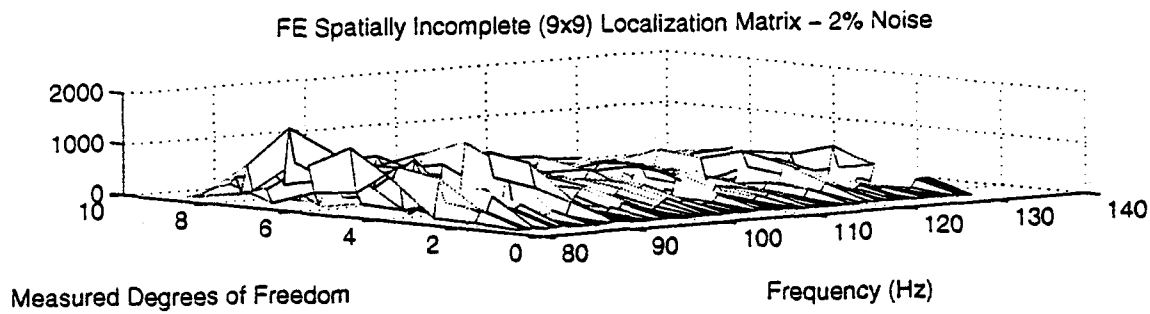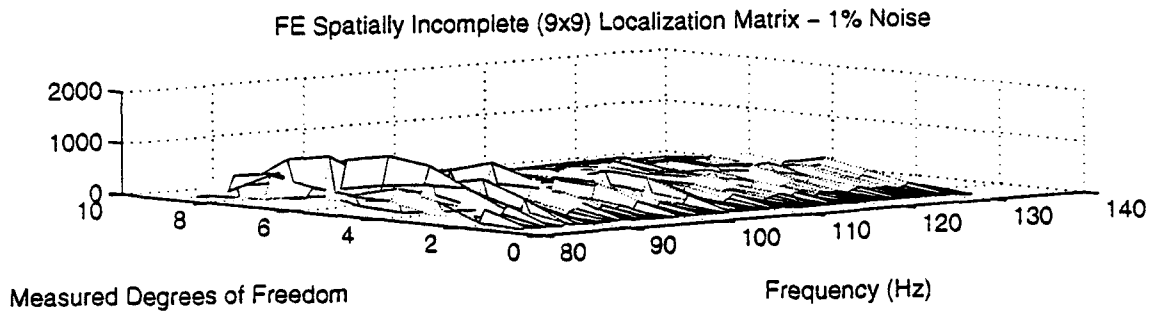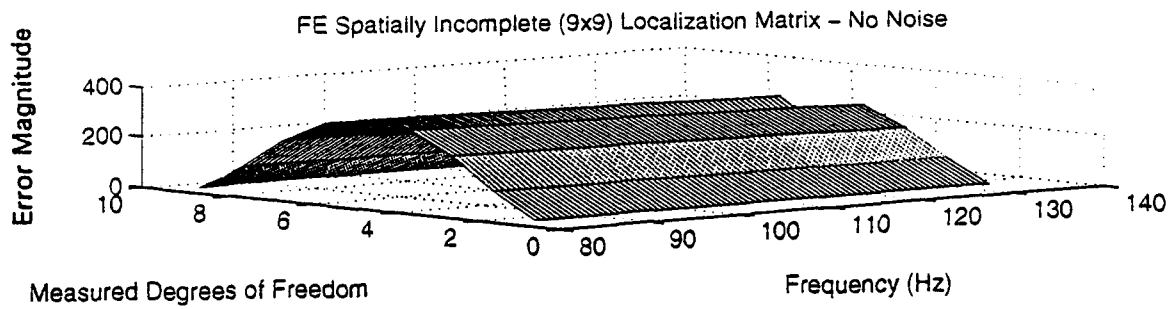
**Figure 4-30** FE noise simulation, 50% rho reduction (mdof 5), various noise conditions, 82-133 Hz.

FE Spatially Incomplete (9x9) Localization Matrix – No Noise

Error Magnitude

Measured Degrees of Freedom

Frequency (Hz)

FE Spatially Incomplete (9x9) Localization Matrix – 1% Noise

Measured Degrees of Freedom

Frequency (Hz)

FE Spatially Incomplete (9x9) Localization Matrix – 2% Noise

Measured Degrees of Freedom

Frequency (Hz)

FE Spatially Incomplete (9x9) Localization Matrix – 5% Noise
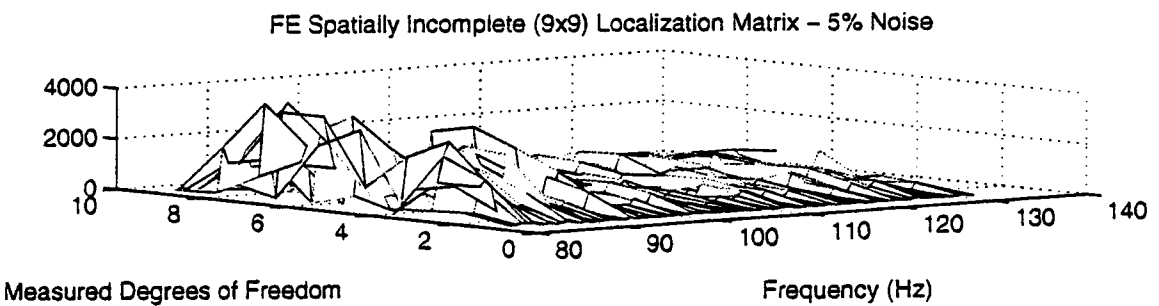
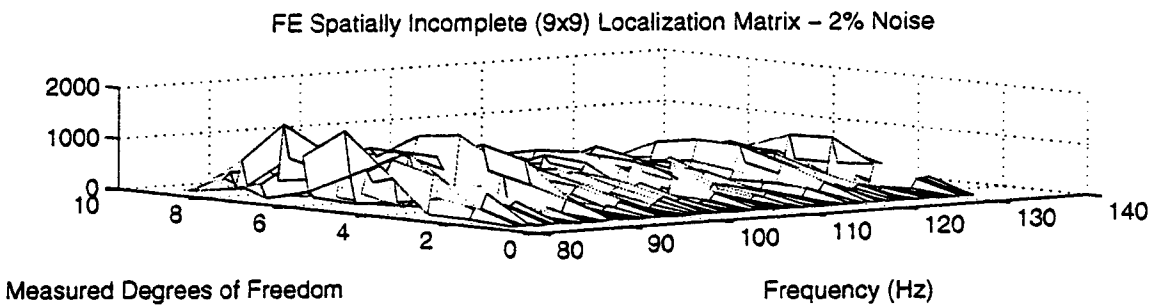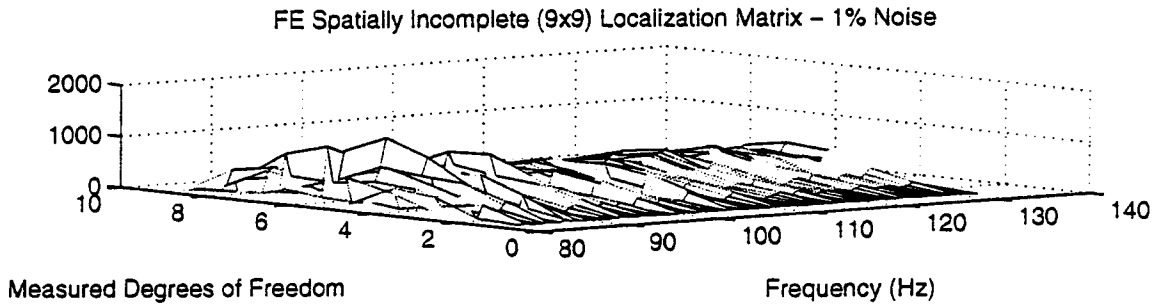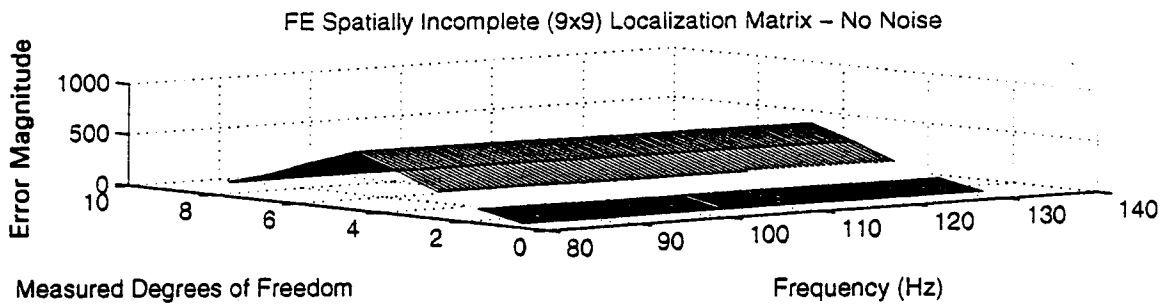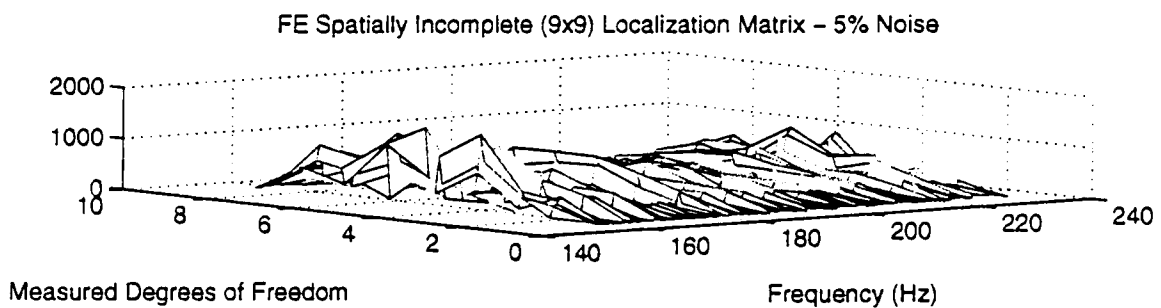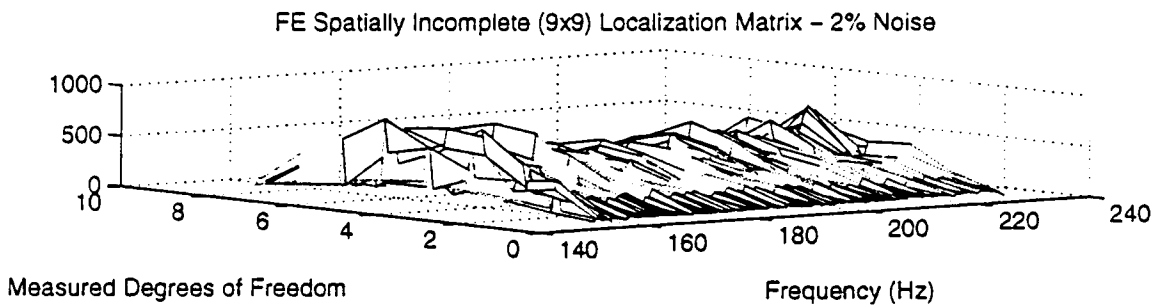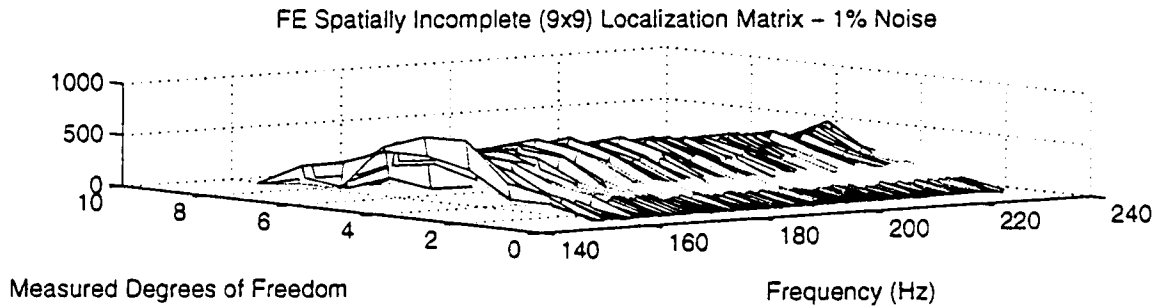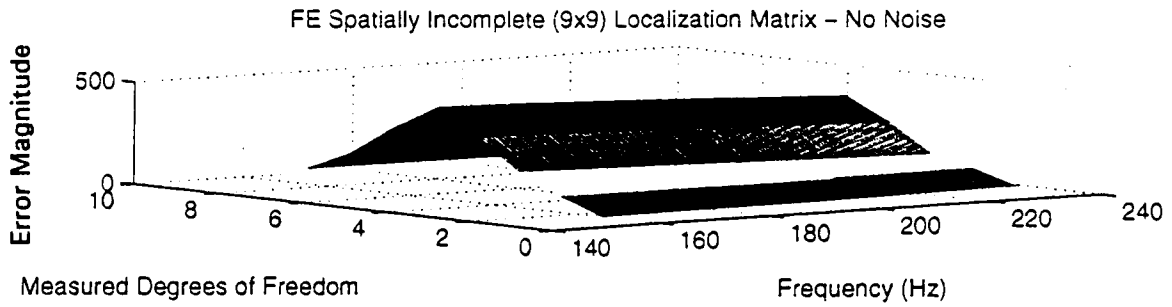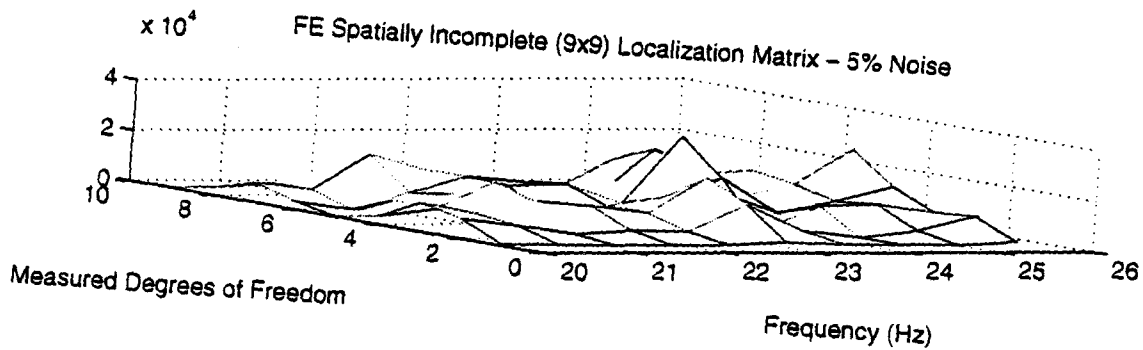Measured Degrees of Freedom

Frequency (Hz)

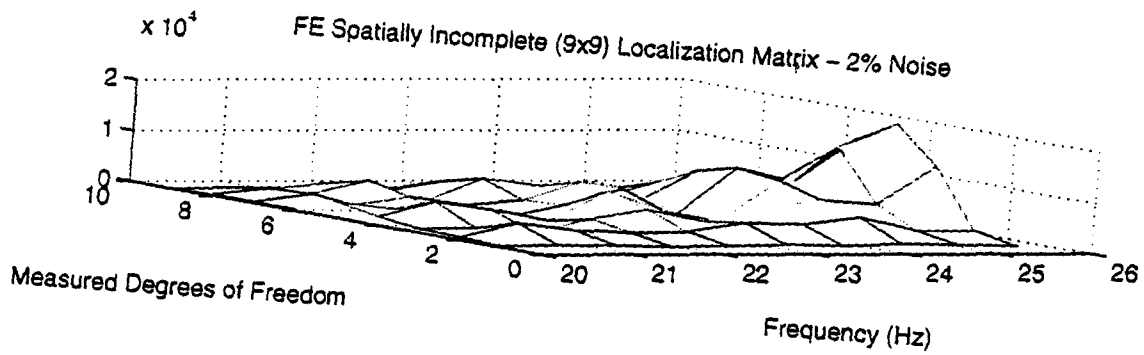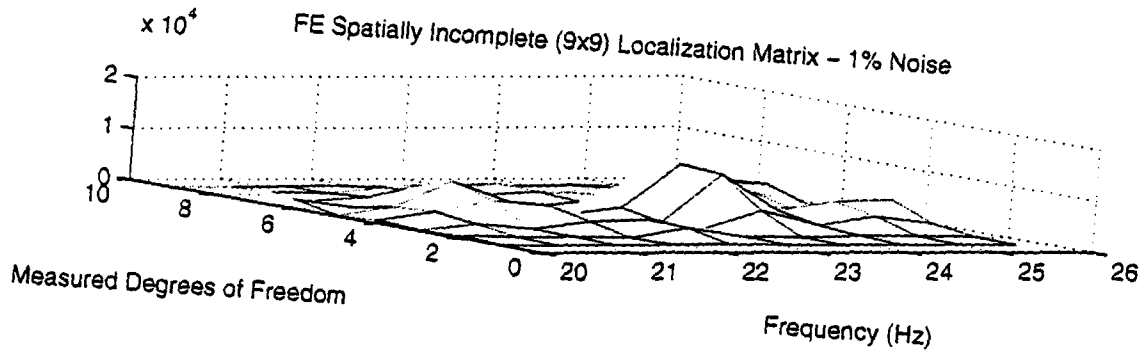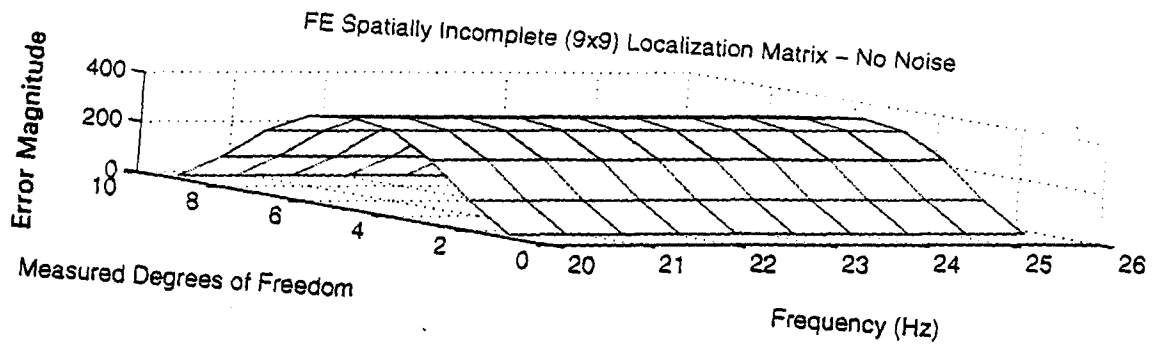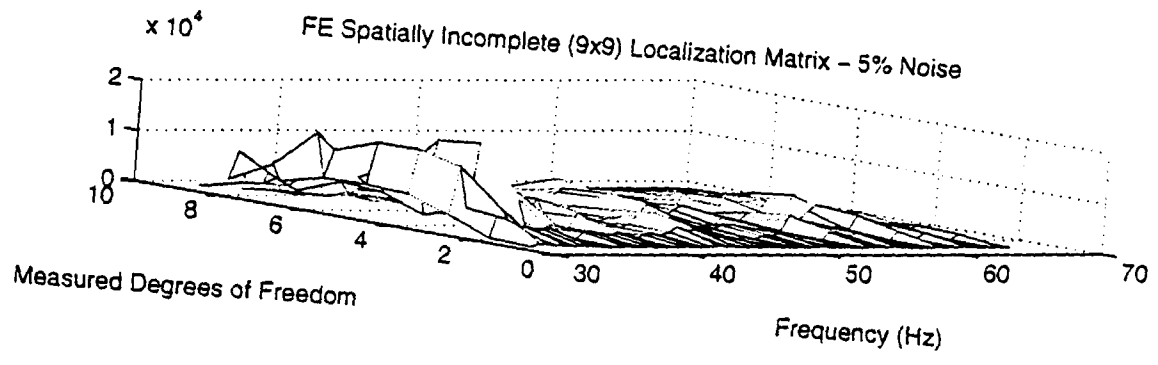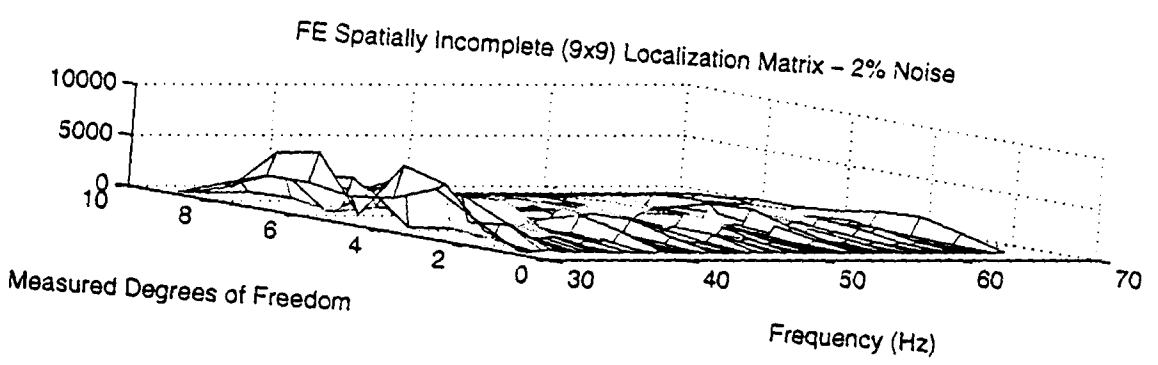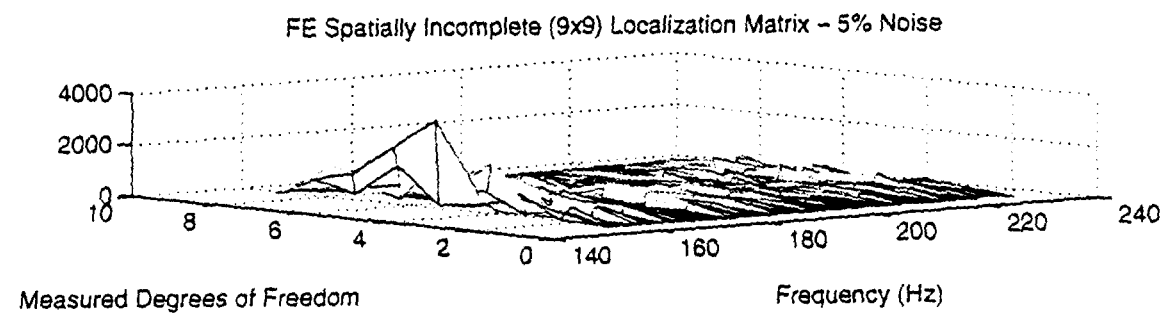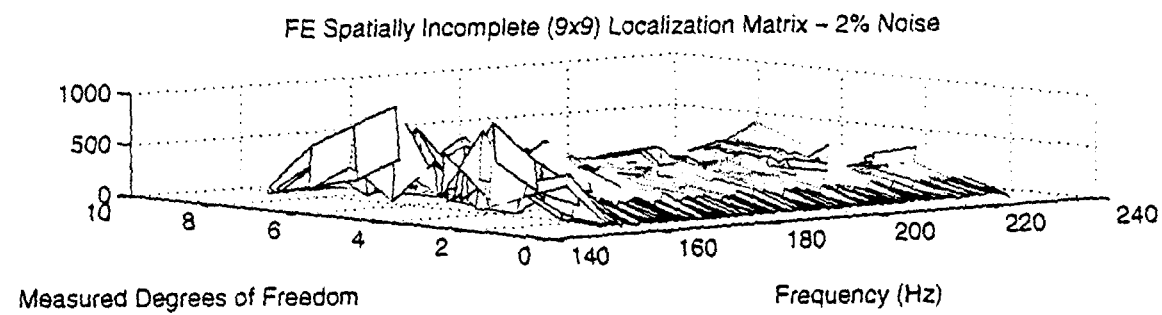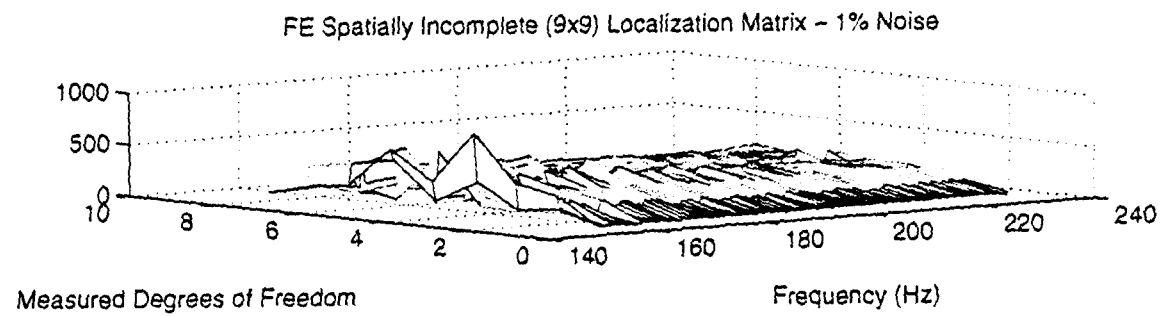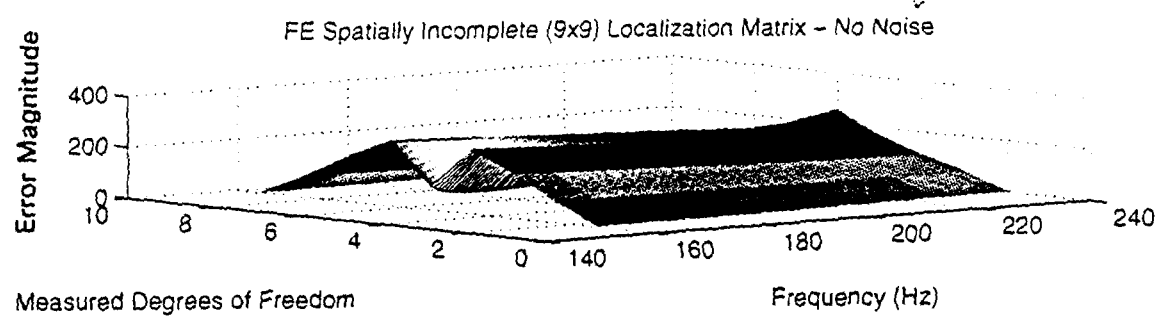**Figure 4-31** FE noise simulation, 50% rho reduction (mdof 5), various noise conditions, 158-233 Hz.

The preceding FE noise simulations reveal a worsening localization trend with increasing noise. Successful localization was performed in the presence of one percent noise. Two percent noise made clear error detection much more difficult, while five percent noise content precluded confident damage assessment. Localization was generally better under the test premise of a reduction in nominal mass density, although as mentioned previously, an EI reduction is more realistic. The inter-resonant frequency bandwidth of 80-140 Hz rendered marginally better localization information than the other test regions. The error magnitudes obtained from localization matrices in the presence of 2% and 5% noise are of comparable order to the error magnitudes obtained experimentally in Chapter V.

## C. DAMAGE SIZE

Having addressed the issues of frequency bandwidth selection and measurement noise, the influence of damage size on localization success remains to be investigated. Consider the 48 element 48-inch beam model of previous sections with a five inch crack centered one foot from a beam end. The damage reflects a 10% EI reduction. Figure 4-32 shows localization in the absence of noise. Figures 4-33 and 4-34 exhibit 1% measurement noise in four inter-resonant regions. Figure 4-35 and Figure 4-36 reflect 2% measurement noise. Figures 4-37 and 4-38 reflect 5% measurement noise. The results of these figures are encouraging because they suggest that larger damage might possibly be detected despite the noise. However, measurement noise provides such scaling distortion that true damage is often obscured at select frequencies. Figure 4-39 contrasts FE localization of 5" damage without noise and with 5% noise at select frequencies between 20 Hz and 100 Hz. Generally, larger damage leads to more discernible localization information.

61
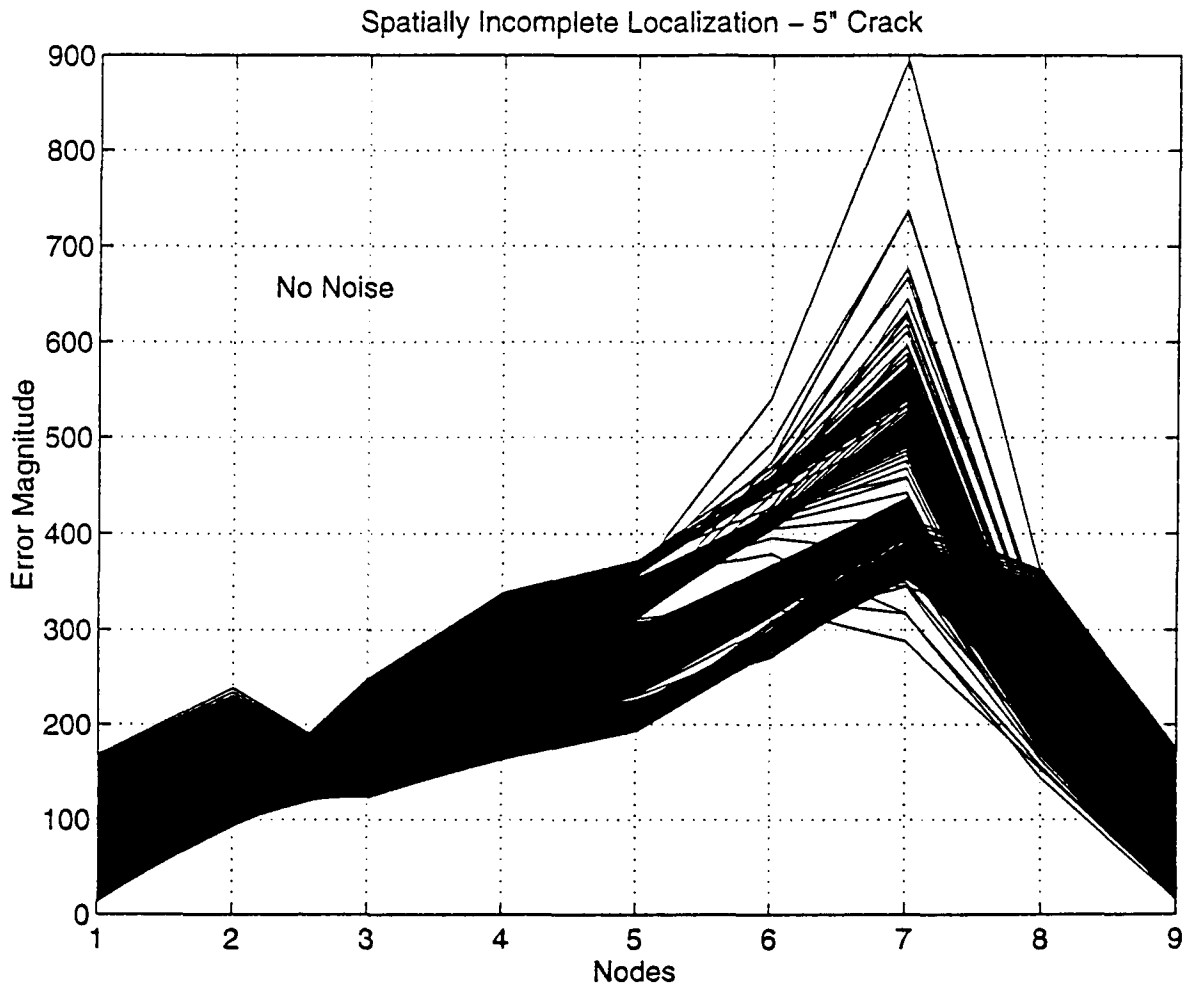
Figure 4-32 FE noise simulation, 5" crack/10% EI reduction, true error only at node 7, no noise, 20-520 Hz.

Spatially Incomplete Localization – 1% Noise



Spatially Incomplete Localization – 1% Noise
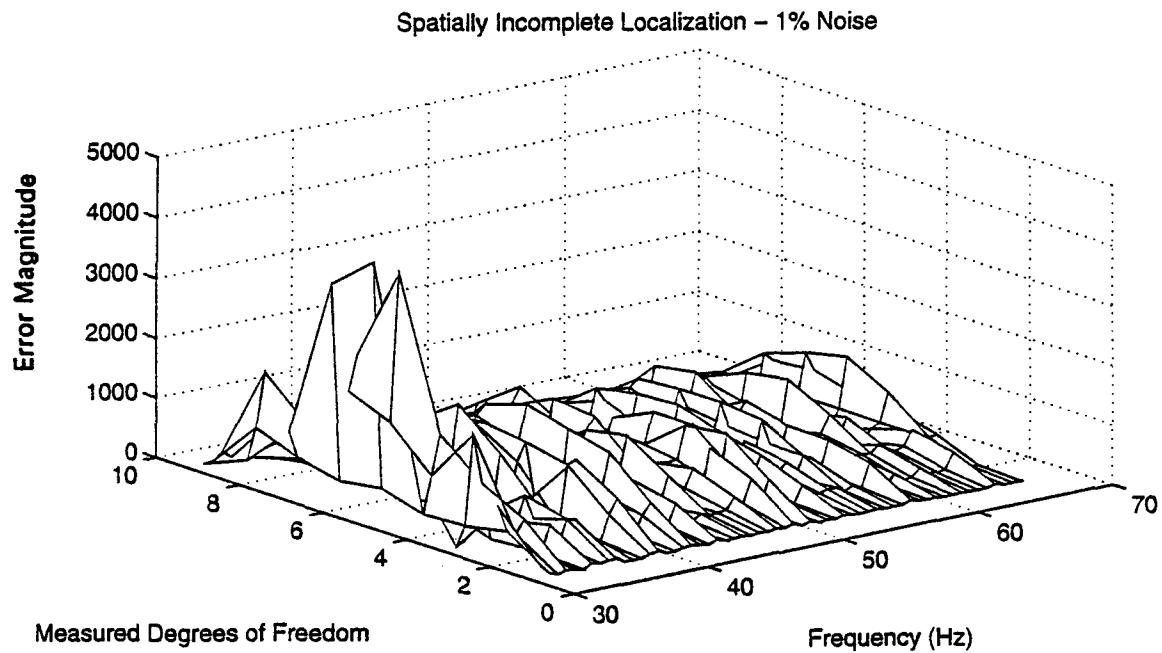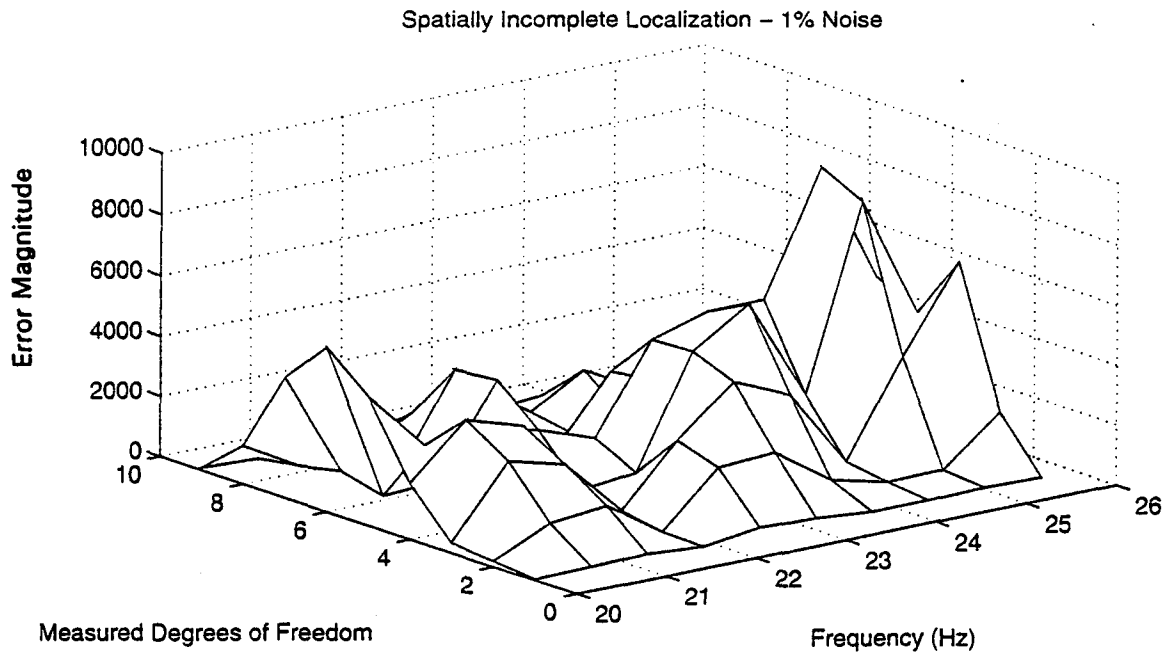
**Figure 4-33**   FE noise simulation, 5" crack/10% EI reduction, true error only at mdof 7, 1% noise, 20-26 Hz and 30-68 Hz.

Spatially Incomplete Localization – 1% Noise
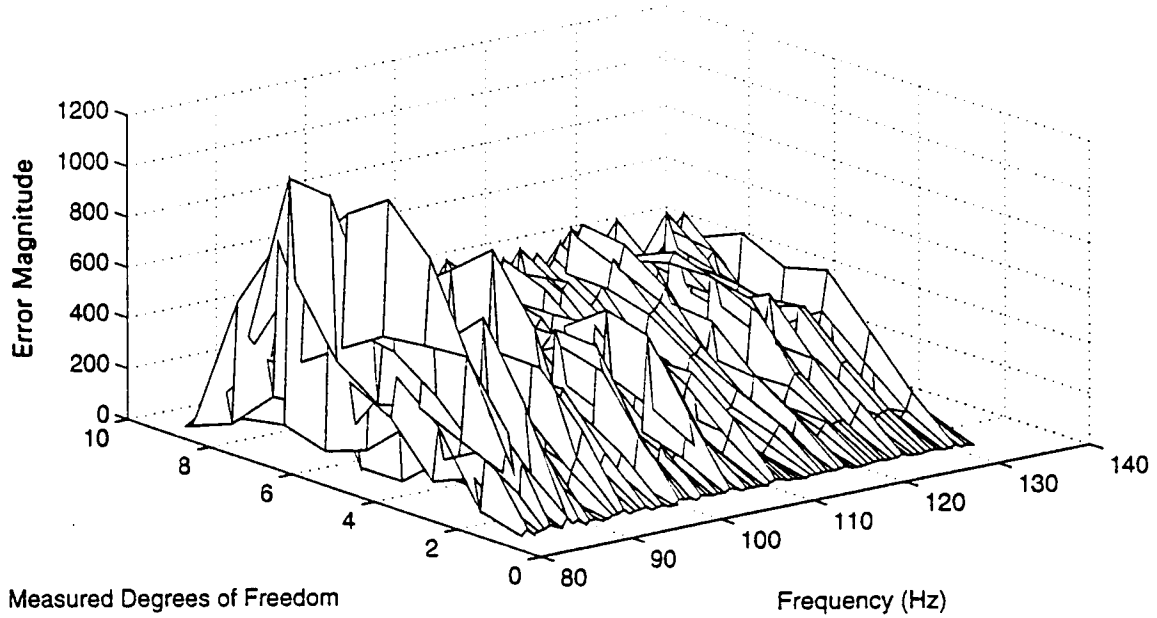


Spatially Incomplete Localization – 1% Noise
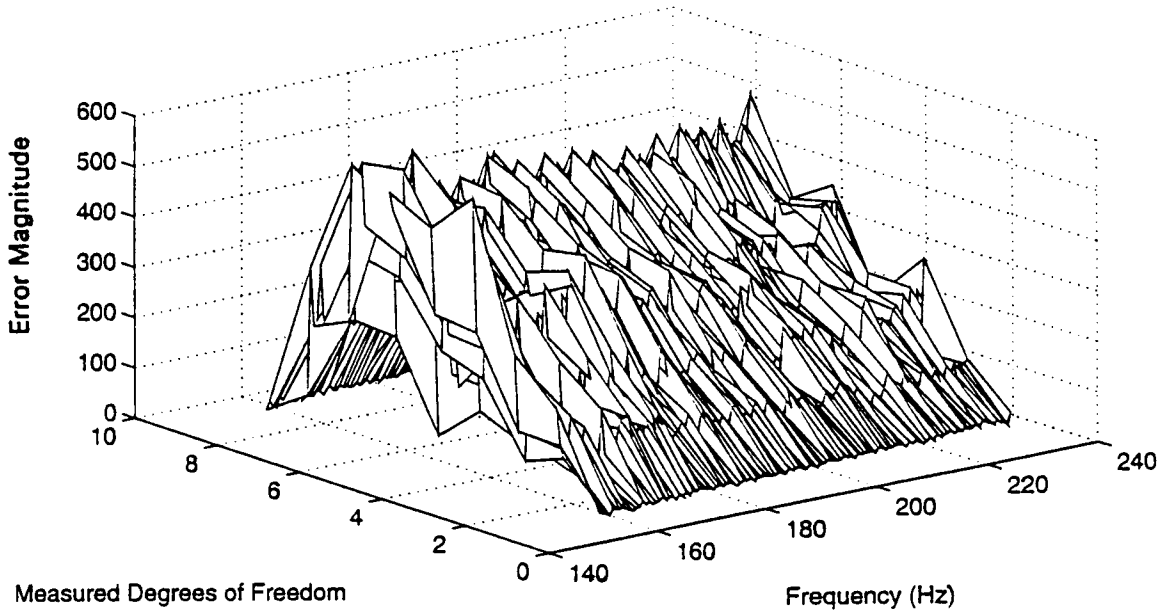
**Figure 4-34**  FE noise simulation, 5" crack/10% EI reduction, true error only at mdof 7, 1% noise, 82-133 Hz and 158-233 Hz.

Spatially Incomplete Localization – 2% Noise
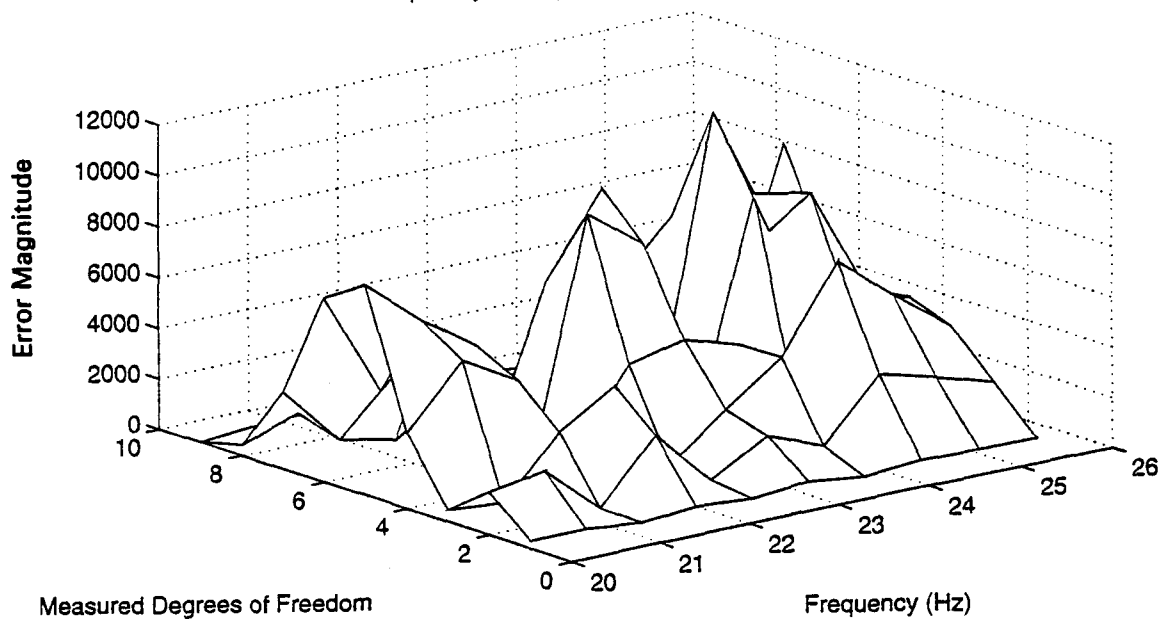


Spatially Incomplete Localization – 2% Noise
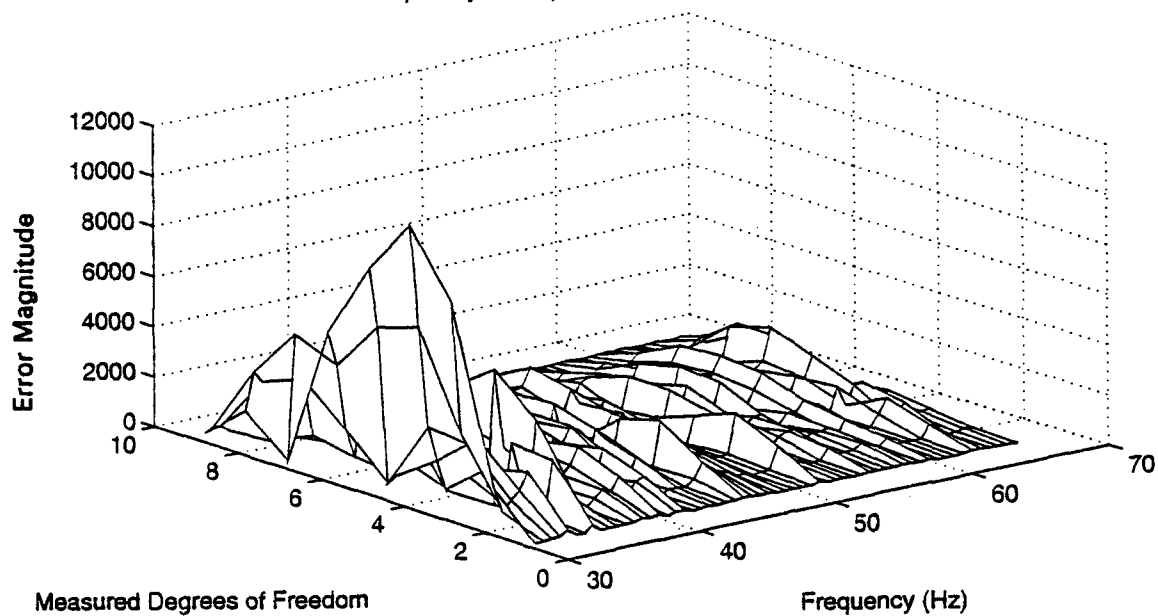
**Figure 4-35**  FE noise simulation, 5" crack/10% EI reduction, true error only at mdof 7, 2% noise, 20-26 Hz and 30-68 Hz.

65

Spatially Incomplete Localization – 2% Noise



Spatially Incomplete Localization – 2% Noise
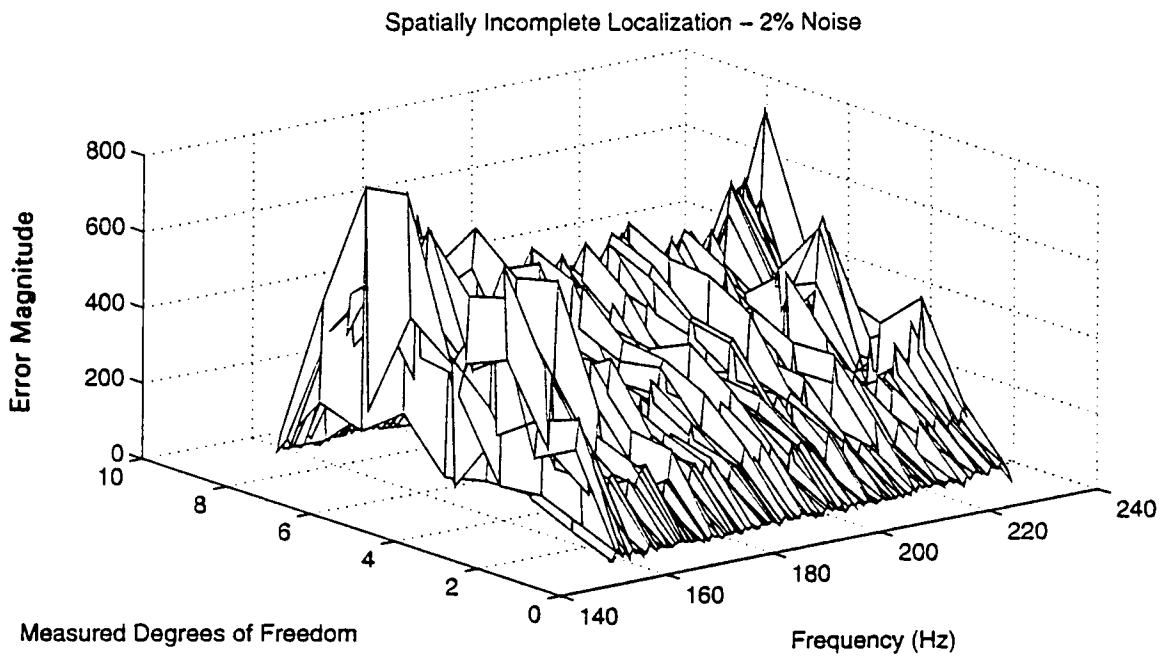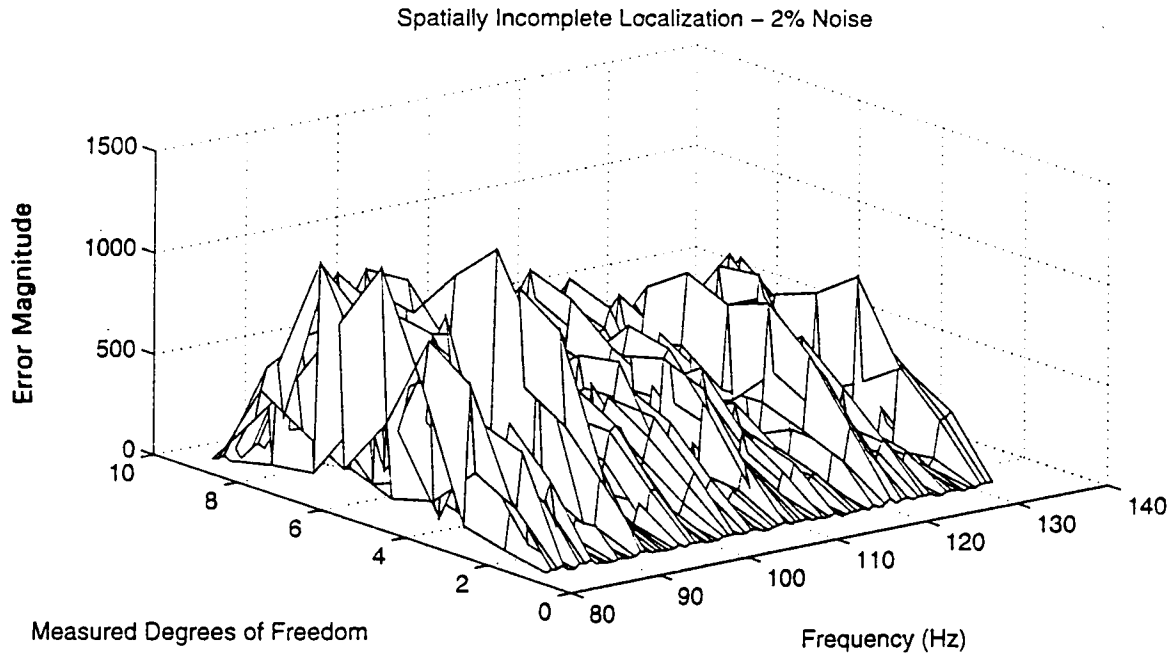
**Figure 4-36**  FE noise simulation, 5" crack/10% EI reduction, true error only at mdof 7, 1% noise, 82-133 Hz and 158-233 Hz.

Spatially Incomplete Localization – 5% Noise



Spatially Incomplete Localization – 5% Noise
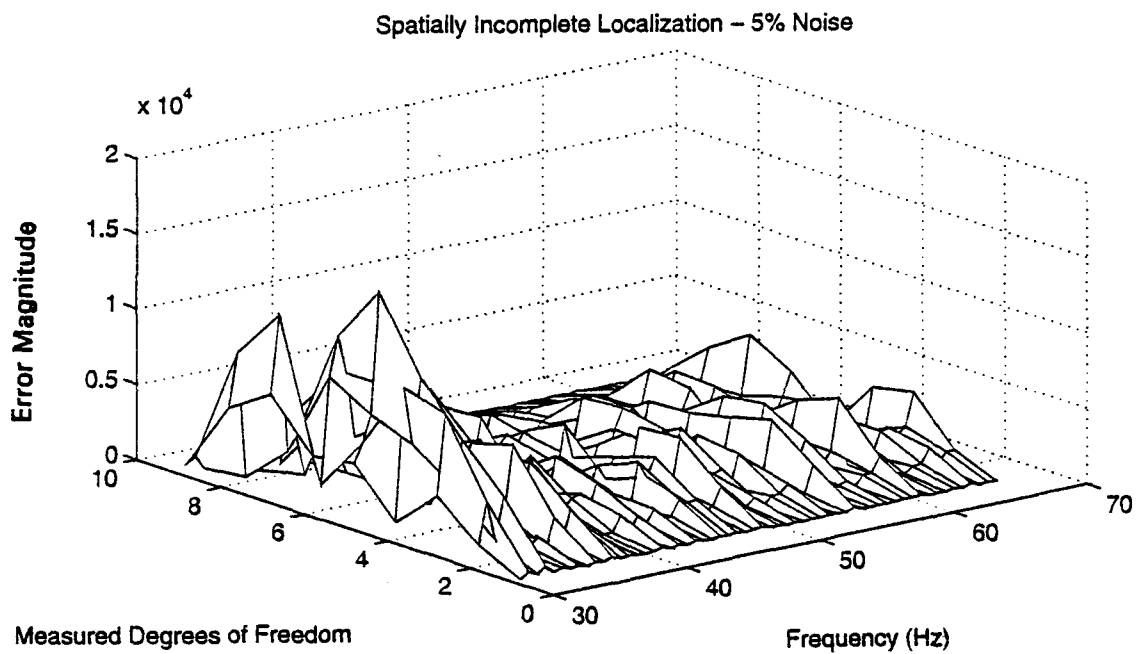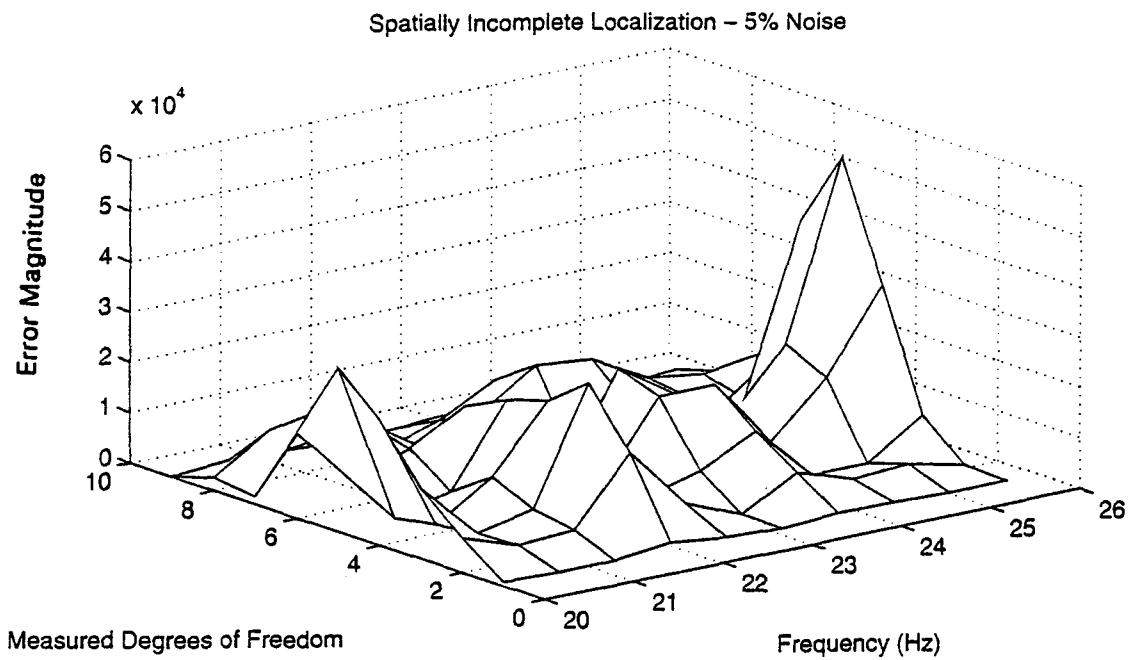
**Figure 4-37** FE noise simulation, 5" crack/10% EI reduction, true error only at mdof 7, 5% noise, 20-26 Hz and 30-68 Hz.

Spatially Incomplete Localization – 5% Noise



Spatially Incomplete Localization – 5% Noise
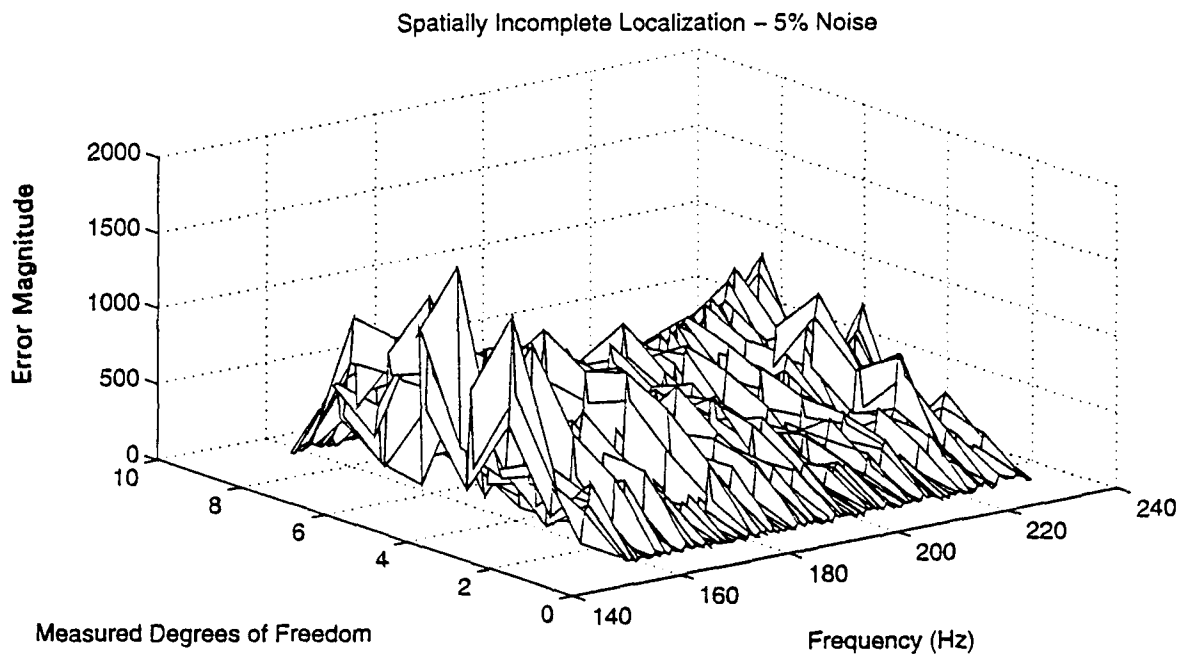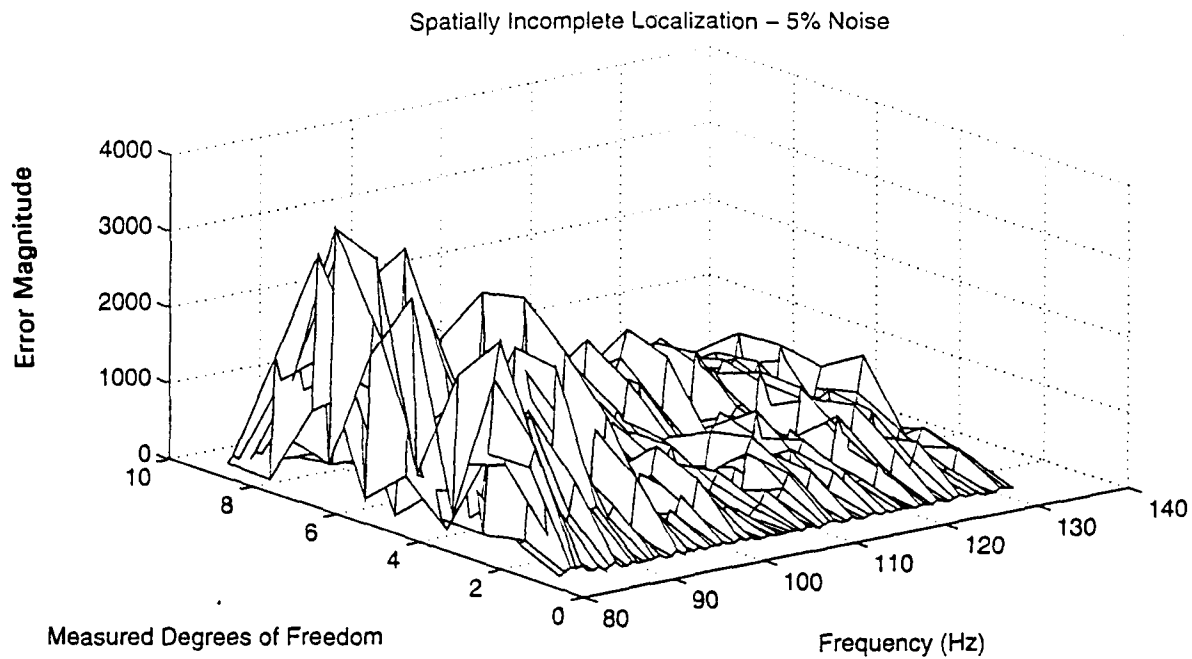
**Figure 4-38**   FE noise simulation, 5" crack/10% EI reduction, true error only at mdof 7, 1% noise, 82-133 Hz and 158-233 Hz.

FE Localization of 5" Damage – No Noise

Damage centered at node 7
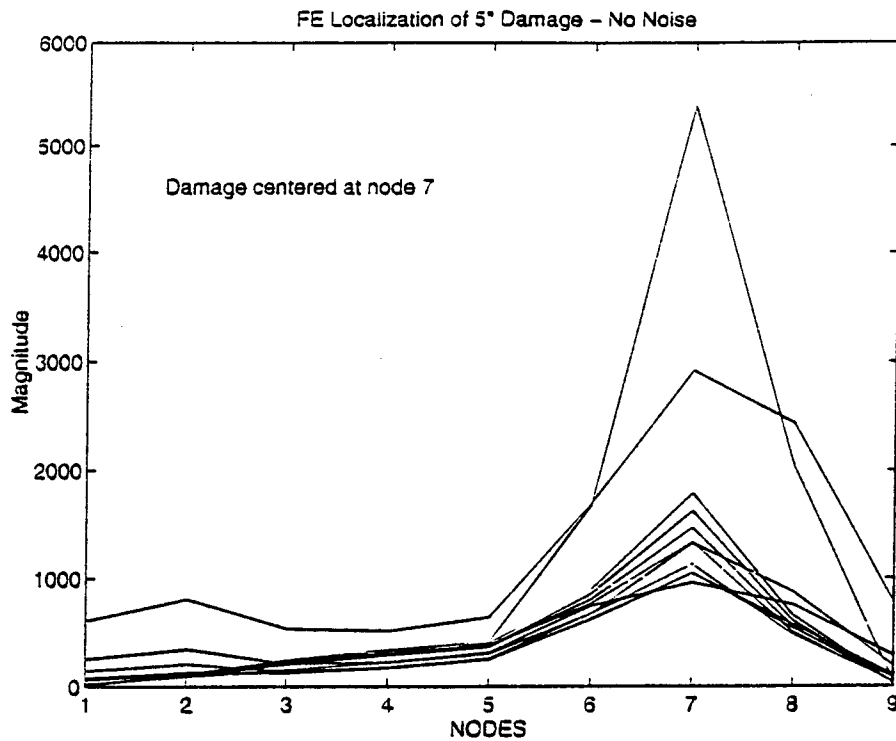
**Figure 4-39a** FE noise simulation, 5" crack/10% EI reduction, true error only at node 7, no noise, 20-100 Hz.



FE Localization of 5" Damage – 5% Noise

Damage centered at node 7
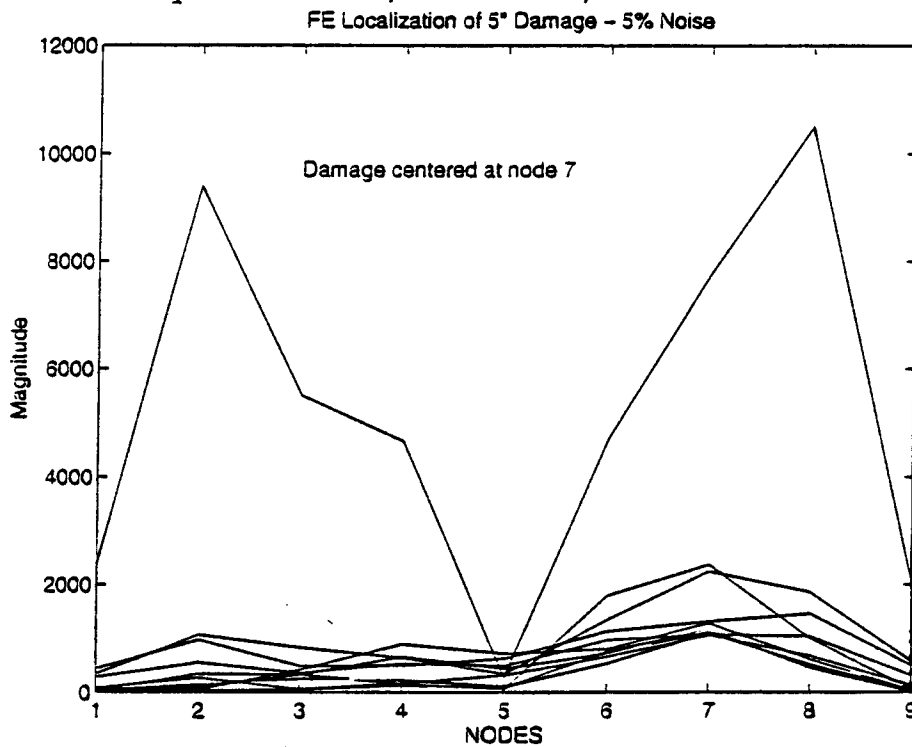
**Figure 4-39b** FE noise simulation, 5" crack/10% EI reduction, true error only at node 7, 5% noise, 20-100 Hz.

69

## V. EXPERIMENT

Continuous carbon fiber/epoxy composite beams were acquired from the Composites Structures Technology Corporation for experimental localization. An undamaged test beam and a beam with 2.25" pre-manufactured delamination were considered for analysis. A mathematical model for the virgin beam was constructed using finite element methods. From experimental measurements, the FE model was refined to reflect system natural frequencies within the frequency bandwidth 20-520 Hz. Having developed an accurate analytical model representative of our test system, localization methods were applied using theoretical-experimental test systems and experimental-experimental test systems.

### A. EXPERIMENTAL MEASUREMENT

Extensive planning and preparation preceded the actual measurement phase. A free-free beam configuration was selected for measurement, largely to facilitate FE modeling and to eliminate constraint considerations. Issues of testpiece suspension and supports were addressed to ensure clean forced vibration analysis results. Two excitation methods were evaluated in frequency impact hammers and attached shakers. Shaker excitation signals and exciter attachment methods were also investigated.

Test beam support mechanisms were selected to ensure that measured linear reponse natural frequencies far exceeded plunge mode and pendulum mode natural frequencies. Filament tackline and rubber bands effectively maintained both plunge and pendulum mode natural frequencies on the order of several hertz, far below the first beam natural frequency of 27.5 Hz. These soft "spring" supports ensure that test structure rigid body modes, although no longer having zero value natural frequencies, have frequencies much less than the bending mode natural frequencies [Ref. 2:p. 90]. Structural supports were

mounted at nodal points for the first mode of vibration. Shaker excitation was selected over hammer blow testing to produce cleaner FRF results. Exciter selection involved comparisons between plastic "stingers" of various lengths and cross-sections and a steel 3" exciter. The test bandwidth natural frequencies obtained from each stinger configuration are compared in Table 5-1 below.

| NATURAL FREQUENCIES in Hz | | | | | |
|---|---|---|---|---|---|

| | | | Stinger Types (Length) | | |
| Mode No. | Frequency Hammer | Steel (3 in) | Plastic (3 in) | Plastic (5 in) | Red. Plastic (5 in) | FE Model |
|---|---|---|---|---|---|---|
| 1 | 28.12 | 28.75 | 27.5 | 27.5 | 27.5 | 27.5 |
| 2 | 76.87 | 77.5 | 76.25 | 76.25 | 76.25 | 75.72 |
| 3 | 151.25 | 150.62 | 149.37 | 148.75 | 148.75 | 148.1 |
| 4 | 250 | 247.5 | 246.25 | 246.25 | 246.25 | 244.4 |
| 5 | 371.87 | 368.12 | 366.25 | 366.87 | 366.25 | 364.4 |
| 6 | 516.25 | 510 | 508.12 | 508.12 | 508.12 | 507.3 |

**Table 5-1**

The five-inch reduced cross-section plastic stinger was selected for testpiece excitation. The shaker itself has an armature loading of several pounds, which in combination with an extremely stiff steel stinger might result in measurement errors as well as unnecessary torque applications on the load cell. The natural frequencies obtained with a steel stinger are significantly higher than those of other methods, rendering the appearance of a stiffer parent structure. Reference (11) describes the optimum configuration for a stinger as (1) providing sufficient axial stiffness to excite the structure, (2) possessing a bending stiffness weak enough to eliminate moment effects, and (3) easily adjustable and cheap. Plastic stingers satisfy these requirements nicely and reducing the cross-sectional area lessens exciter stiffness influence in the test structure response.

72

Reference (12) describes the constraints and considerations involved in excitation signal selection. Burst random excitation signals were selected for our experiment over the other available methods, i.e., swept sine, periodic, and random excitation, due to their large signal to noise ratio and expedience in frequency bandwidth dynamic response measurement. Burst random excitation is similar to random excitation, with the exception that the input history function rapidly decays to zero within the sample period [Ref. 12:p. 567]. This feature is particularly useful for lightly damped structures, such as our composite testpiece, because the excitation system attempts to maintain a zero input force, dragging the response history to zero very quickly.

Nine equidistant aluminum disks were mounted on the test structure to allow for stinger and force transducer attachment at measurement node locations. Simulations of Chapter 4 reflected these nine measurement nodes. A force transducer measured the excitation force input, while an accelerometer captured linear and angular structural response. Signal information was processed by a two-channel dynamic system analyzer which performed fast fourier transforms on each input channel before generating the FRF in units {g's/lbf}. Response information for all nine measurement nodes was gathered sequentially for each of the nine shaker locations and organized in a manner consistent with the theoretical formulation of a FRF matrix. Ensemble averaging was employed to smooth noise effects in measured FRF. Test equipment and experimental setup are detailed in Appendix B.

## B. THEORETICAL MODEL DEVELOPMENT

Experimental beam dimensions and material properties provide the basis for the FE model development. Composite beam layup specifications are detailed in Appendix A. Test structure dimensions were obtained by measurement, but

material properties were unavailable from source documentation. Hence, four-point bending tests were performed on 4.5" coupons of the the virgin composite beam. The coupons, representing particular layup orientations, yielded results leading to subsequent determination of an effective EI for the test structure. Complete listings of results are found in Appendix A. The EI obtained from the four-point bending tests, conducted upon coupons, provided an approximation to permit FE formulation. The true EI value for our test system was obtained iteratively by correcting the FE model to reflect measured eigenvalues. The resulting EI was independently verified by comparing vibration handbook calculated free-free beam resonant frequencies to those obtained experimentally. Figure 5-1 demonstrates the bending test apparatus and Figure 5-2 demonstrates strain gage orientation.
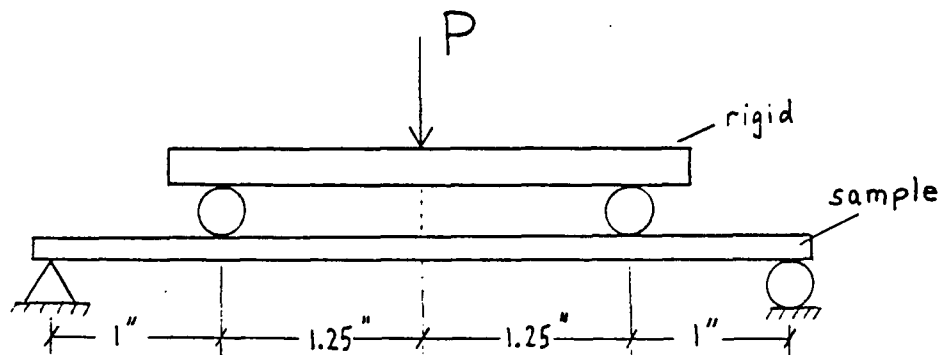


**Figure 5-1** Four-point bending test setup.
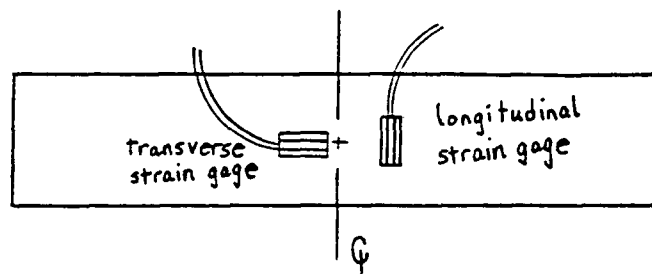


**Figure 5-2** Coupon strain gage alignment.

From the composite material properties and specifications, a FE model was developed. Experimental FRF verification, found in Appendix C was obtained by evaluating its coherence and reciprocity. Experimental natural frequencies drove the theoretical model correction process. FE model corrections were required to account for mass and inertia components of the nine aluminum discs and attached measurement devices, described in the previous section. Angular and linear displacement measurements were obtained for a test frequency bandwidth of 20-520 Hz. Figure 5-3 shows FE-test natural frequency correlation in percent error. Figures 5-4 and 5-5 show FE-experimental FRF correlation for translational and rotational response coordinates, respectively. Experimental FRF is represented in the thick dotted lines. The FE code is enclosed in Appendix D.
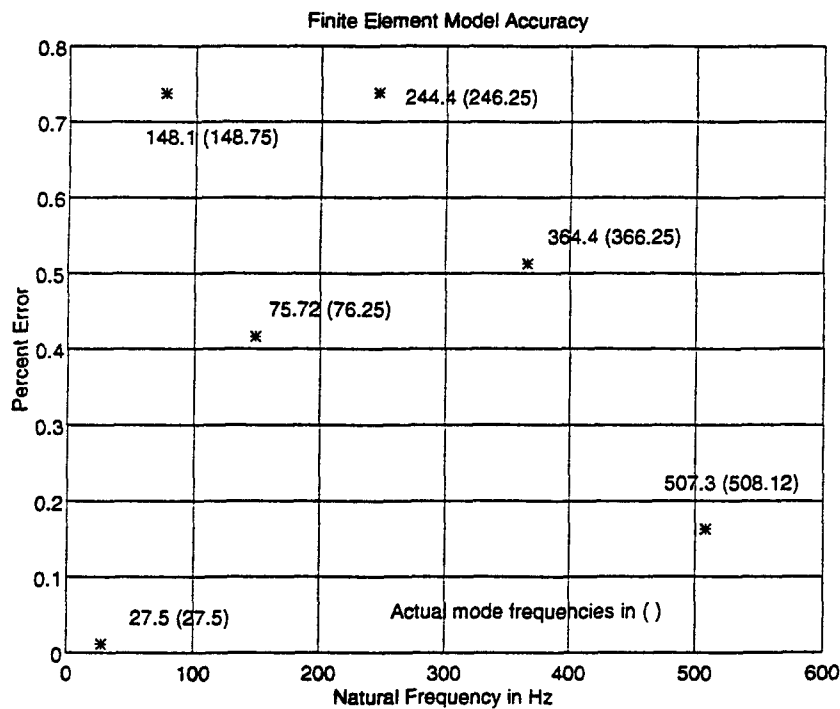


Figure 5-3    FE-experimental natural frequency correlation.

FE Model vs Experimental No Crack Beam ( Translation H99 )
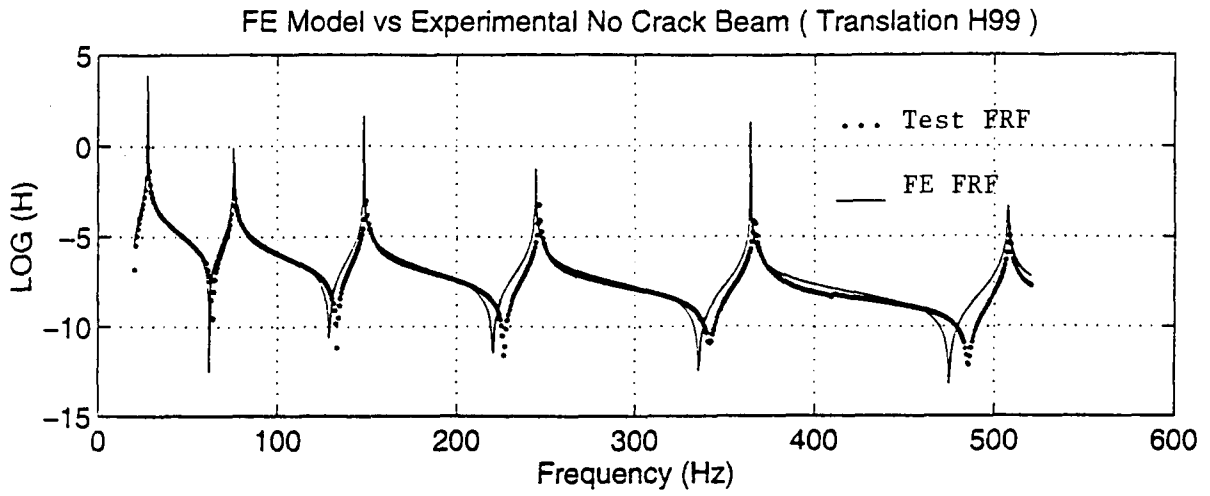
**Figure 5-4** FE-experimental driving point FRF correlation, translational response {in/lbf} only.



FE Model vs Experimental No Crack Beam ( Rotation H99 )
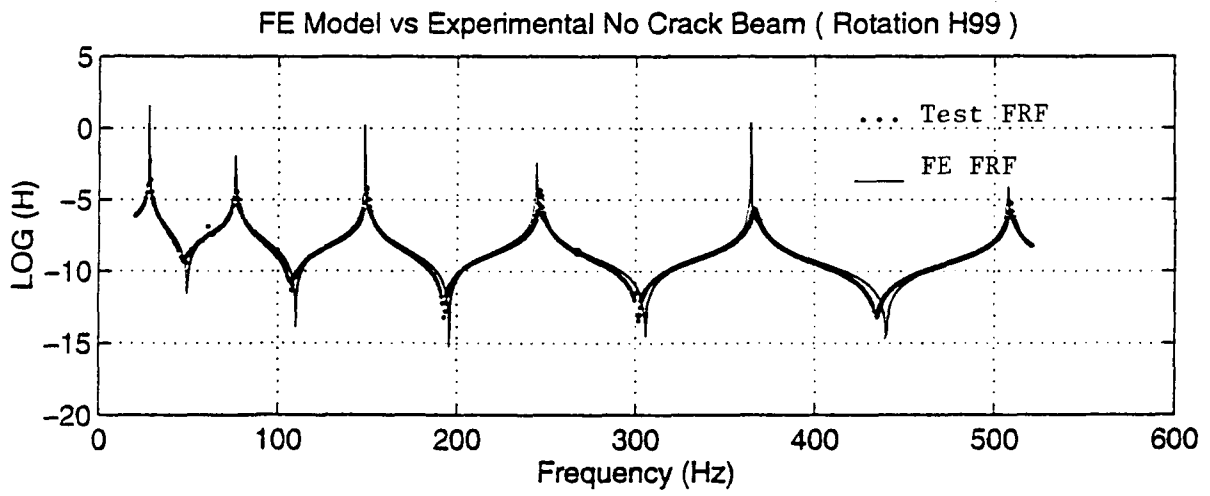
**Figure 5-5** FE-experimental driving point FRF correlation, rotational response {rad/lbf} only.

76

## C. LOCALIZATION

Localization was performed on the 2.25" crack composite beam using both the FE model and the undamaged composite beam as a reference structure. Figures 5-3 and 5-4 demonstrated translational and rotational FRF for the FE and test systems. Figures 5-6 and 5-7 demonstrate equivalent information for damaged and undamaged experimental beams. Damaged beam FRF is represented with the thick dotted lines.
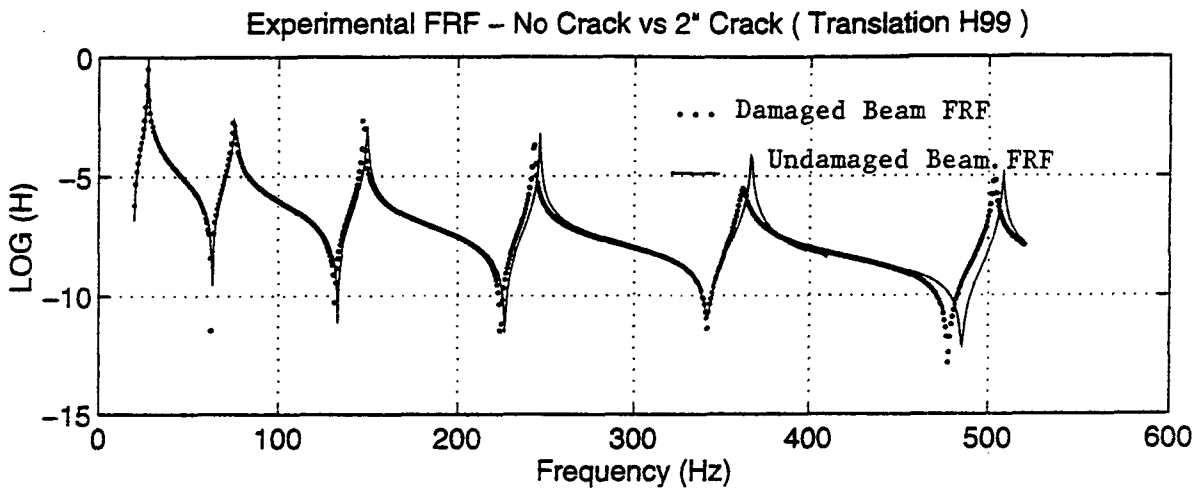


Figure 5-6
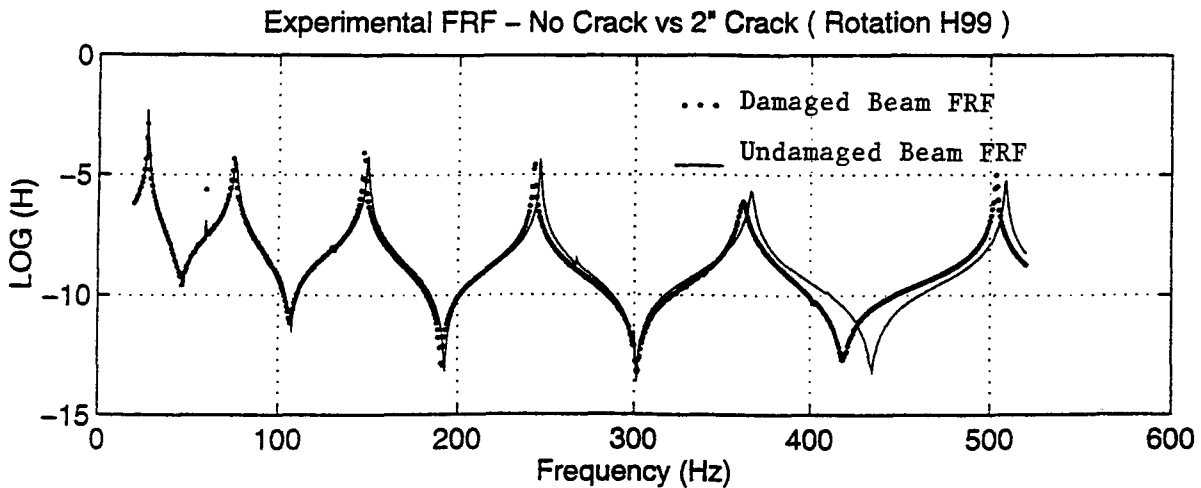


Figure 5-7

Localization methods, Equation (2.26), were applied to FE-experimental no crack systems, FE-experimental crack systems, and experimental crack-no crack sytems in the frequency bandwidth 20-520 Hz. Results are shown in Figures 5-8 through 5-10. Figures 5-11 through 5-18 show FE-experimental results and experimental-experimental results in inter-resonant regions.

Figures 5-19 through 5-29 repeat the above analysis, but the magnitude of the test FRF is used in Equation (2.26) in an attempt to improve error identification results. The localization equation used in generating these figures is as follows:

$$L_{mag} = Z_{ee}^{a} \cdot \left[ H_{ee}^{a} - |H_{ee}^{x}| \right] \cdot Z_{ee}^{a} \qquad (5.1)$$

Figures 5-19 through 5-21 show "magnitude" localization results for our test bandwidth. Figures 5-22 through 5-29 show localization results using test FRF magnitude in the inter-resonant regions.

Magnitude localization for the test frequency bandwidth added no useful information and failed to cleanup error identification information as desired. In most cases, as the figures demonstrate, magnitude localization scaling effects magnify surrounding information and distort valid information provided by ordinary localization methods. Inter-resonant regions between second and third natural frequencies showed improved localization over other regions. Localization using experimental systems provided encouraging results, but the inability of theoretical-experimental localization to consistently and accurately differentiate between the damaged and undamaged test systems prompts further investigation the experimental application of the localization theory.
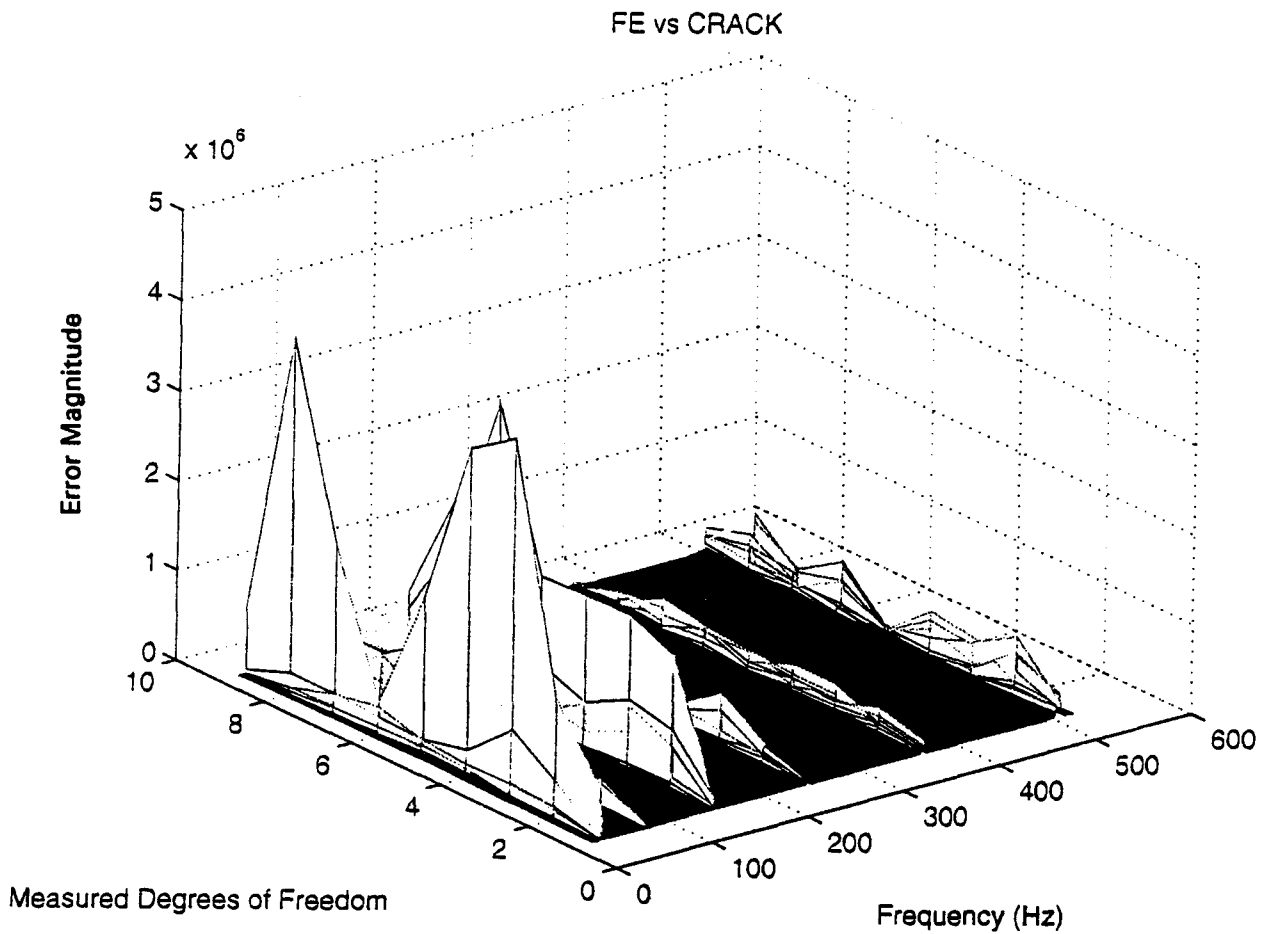
**Figure 5-8** FE model/composite beam localization at all
frequencies between 20-520 Hz, composite beam damage: 2.25"
length delamination.
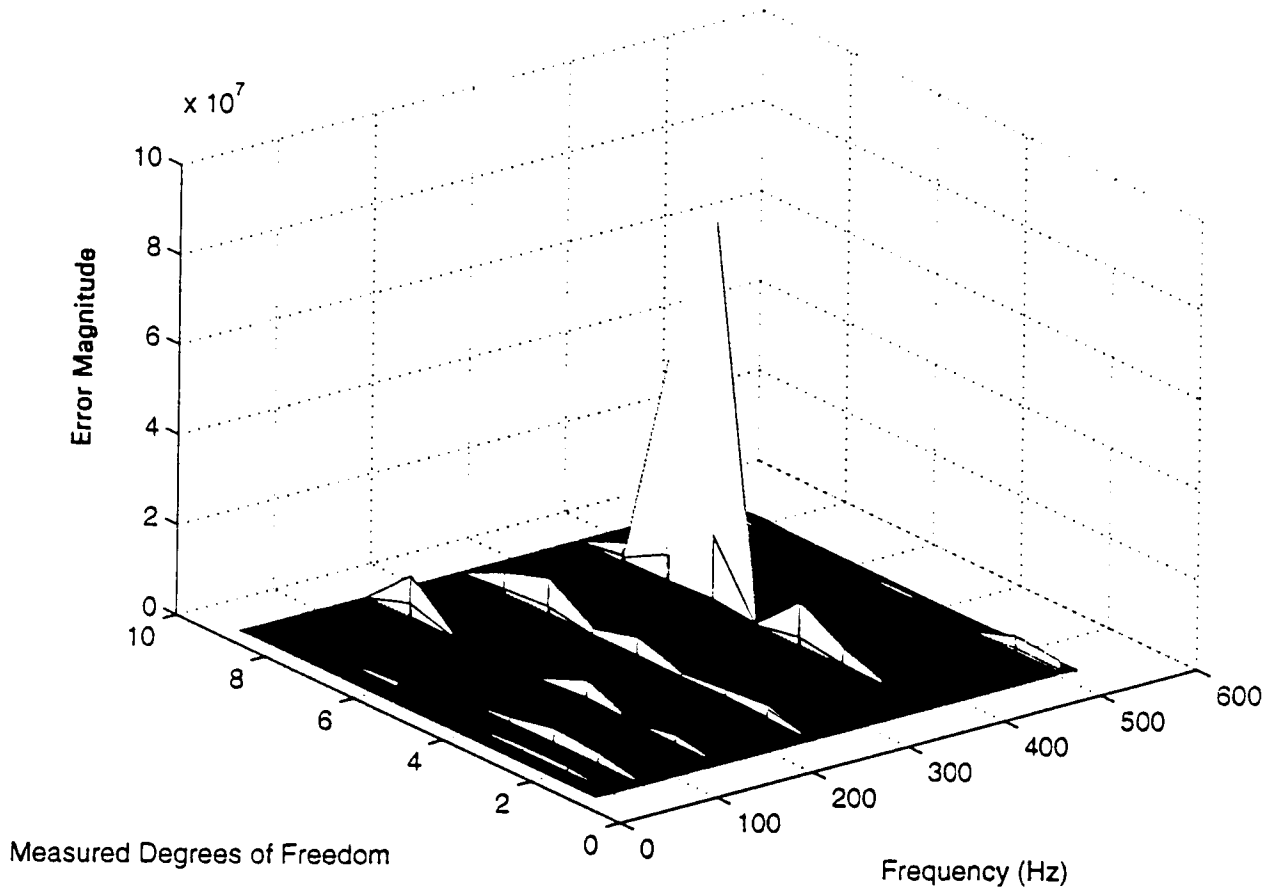
**Figure 5-9** Undamaged composite beam/damaged composite beam localization at all frequencies between 20-520 Hz, composite beam damage: 2.25" length delamination.
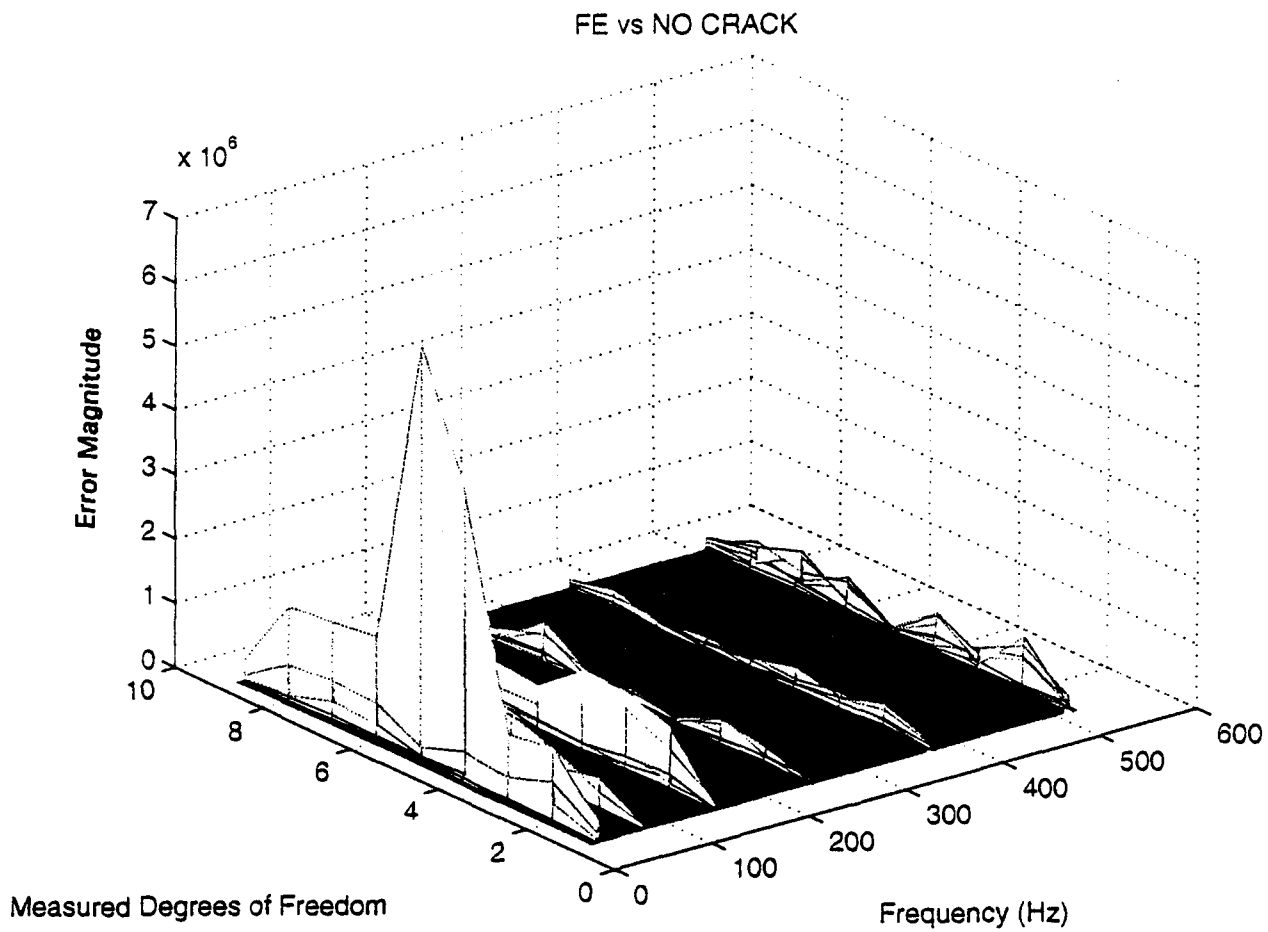
**Figure 5-10** FE model/composite beam localization at all frequencies between 20-520 Hz, undamaged composite beam.
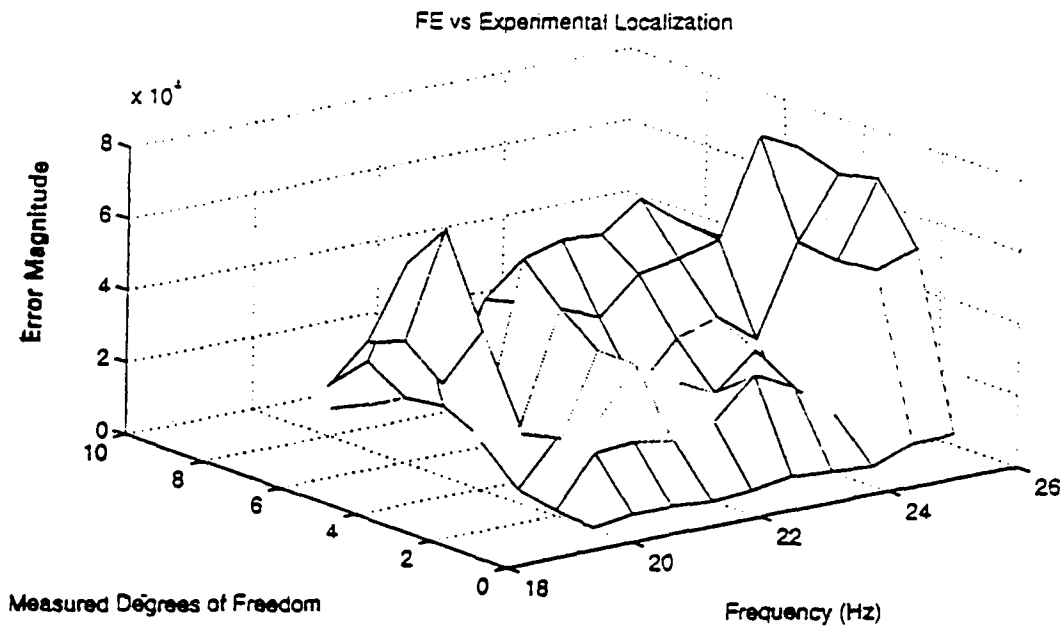
**Figure 5-11** FE model/composite beam localization, 20-26 Hz, composite beam damage: 2.25" length delamination.
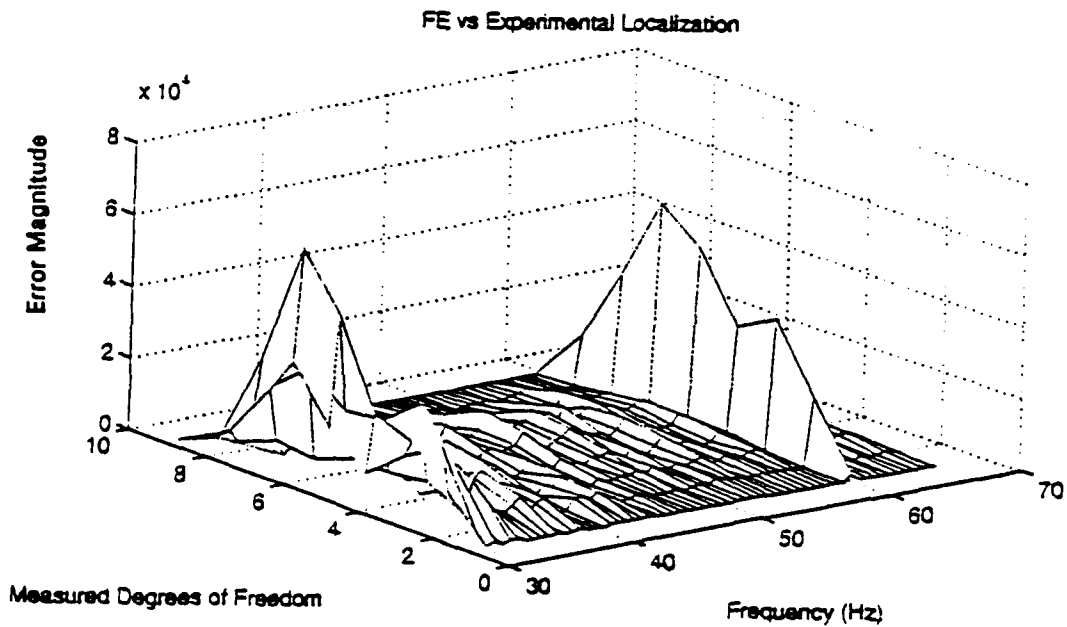


**Figure 5-12** FE model/composite beam localization, 30-68 Hz, composite beam damage: 2.25" length delamination.

FE vs Experimental Localization
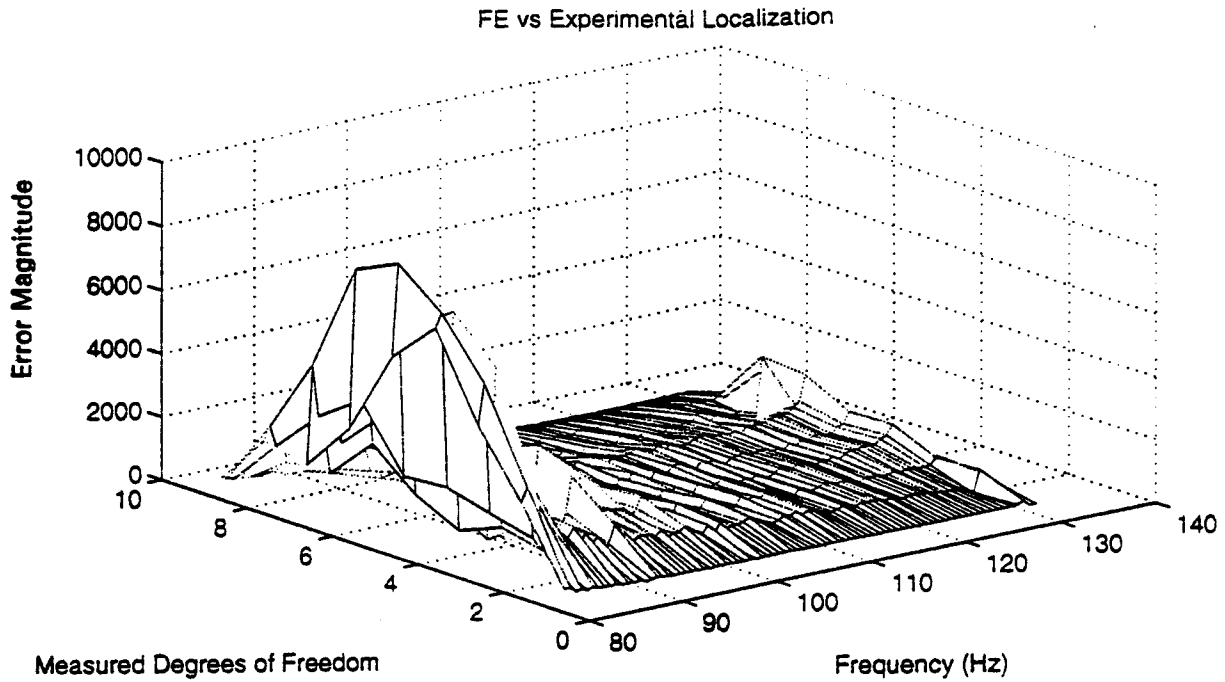


**Figure 5-13** FE model/composite beam localization, 82-133 Hz, composite beam damage: 2.25" length delamination.

FE vs Experimental Localization
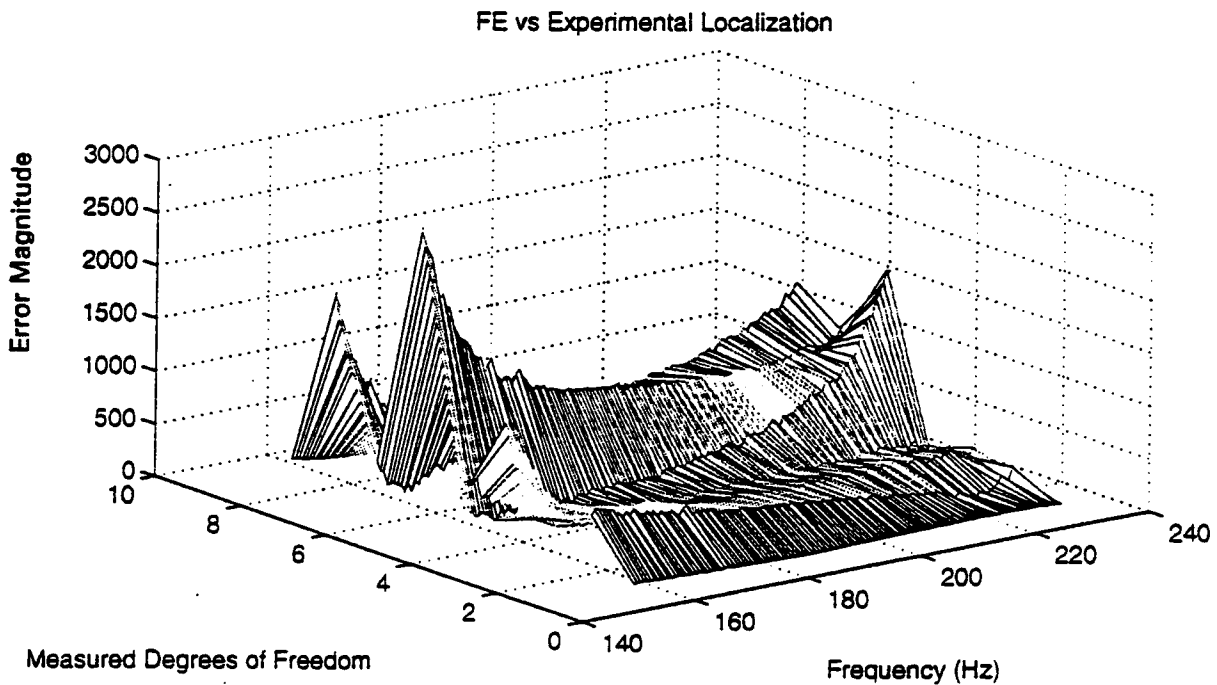


**Figure 5-14** FE model/composite beam localization, 158-233 Hz, composite beam damage: 2.25" length delamination.

Experimental vs Experimental Localization
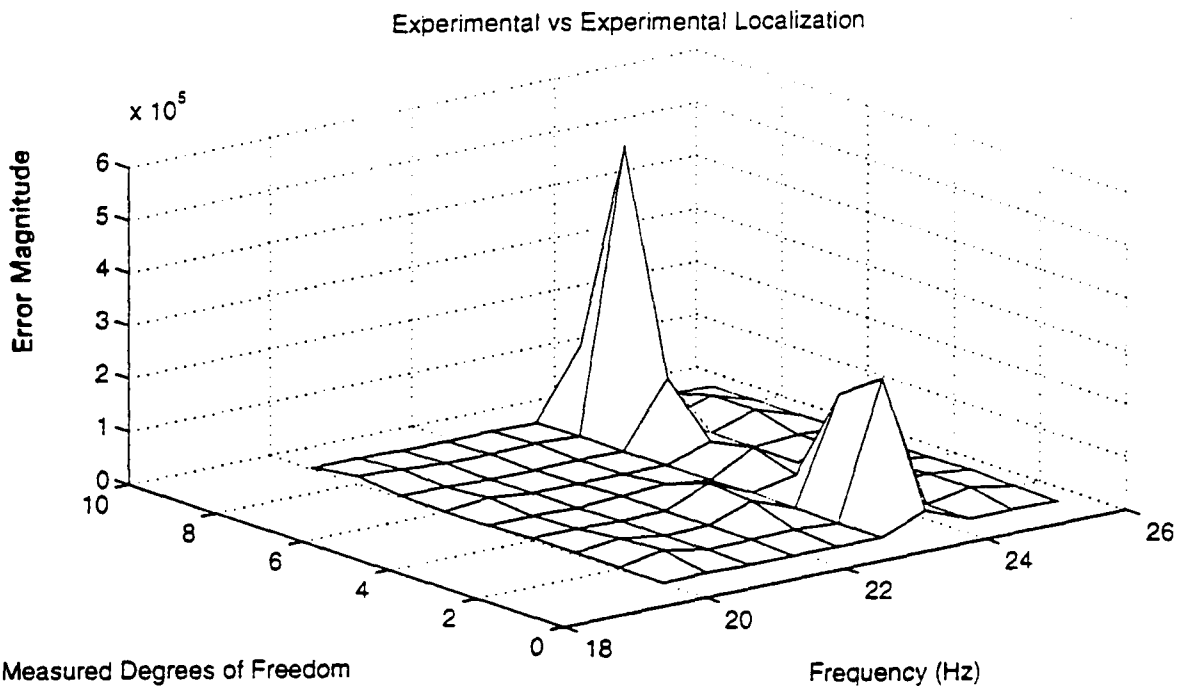


**Figure 5-15** Undamaged/damaged composite beam localization, 20-26 Hz, composite beam damage: 2.25" length delamination.

Experimental vs Experimental Localization
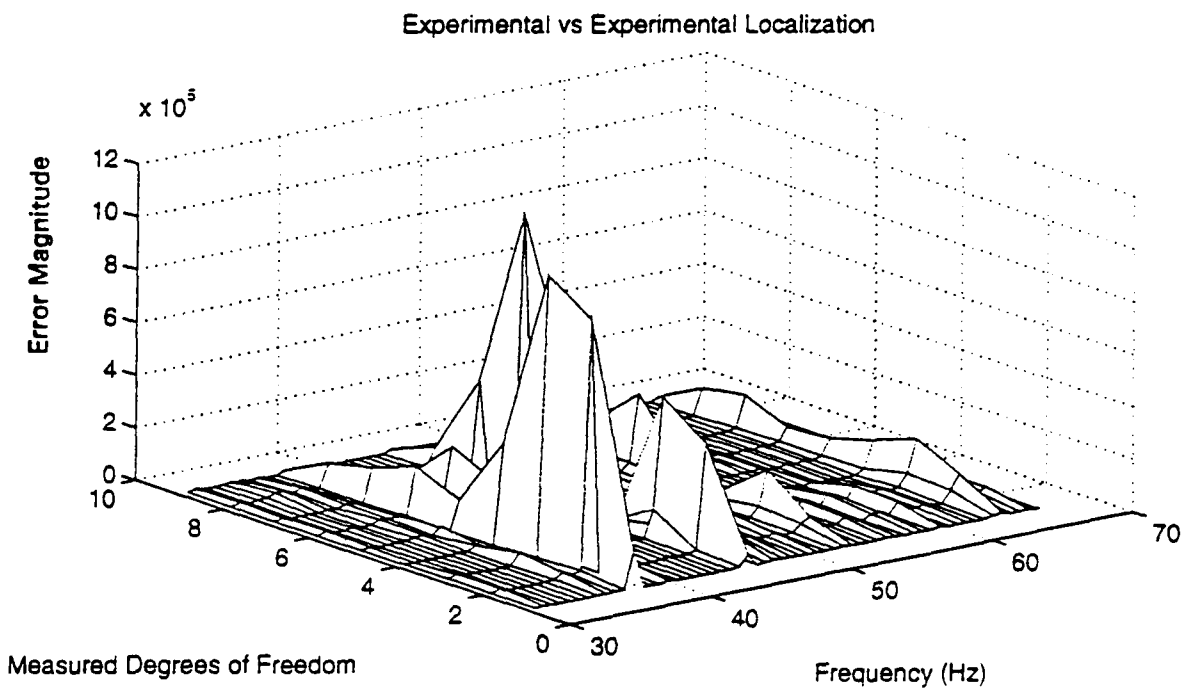


**Figure 5-16** Undamaged/damaged composite beam localization, 30-68 Hz, composite beam damage: 2.25" length delamination.

84
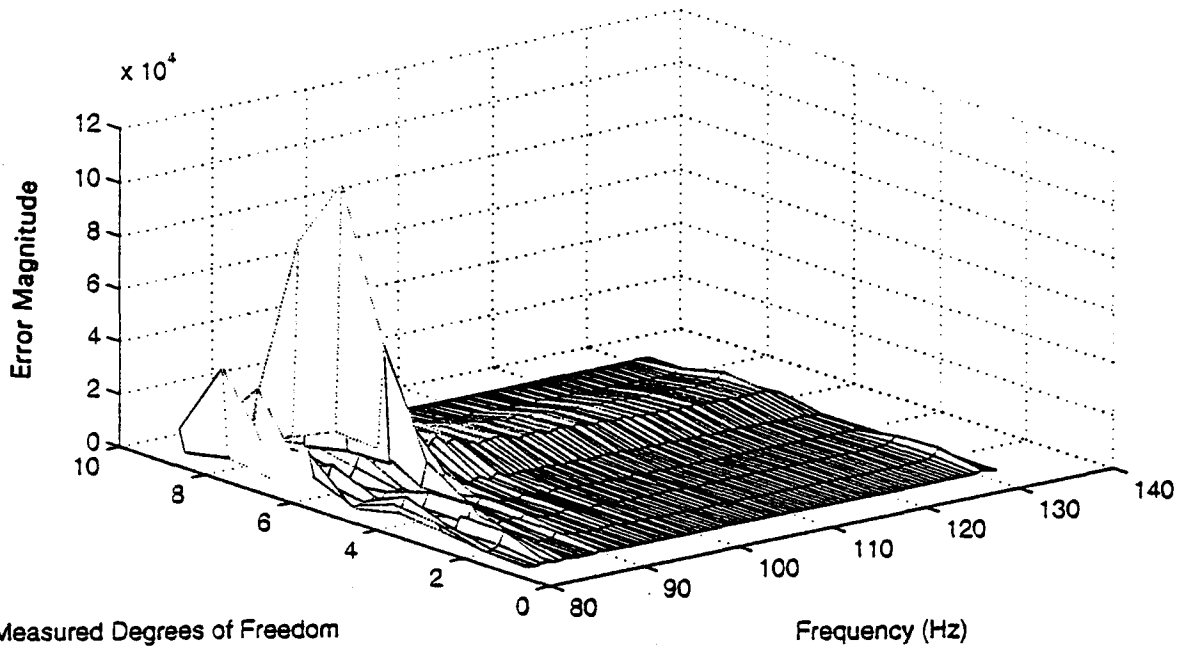
Experimental vs Experimental Localization



**Figure 5-17** Undamaged/damaged composite beam localization, 82-133 Hz, composite beam damage: 2.25" length delamination.

Experimental vs Experimental Localization
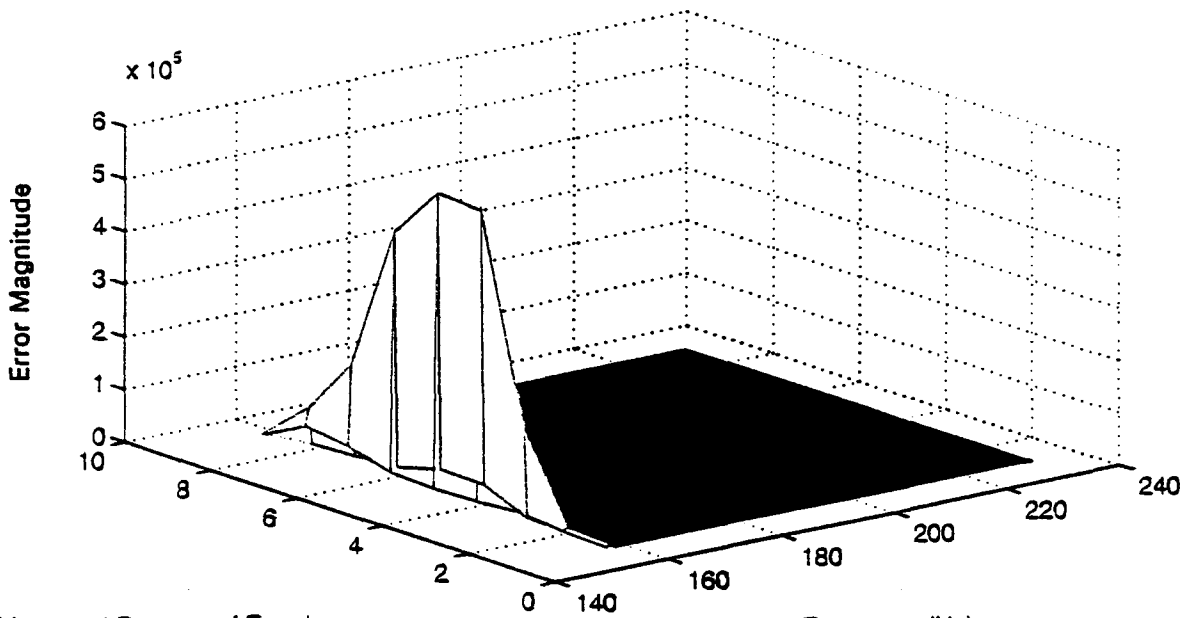


**Figure 5-18** Undamaged/damaged composite beam localization, 158-233 Hz, composite beam damage: 2.25" length delamination.
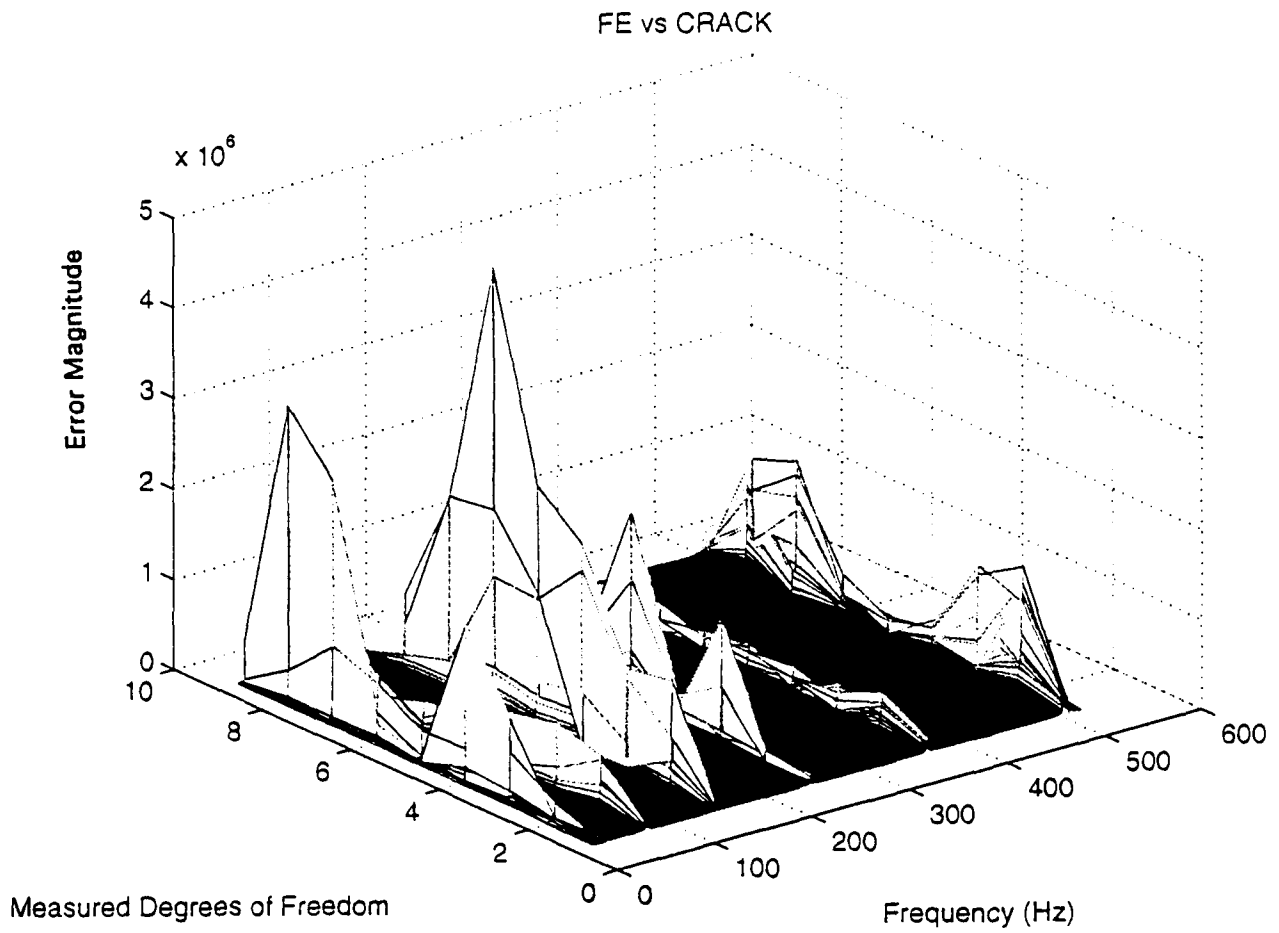
**Figure 5-19** FE model/composite beam magnitude localization at all frequencies between 20-520 Hz, composite beam damage: 2.25" length delamination.
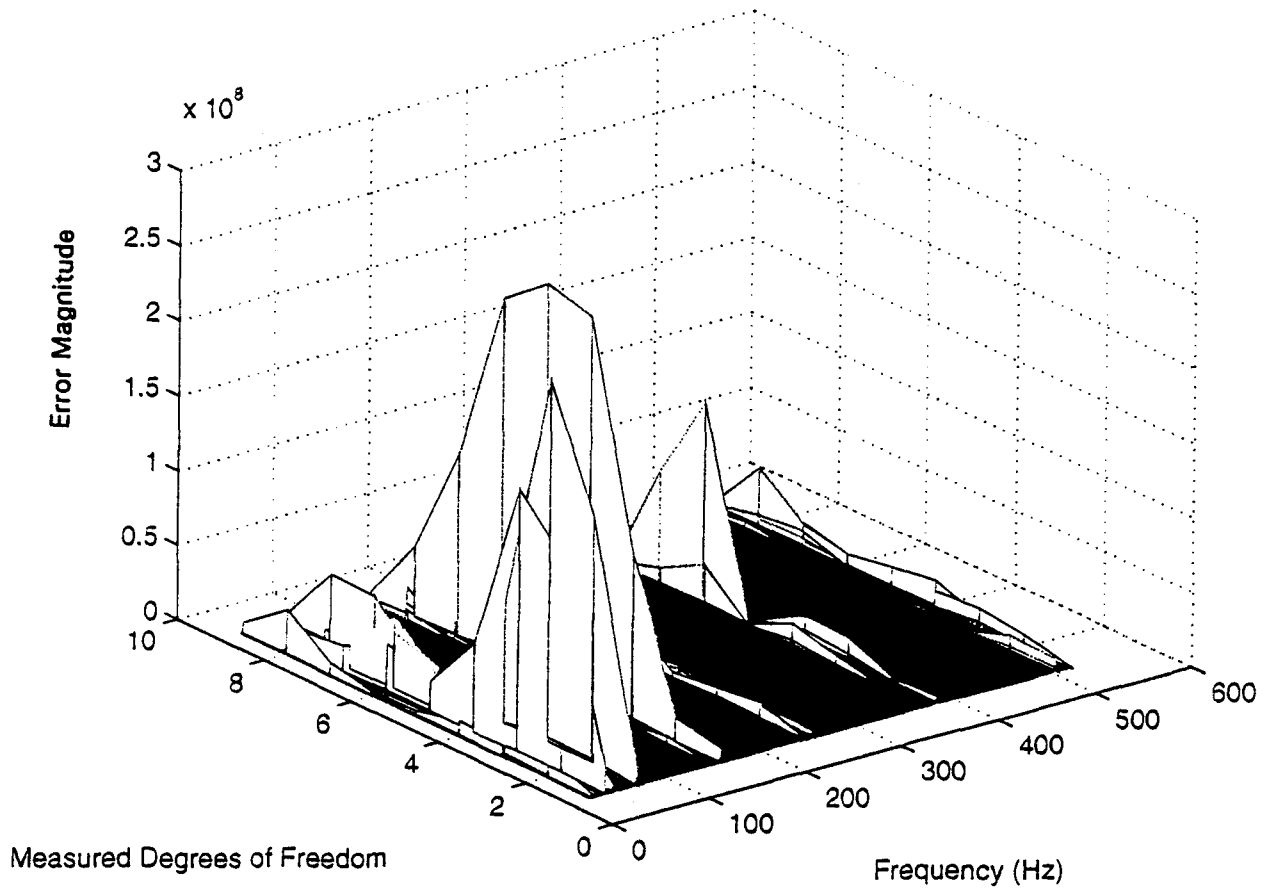
**Figure 5-20** Undamaged/damaged composite beam magnitude localization at all frequencies between 20-520 Hz, composite beam damage: 2.25" length delamination.
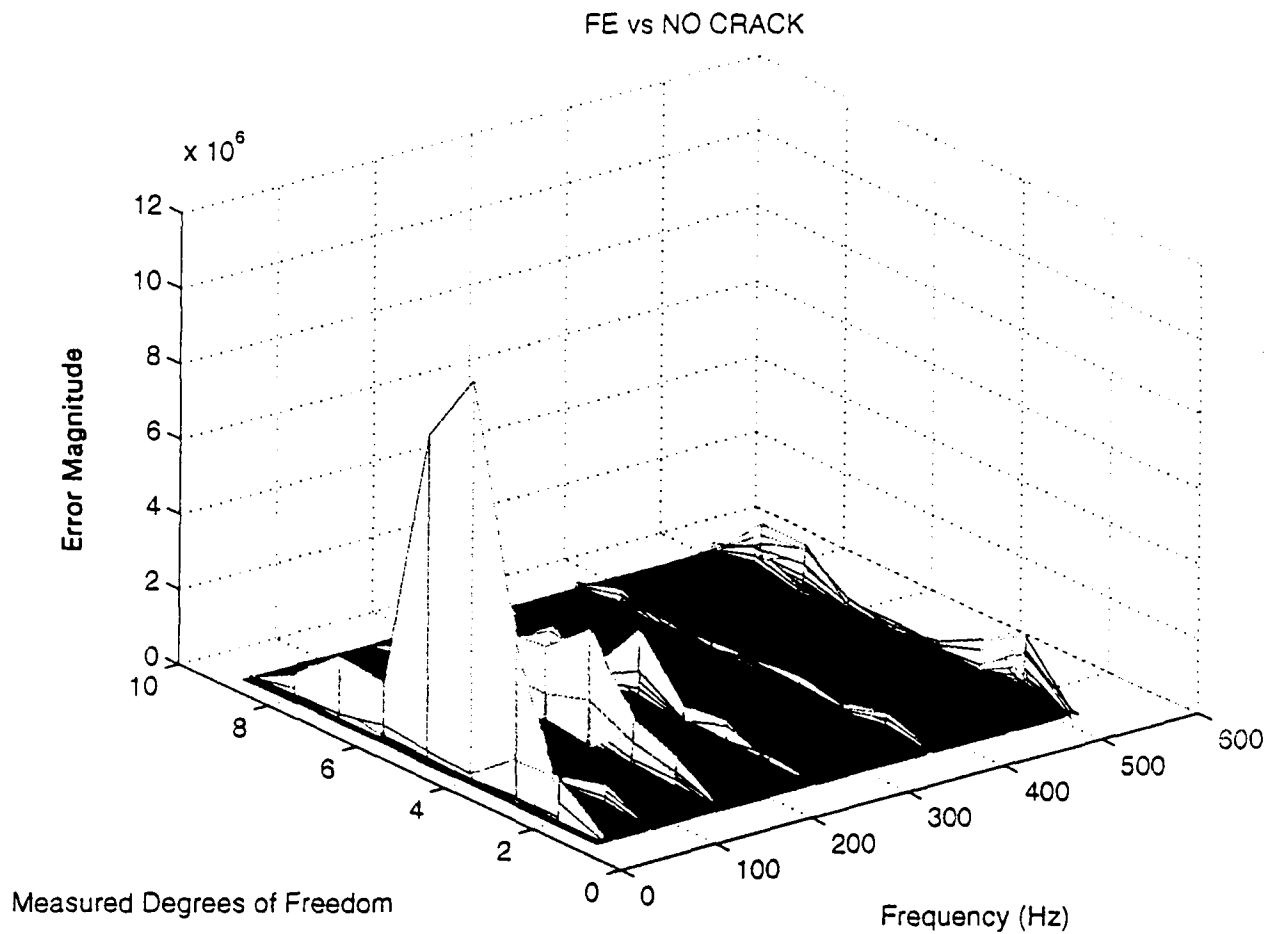
**Figure 5-21** FE model/composite beam magnitude localization at all frequencies between 20-520 Hz, undamaged composite beam.
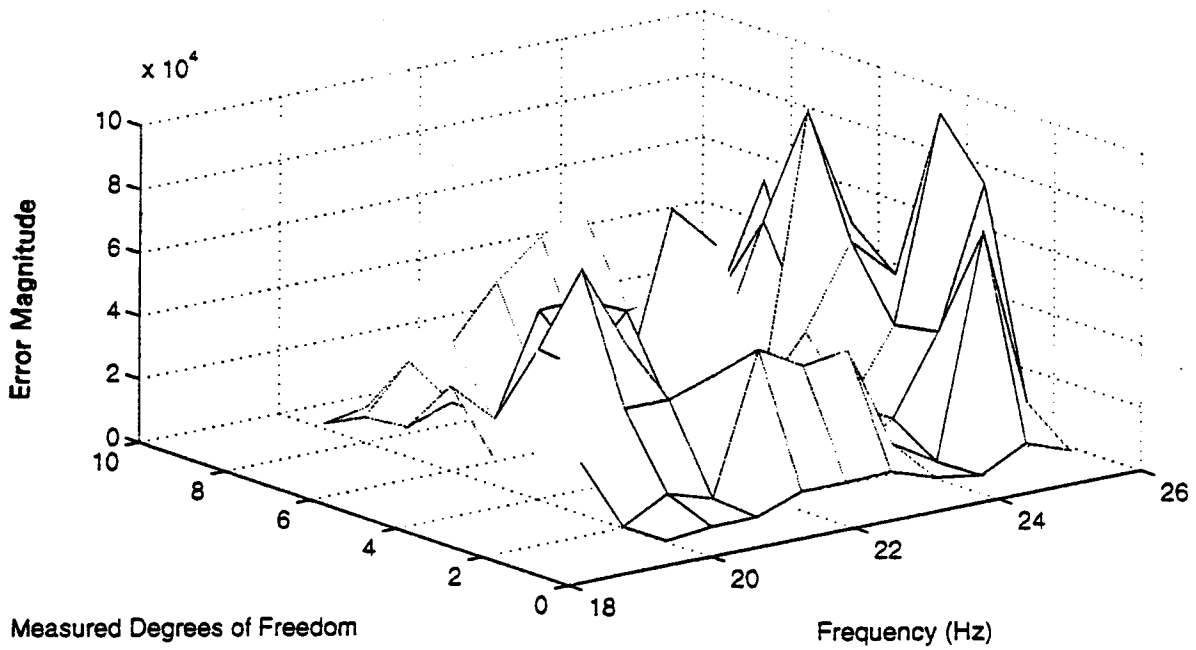
**Figure 5-22** FE model/composite beam magnitude localization, 20-26 Hz, beam damage: 2.25" length central delamination.
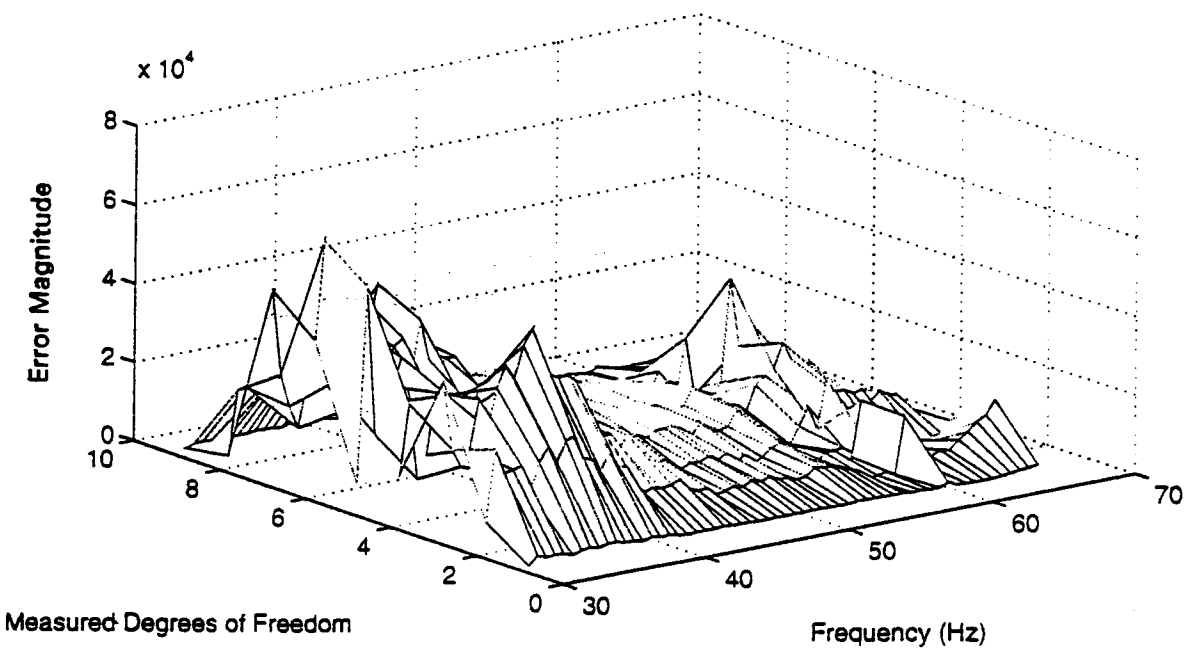


**Figure 5-23** FE model/composite beam magnitude localization, 30-68 Hz, beam damage: 2.25" length central delamination.
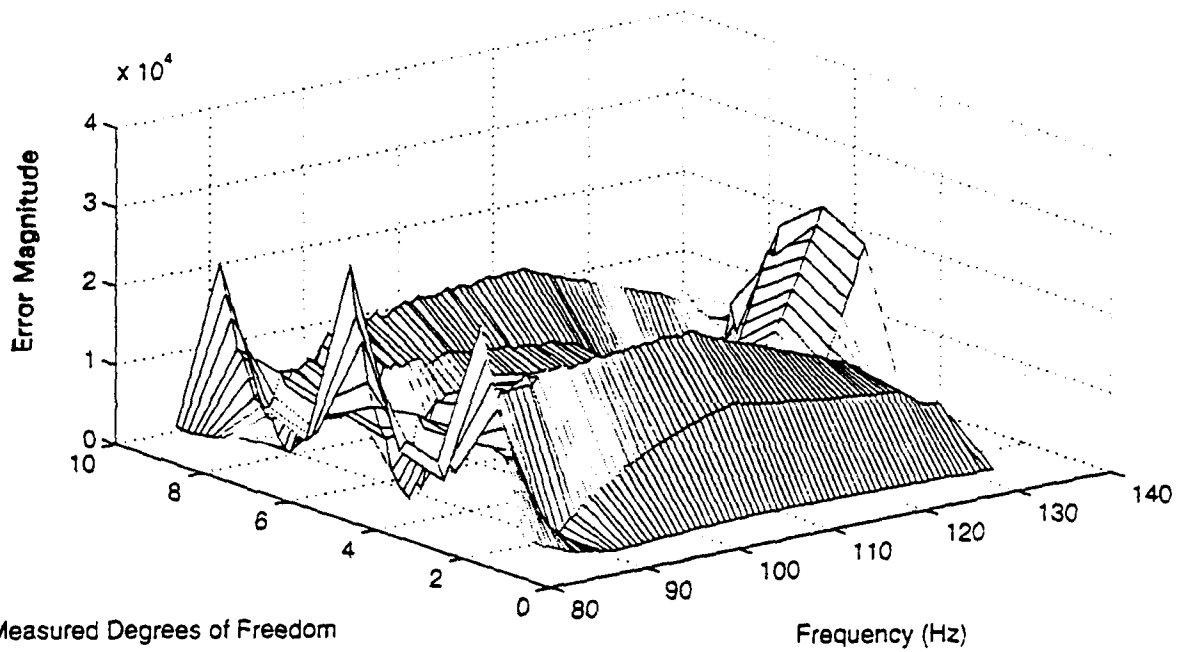
FE vs Experimental Localization



**Figure 5-24** FE model/composite beam magnitude localization, 82-133 Hz, beam damage: 2.25" length central delamination.
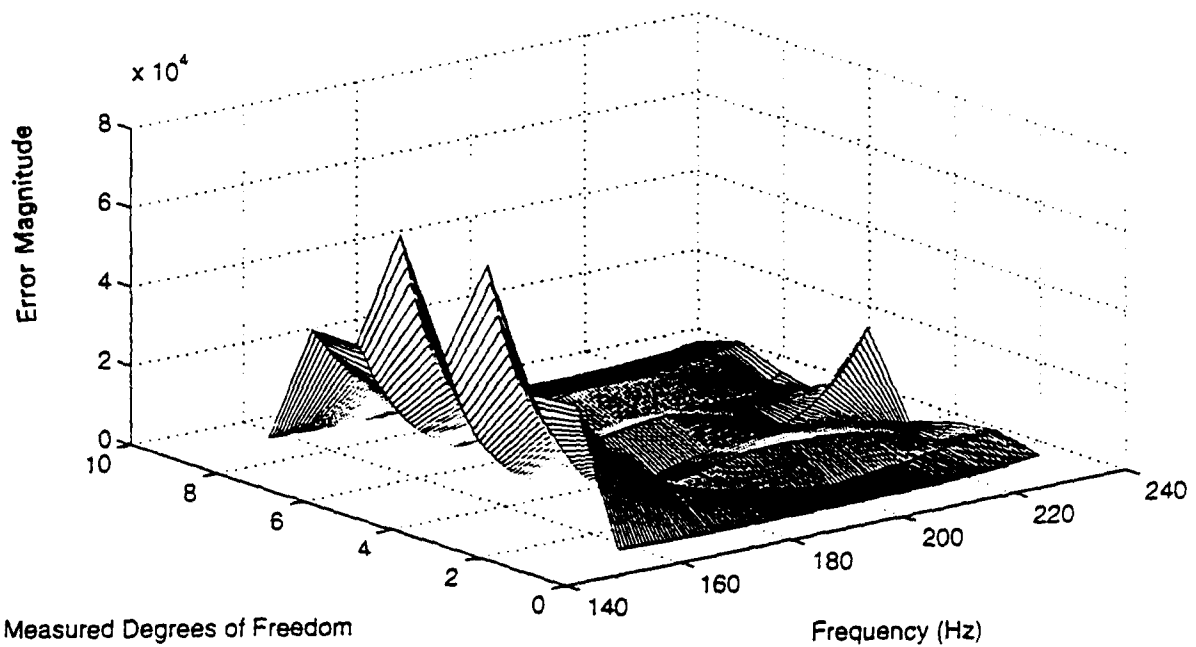
FE vs Experimental Localization



**Figure 5-25** FE model/composite beam magnitude localization, 158-233 Hz, beam damage: 2.25" length central delamination.
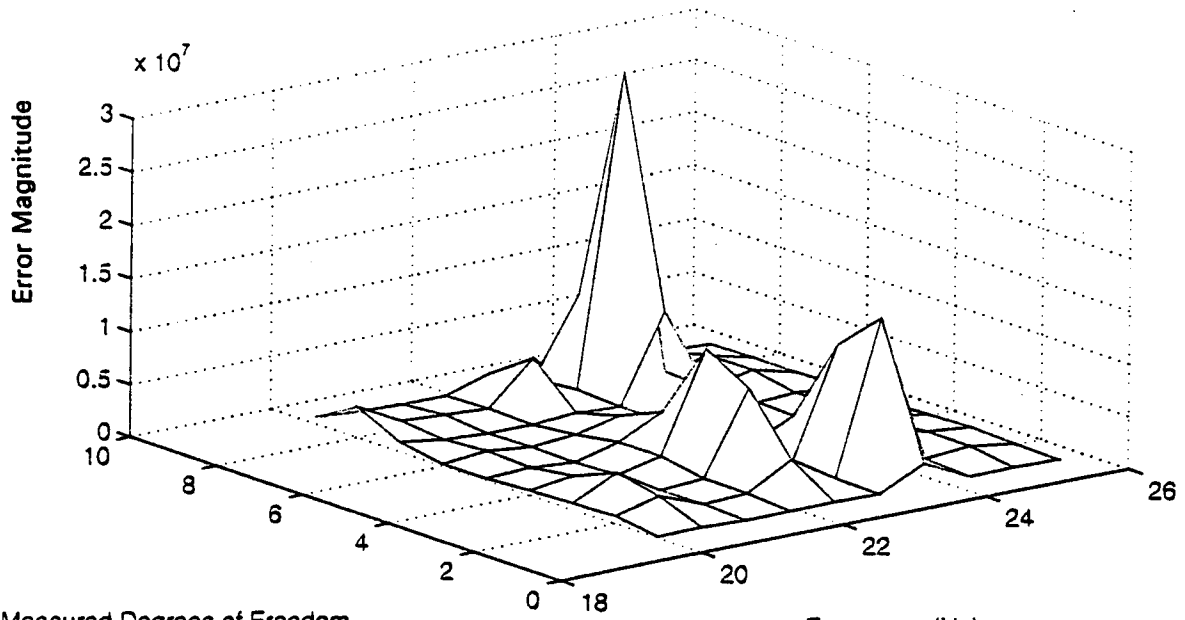
Experimental vs Experimental Localization

**Figure 5-26** Undamaged/damaged composite beam magnitude localization, 20-26 Hz, damage: 2.25" central delamination.
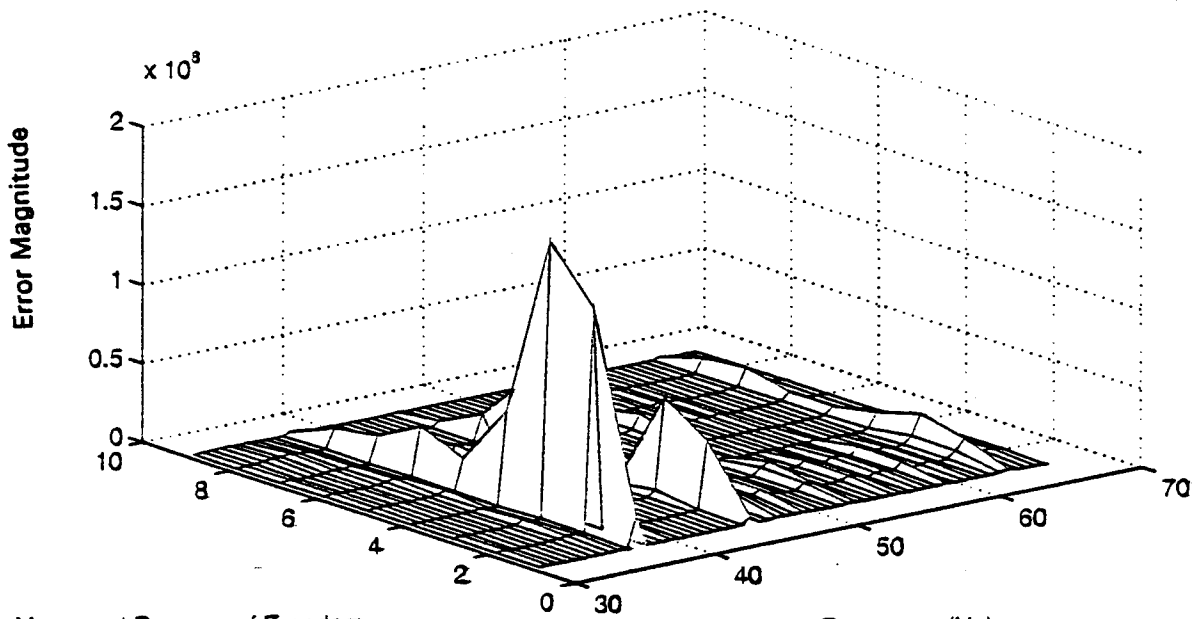


Experimental vs Experimental Localization

**Figure 5-27** Undamaged/damaged composite beam magnitude localization, 30-68 Hz, damage: 2.25" central delamination.

91
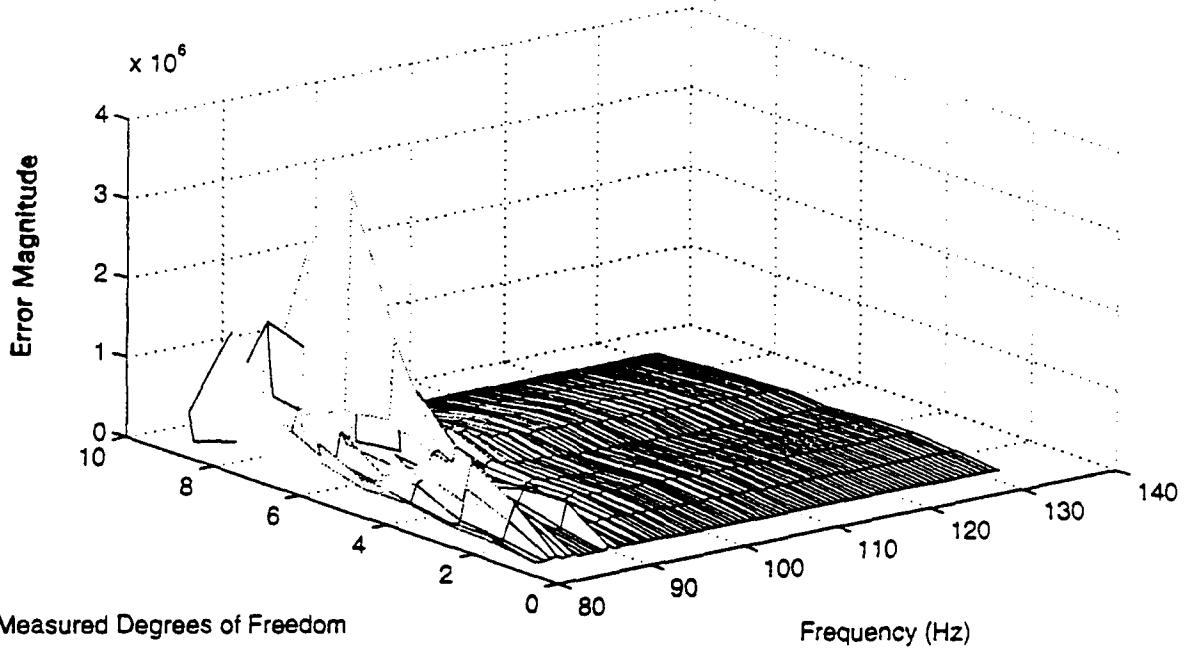
Experimental vs Experimental Localization

**Figure 5-28**    Undamaged/damaged composite beam magnitude localization, 82-133 Hz, damage: 2.25" central delamination.



Experimental vs Experimental Localization
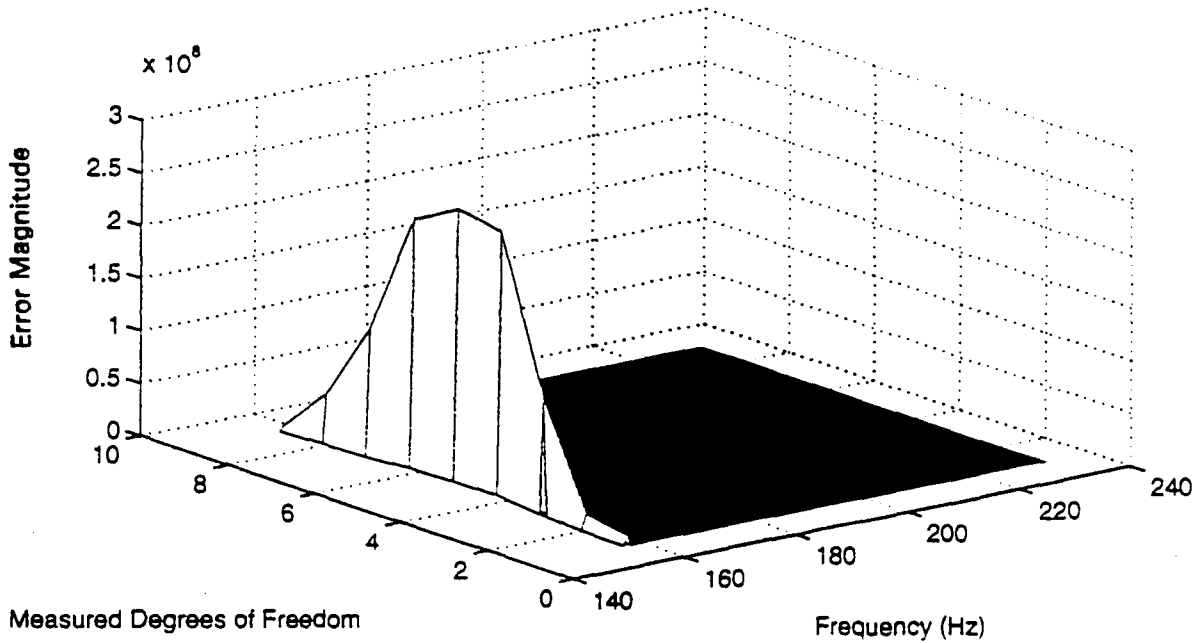
**Figure 5-29** Undamaged/damaged composite beam magnitude localization, 158-233Hz, damage: 2.25" central delamination.

## VI.  CONCLUSIONS / RECOMMENDATIONS

### A.  SUMMARY

Frequency domain error localization was applied to the damage detection problem.  Structural dynamic model error identification using spatially incomplete data was performed both theoretically and experimentally.  The investigations into structural damage detection using frequency domain analysis have shown the following:

- frequency domain localization is preferred over traditional modal methods because modal identification requirements are eliminated, permitting direct updating of FRF models and avoiding modal truncation errors

- the localization theory presents an exact solution for the location of differences between two frequency response functions, given spatially complete data

- localization must be performed over a frequency bandwidth to provide sufficient information to draw error location conclusions

- frequency bandwidth selection is important; lower frequency ranges revealed a greater propensity for error detection, and inter-resonant regions in general, devoid of natural frequency scaling, yielded more reliable localization information

- damage size impacts localization in that minor changes in structural stiffness can potentially go undetected, ergo, FE-experimental analyses inability to distinguish delamination damage

- localization using all experimental data demonstrates merit and warrants further investigation

- measurement noise, as expected, is detrimental to the error identification process and needs to be significantly reduced

93

## B. CONCLUSIONS

Factors which greatly detracted from the localization process were data incompleteness, noise, test frequency bandwidth selection, and damage size. Spatially incomplete localization results in smeared error location information in the absence of noise. Adding measurement noise, inherent in all real experimental measurement, further distorts error detection information by magnifying spurious, or alien errors and suppressing true error information. Test noise complicates the localization process by challenging the analyst to differentiate noise contribution from true errors, an impossibility without quantifiable noise measurements. Frequency bandwidth selection analysis, in FE simulation, indicated that perhaps there exists a preferred frequency region for localization which is a function of FE-experimental FRF correlation. Our FE model FRF matched the experimental no crack beam FRF very closely in the lower frequency range of our test bandwidth and worsened with increasing frequency. Results demonstrated greater localization trends in this region. Were the FE model constructed to accurately describe higher mode natural frequencies at the expense of lower mode frequencies, the trend might differ. FE-experimental localization results did not distinguish between damaged and undamaged beams. Interestingly, both beams reflected central damage of comparable magnitude, whereas the experimental-experimental localization revealed central damage an order of magnitude greater. Unable to quantify the measurement noise content in the localization methods, we are unable to assess whether experimental-experimental localization results are valid or an anomaly resulting from the combination of spatially incomplete test data and measurement noise. Whatever the mechanism, the fact that central damage is identified consistently, although badly scaled, warrants

94

further investigation of experimental localization. FE simulation demonstrated that larger cracks have greater chance of detection through the measurement noise floor, but this would have to be shown experimentally to validate FE model results.

## C. RECOMMENDATIONS

Frequency domain error localization methods showed positive results, theoretically and experimentally. However, several problems were revealed that prevent the localization theory from being employed exclusively when investigating structural damage. Recommendations to address the problems revealed in this thesis include:

- perform tests with multi-channel acquisition system

- employ advanced definitions of the frequency response function in FRF estimators such as H1 and H2 which account for output and input noise, respectively

- conduct localization using expanded test matrices to eliminate spurious errors stemming from FE model reduction methods

- reconstruct FRF using modal curve fitting methods to deal with noise

- use multi-exciter testing to ensure more even distribution of energy throughout structure, while maintaining reasonable force levels

- employ laser-based dynamic response measurement methods to collect "noise-free" FRF

Multi-channel acquisition systems permit higher quality tests, because the analyst acquires data on all response channels simultaneously, thereby ensuring structure invariance during testing. Newer acquisition systems employ advanced FRF definitions, designed specifically to deal with noisy situations [Ref. 13:p. 1049].

Reduction methods impose distortion in localization methods. Matrix expansion methods are available which would build test data FRF to a full order matrix, which is then compared to its full order FE model. Localization under these circumstances should be significantly improved.

Curve fitting FRF to identify modal parameters of a damaged structure and then reconstructing test FRF from smoothed data could greatly reduce the noise contribution and improve error localization. Constructing FRF from modal parameters calculated independently of load measurement also should result in improved localization.

Laser-based methods of dynamic response measurement eliminate virtually all of the problems encountered in this thesis, with the exception of spatially incomplete measurement.

# APPENDIX A.   COMPOSITE BEAM SPECIFICATIONS

Composite beams were obtained from Composite Structures Technology, Inc. for experimental localization.  The ordered design specifications were as follows:
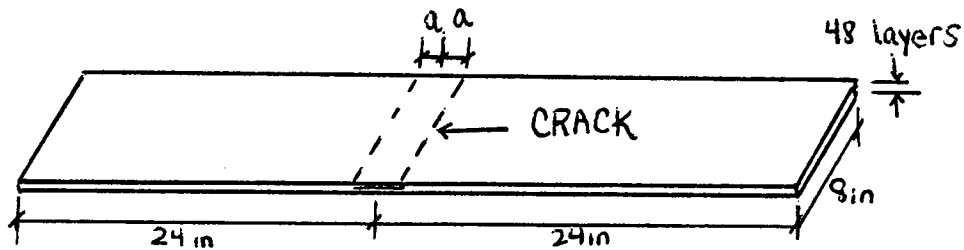


Crack:   through the width; located at the center of the length as well as in the middle of the thickness.

lengths(za) = 0 (no crack) and 2.25 in

layup orientations:  $[[0 \deg/90 \deg/+45 \deg/-45 \deg]_6]_{symmetric}$
(total 48 layers)
<--> 0 degree direction

Material:   Continuous carbon fiber/epoxy

## CARBON PREPREG TAPE

CST carbon laminates, panels and plates are composed of single or multiple layers of unidirectional carbon prepreg and may include other composite materials per part specification. The carbon prepreg tape in these parts is a hotmelt, 250 degree F, curable epoxy resin reinforced with unidirectional carbon fibers. The carbon fiber characteristics are:

| | |
|---|---|
| 0° Tensile strength at 77° F | 520,000 psi |
| 0° Tensile modulus at 77° F | $34 \times 10^6$ psi |
| Density | 0.065 lb/in$^3$ |

This information has been furnished by the prepreg manufacturer and is not guaranteed to be completely accurate. Users are advised to make their own tests to determine the safety and suitability of each such product or product combinations for their own purposes. Unless otherwise agreed in writing, we sell the products without warranty, and buyers and users assume all responsibility and liability for loss or damage arising from the handling and use of our products, whether used alone or in combination with other products.

Upon receipt of the composite beams, the following measurements were obtained:

length: 48 inches

width: 5.723 inches

thickness: 0.2911 inches

weight: 4.094 lbs

Material properties were not provided. Composite EI was determined by performing four-point bending tests on representative coupons. Load increments were applied to composite samples of 0, 45, and 90 degree layup orientations. The resultant longitudinal and transverse strains were measured from attached strain gages. Figures 5-1 and 5-2 demonstrate the test configuration. MATLAB routines COMP.M and PROPS.M determine the modulus of elasticity for each layup orientation and the aggregate EI for our test beam. Variables load#, longx#, and transx#, represent the applied load, longitudinal strain, and transverse strain, respectively, for each layup.

% Composite Measured Strain For Four Point Bending Model

------------------------------------
% 0 degree layup orientation
------------------------------------

```
load0=[0 28 30 51 52 52.5 75 77 100.5 101.5 102.5 125.5 126.5 152 153 153.5 ...
       175.5 201.5 203 227 253 253.5 255 302.5 352 377.5 403 427.5 452 476 ...
       501 502 527 552 577 602.5 626.5 652 675.5 703 727.5 749.5 778 778.5 ...
       798 827 851 877 902 904 925 950 978 1001 1025 1070];
longx0=[0 216 221 371 375 396 543 577 723 743 744 914 911 1091 1086 1103 1255 ...
       1438 1424 1608 1763 1781 1786 2087 2416 2583 2754 2911 3063 3216 3376 ...
       3410 3530 3679 3832 3982 4116 4265 4396 4540 4674 4802 4943 4953 5059 ...
       5207 5326 5464 5568 5562 5679 5777 5914 5998 5996 6260];
transx0=[0 -74 -63 -107 -111 -126 -155 -171 -207 -218 -214 -269 -264 -318 -316 ...
       -324 -371 -425 -417 -476 -518 -528 -524 -615 -713 -763 -813 -857 -903 ...
       -945 -990 -1011 -1032 -1075 -1115 -1157 -1192 -1232 -1265 -1304 -1336 ...
       -1369 -1402 -1424 -1430 -1464 -1503 -1544 -1575 -1569 -1586 -1609 ...
       -1664 -1709 -1687 -1804];

c0=polyfit(load0,longx0,1);
d0=polyfit(load0,transx0,1);
fit10=polyval(c0,load0);
fit20=polyval(d0,load0);

figure (1)

subplot(211), plot(load0,fit10)
title('Strain vs. Load - 0')
xlabel('Applied Load (lbs)')
ylabel('Longitudinal Strain (in^-6)')
grid
gtext('U = 6.0166*P + 199.6878')

subplot(212), plot(load0,fit20)
title('Strain vs. Load - 0')
xlabel('Applied Load (lbs)')
ylabel('Transverse Strain (in^-6)')
grid
gtext('U = -1.6948*P - 73.7285')
```

```
-------------------------------------
% 45 degree layup orientation
-------------------------------------
load45=[0 9.5 19.5 20.5 30.5 39.5 40 49.5 58.5 60 70 80 80 86.5 90.5 ...
       95 100 105 110 115 120.5 125 130 135.5 140 145.5 150 155 160 ...
       165 170 175 180 185 190 195 200 205.5 210 215 220];
longx45=[0 428 993 1032 1612 2160 2229 2780 3356 3378 4020 4620 4466 ...
        4869 5161 5489 5803 6175 6570 6922 7308 7702 8133 8527 8937 ...
        9301 9664 10013 10409 10880 11186 11472 11875 12242 12552 ...
        12849 13129 13419 13729 14021 14268];
transx45=[0 -358 -789 -816 -1235 -1621 -1661 -2051 -2460 -2465 -2927 ...
         -3360 -3256 -3556 -3769 -4020 -4247 -4538 -4815 -5105 -5380 ...
         -5689 -5996 -6305 -6582 -6892 -7165 -7461 -7769 -8194 -8452 ...
         -8740 -9101 -9478 -9740 -10079 -10325 -10636 -10924 -11235 -11476];

c45=polyfit(load45,longx45,1);
d45=polyfit(load45,transx45,1);
fit145=polyval(c45,load45);
fit245=polyval(d45,load45);

figure (2)

subplot(211), plot(load45,fit145)
title('Strain vs. Load - 45')
xlabel('Applied Load (lbs)')
ylabel('Longitudinal Strain (in^-6)')
grid
gtext('U = 68.0480*P - 612.0741')

subplot(212), plot(load45,fit245)
title('Strain vs. Load - 45')
xlabel('Applied Load (lbs)')
ylabel('Transverse Strain (in^-6)')
grid
gtext('U = -53.5477*P + 684.0852')
```

```
---------------------------------------
% 90 degree layup orientation
---------------------------------------

load90=[0 3 5 5 6 6 9 10 10 12 14 15 16.5 18.5 20 20 25 30 35 40 45 50 55 60 65 70];
longx90=[0 185 466 475 454 562 714 964 1017 1126 1490 1657 1754 1982 ...
        2167 2189 2752 3327 3863 4386 4883 5426 5892 6386 6806 7270];
transx90=[0 -4 -5 -9 -7 -6 -13 -15 -24 -20 -24 -37 -31 -33 -39 -50 -59 ...
        -73 -82 -95 -102 -116 -122 -132 -136 -145];
c90=polyfit(load90,longx90,1);
d90=polyfit(load90,transx90,1);
fit190=polyval(c90,load90);
fit290=polyval(d90,load90);

figure (3)

subplot(211), plot(load90,fit190)
title('Strain vs. Load - 90')
xlabel('Applied Load (lbs)')
ylabel('Longitudinal Strain (in^-6)')
grid
gtext('U = 107.7238*P - 49.5720')


subplot(212), plot(load90,fit290)
title('Strain vs. Load - 90')
xlabel('Applied Load (lbs)')
ylabel('Transverse Strain (in^-6)')
grid
gtext('U = -2.2546*P + 2.8920')
```

```
format long
%  Aggregate Properties of Composite Beam

step = 0.2911/48;
z = 0:step:0.2911;
modulus = [24384000 1362000 2156000 2156000 24384000 1362000 2156000 ...
          2156000 24384000 1362000 2156000 2156000 24384000 1362000 ...
          2156000 2156000 24384000 1362000 2156000 2156000 24384000 ...
          1362000 2156000 2156000 2156000 2156000 1362000 24384000 ...
          2156000 2156000 1362000 24384000 2156000 2156000 1362000 ...
          24384000 2156000 2156000 1362000 24384000 2156000 2156000 ...
          1362000 24384000 2156000 2156000 1362000 24384000];
modulus_sum = 0
for i= 1:48
   modulus_sum = modulus_sum + (modulus(i)*((z(i+1).^3 - z(i).^3)));
end
modulus_eff = modulus_sum./3
```

## APPENDIX B.  EXPERIMENTAL SETUP

The experimental setup involved the selection of test equipment, test equipment calibration (as necessary), and the determination of test settings.  Test equipment, experimental setup, system calibration, and measurement unit analysis are discussed below.  Signal analyzer test settings are listed at the rear of this Appendix.

### A.  TEST EQUIPMENT / EXPERIMENTAL SETUP

The following test equipment was employed for frequency response function measurement and data transfer:

- HP 3562A Dynamic System Signal Analyzer

- PM25A Vibration Exciter (Shaker)

- MB Dynamics SS250VCF Amplifier

- Translational Angular Piezobeam (TAP) System Model 8832

- (TAP) Accelerometer

- Integrated Circuit Piezoelectric (ICP) Transducer

- HP9122 Disk Drive

- Datastor 486DX-66MHz computer

Figure B-1 demonstrates the experimental setup.  Figure B-2 describes the measurement chain.
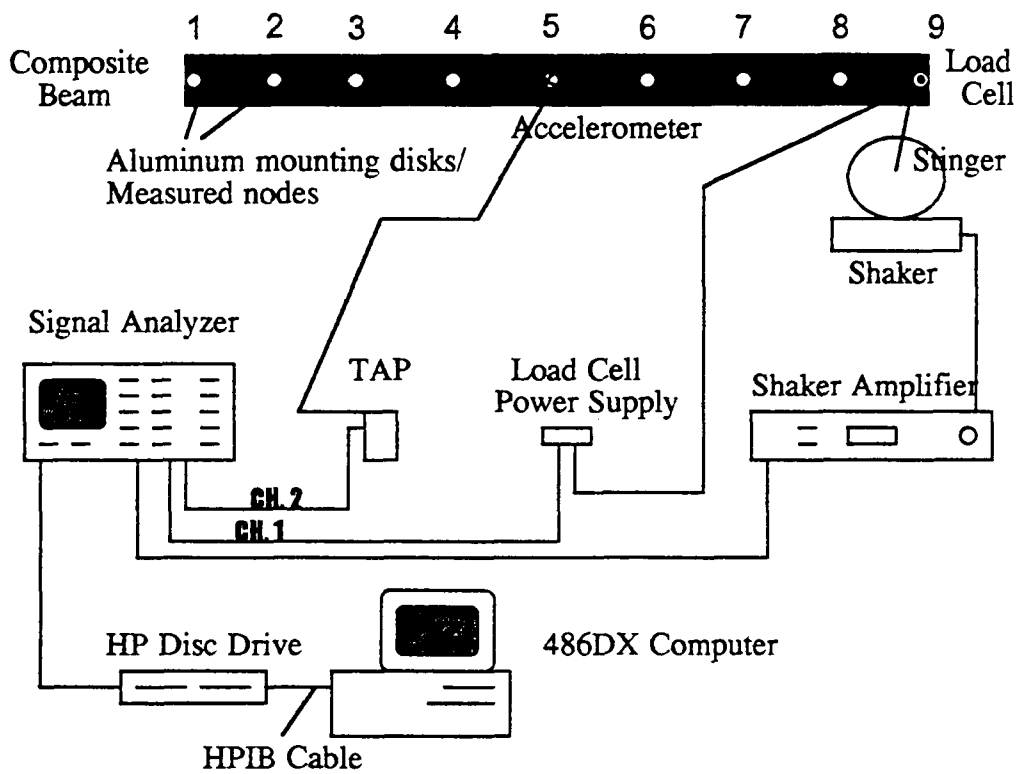
**Figure B-1** Experimental setup.
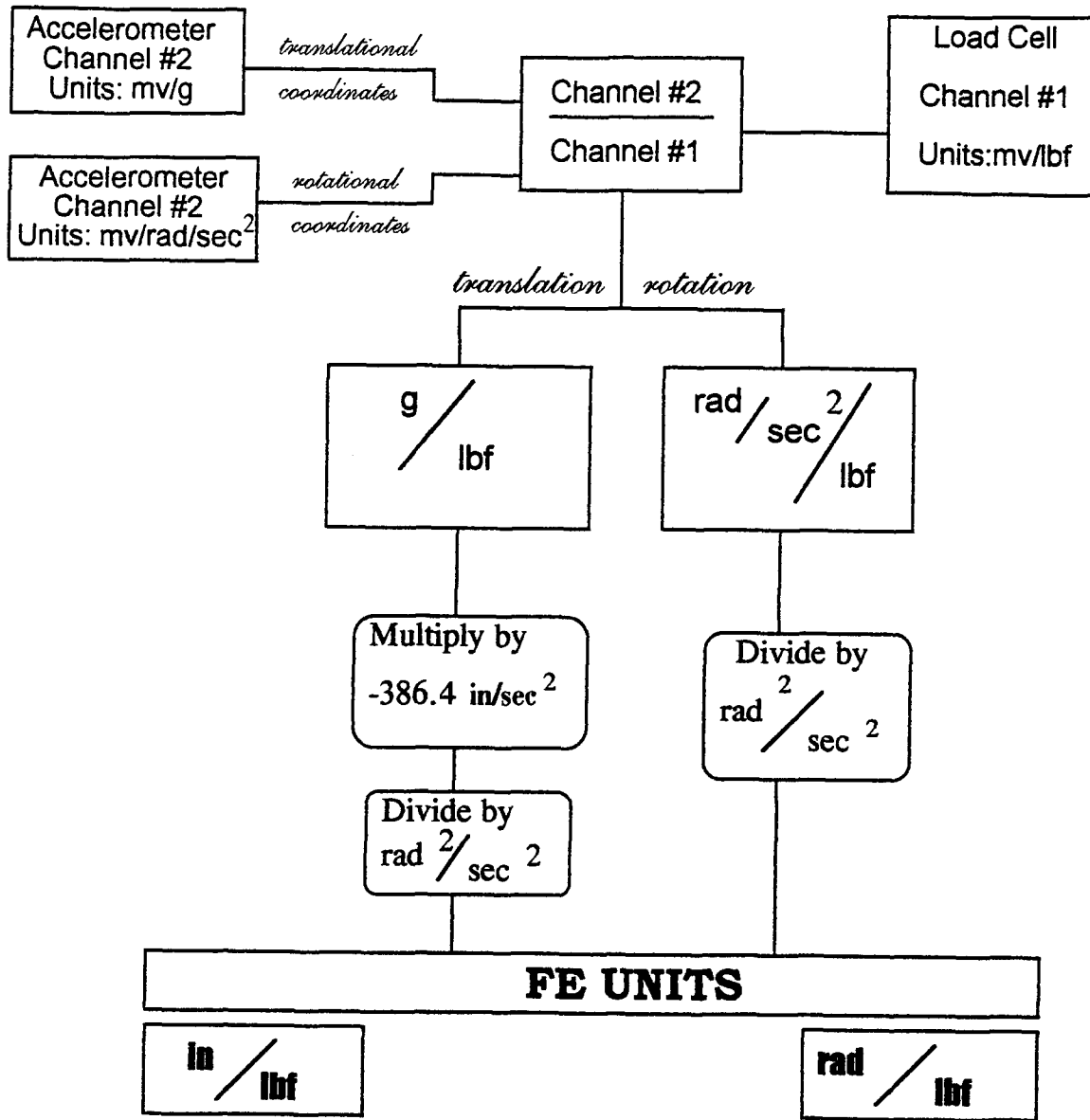
**Figure B-2** Unit measurement chain.

## B. LUMPED MASS TEST

Preparing the test system for measurement involved verification of measurement device sensitivities, which are listed at the end of this Appendix. The sensitivities specified by the manufacturer for the load cell and the accelerometer were entered into the signal analyzer. A lumped mass of comparable weight to our composite beam was used to assess whether sensitivities provided were still valid. The FRF for a lumped mass is the inverse of its mass. Hence, our measured FRF should reflect this condition. The load cell sensitivity is adjusted until this condition is satisfied. The manufacturer provided sensitivity for our force transducer was 52.56 mv/lbs. The sensitivity determined by our lumped mass test was 55.8 mv/lbf. The following calculations demonstrate the lumped mass verification process:

Lumped mass {aluminum disk} analysis

aluminum disk mass     =  3.744 lbf     (as measured)
accelerometer mass     =  0.02513 lbf
force transducer mass  =  0.05203 lbf
        >>      total mass = 3.821 lbf


HP DSA output using load cell sensitivity 55.8 mv/lbs,
avg. left of 60Hz spike, -11.633 dB
avg. right of 60Hz spike, -11.642 dB
        overall avg     =       -11.642 dB


    20 log x =  [ ] dB
20 log (1/m) = -11.642 dB
   log (1/m) = -0.5821
         1/m = 0.26176
           m = 3.8207 lbf (checks!)

106

# KISTLER

## Calibration Certificate

## TAP™

### TRANSLATIONAL ANGULAR PIEZOBEAM SYSTEM MODEL 8832

```
Accelerometer Model 8696.............................SN C58086
Coupler Model 5130..................................SN C33406
```

| | |
|---|---|
| Angular Sensitivity at 250 Hz, 130 rad/s² | 0.483 mV/rad/s² |
| Linear Sensitivity at 100 Hz, 3g$_{ras}$ | 1024 mV/g |

```
        Linear Range ...................... ±10 g
        Angular Range ..................... ±18,000 rad/s²
        Mounted Resonant Frequency (nom.) . 8 kHz
        Transverse Sensitivity max. ....... 2%
        Bias Voltage ...................... 11 ±3 VDC
        Time Constant (nom.) .............. 1.0 s
```

All measurements at 21°C
$g = 9.807 \ m/s^2$

### NIST TRACEABILITY

This accelerometer was calibrated using a back to back comparison technique against a Kistler Working Standard. The Working Standard is periodically calibrated against a Kistler Reference Standard System which in turn is periodically recertified by the National Institute of Standards and Technology. The calibration of all Kistler acceptance test instrumentation is in conformance with MIL-STD-45662A.

|  | Working Standard | Reference Standard |
|---|---|---|
| Linear Acceleration: | | |
| Accelerometer | Model 809K112 SN C51785 | Model 8002K SN C17447 |
| Charge Amplifier | Model 5020 SN C31904 | Model 5020 SN C4870 |
| NIST Test Report Number: | | 822/250337 |
| Angular Acceleration: | | |
| Accelerometers | Model 8602A500M1 | Model 808K1 SN 1263 |
| | SN C36072/SN C36073 | |
| Charge Amplifiers | Model 504E10 | Model 561T SN 251 |
| | SN C4797/SN C4623 | |
| Summing Amplifier | Model 5217 SN 186396 | |

SEP 24 1993

By: _Mark Thomas_          Date: 09-24-1993
        Mark Thomas

107

# ICP CALIBRATION DATA

Model 208A02

S/N 10539

Cal Range 0 - 100 lbs.

Sens. 52.56 mv/lbs.

Linearity <1.0 %FS

* By comparison with reference standard per ISA S37.10. Zero Based best straight line.

Input TC >500 sec

Rise Time 10 usec

Nat'l Freq 70 kHz

Output Imp < 100 ohms

By Gary Redmond

Date Aug 31, 1993



Calibration of instrumentation used to certify this sensor is traceable to NIST.

PCB Piezotronics' calibration procedure is in compliance with MIL-STD-45662A.

5260 mV

4210 mV

3150 mV

2090 mV

1050 mV

OUTPUT-MILLIVOLTS (mV)

INPUT lbs.
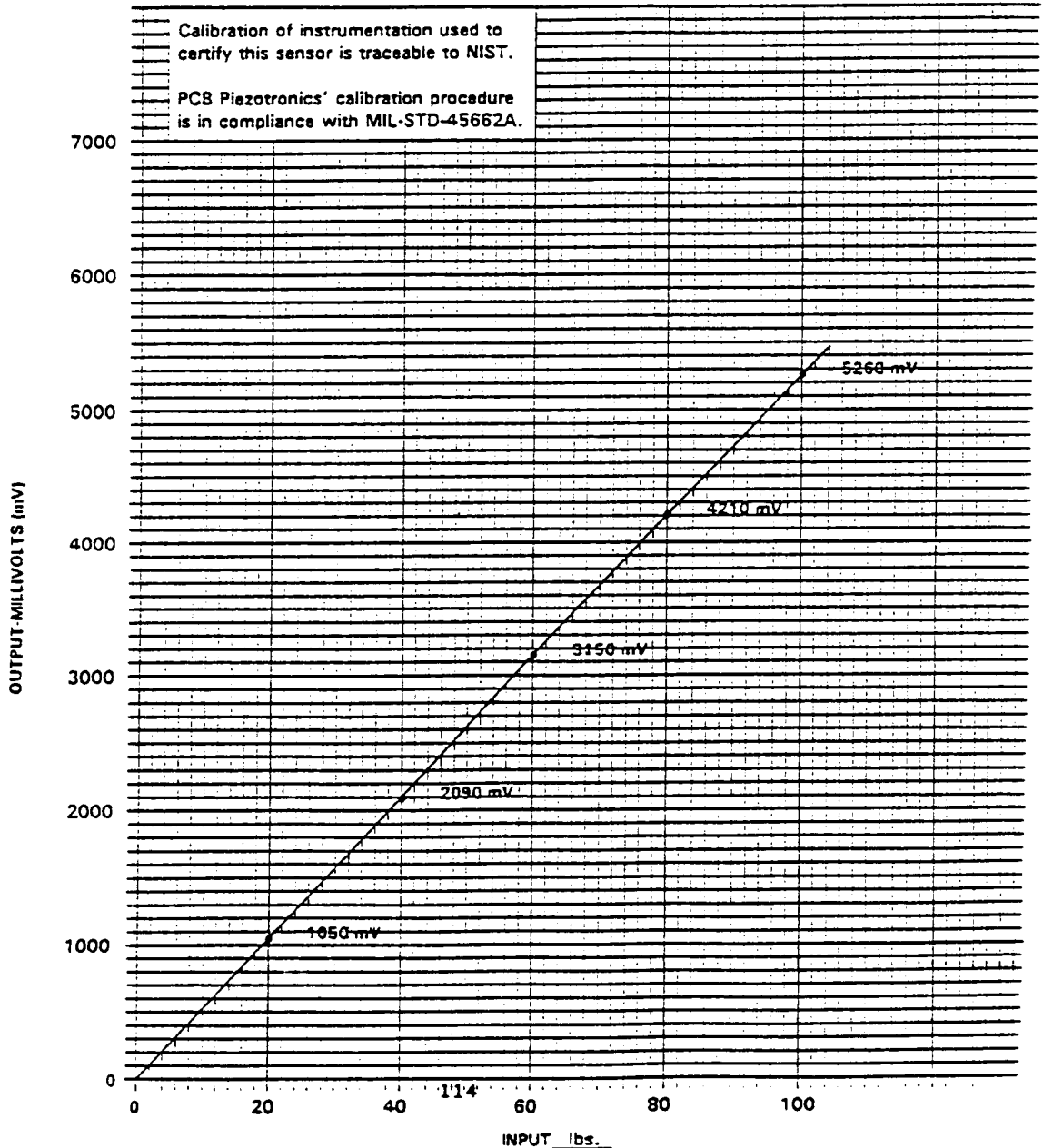
PCB PIEZOTRONICS. INC.
3425 Walden Avenue, Depew NY 14043
Tel:716-684-0001 TWX:710-263-1371

Customer _____

PO Number _____

108

# Linear Resolution

| | | | |
|---|---|---|---|
| **MEASURE:** | CHAN 1<br>Freq Resp | CHAN 2<br>Freq Resp | |
| **WINDOW:** | CHAN 1<br>Uniform | CHAN 2<br>Uniform | |
| **AVERAGE:** | TYPE<br>Stable | # AVGS<br>10 | OVERLAP<br>0% | TIME AVG<br>Off |
| **FREQ.** | CENTER<br>270 Hz | | SPAN<br>500 Hz | BW<br>625mHz |
| | REC LGTH<br>1.6 S | $\Delta$t<br>1.56mS | | |
| **TRIGGER:** | TYPE<br>Chan 1 | LEVEL<br>30.0$\mu$Vpk | SLOPE<br>Pos | PREVIEW<br>Off |
| **INPUT:**<br>CH 1<br>CH 2 | RANGE<br>39.9mVpk<br>200mVpk | ENG UNITS<br>55.8mV/EU<br>1.02 V/EU | COUPLING<br>AC (Flt)<br>AC (Flt) | DELAY<br>-50.0mS<br>-50.0mS |
| **SOURCE:** | TYPE<br>Burst Rndm | BURST<br>50% | LEVEL<br>250mVpk | OFFSET<br>0.0 Vpk |

## APPENDIX C.  FRF VERIFICATION

The following plots are provided for experimental FRF verification:

- transfer FRF reciprocity (H91), (H19)
- driving point coherence (H99)
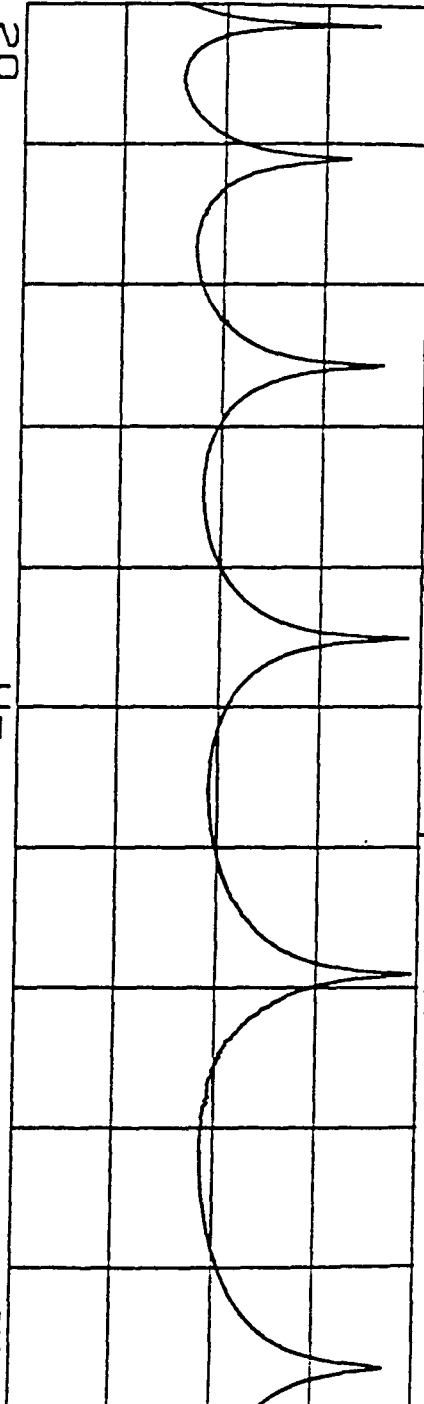
FREQ RESP H91    10Avg    0%Ovlp    Unif

FREQ
50.0

dB

G
LBF
-30.0

Fxd Y 20                                    Hz                      520

FREQ RESP    10Avg    0%Ovlp    Unif

FREQ
320

Imag

G
LBF
-320

Fxd Y 20                                    Hz                      520

112

FREQ RESP H19    20Avg    0%Ovlp Unif

dB

G
LBF
-30.0

Fxd Y 20                                    Hz                               520

FREQ RESP    20Avg    0%Ovlp Unif
320

Imag

G
LBF
-320

Fxd Y 20                                    Hz                               520

113
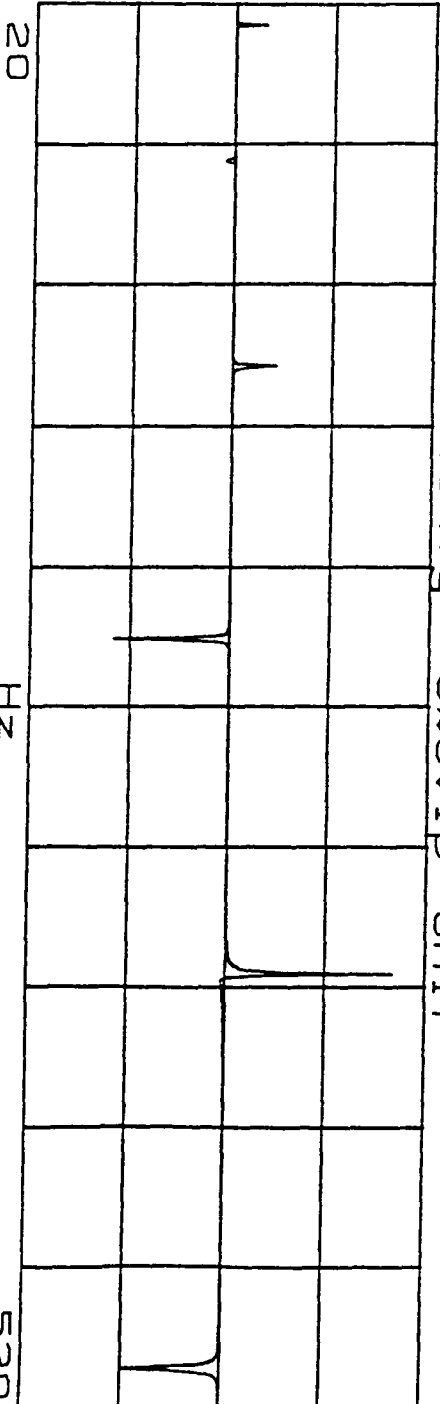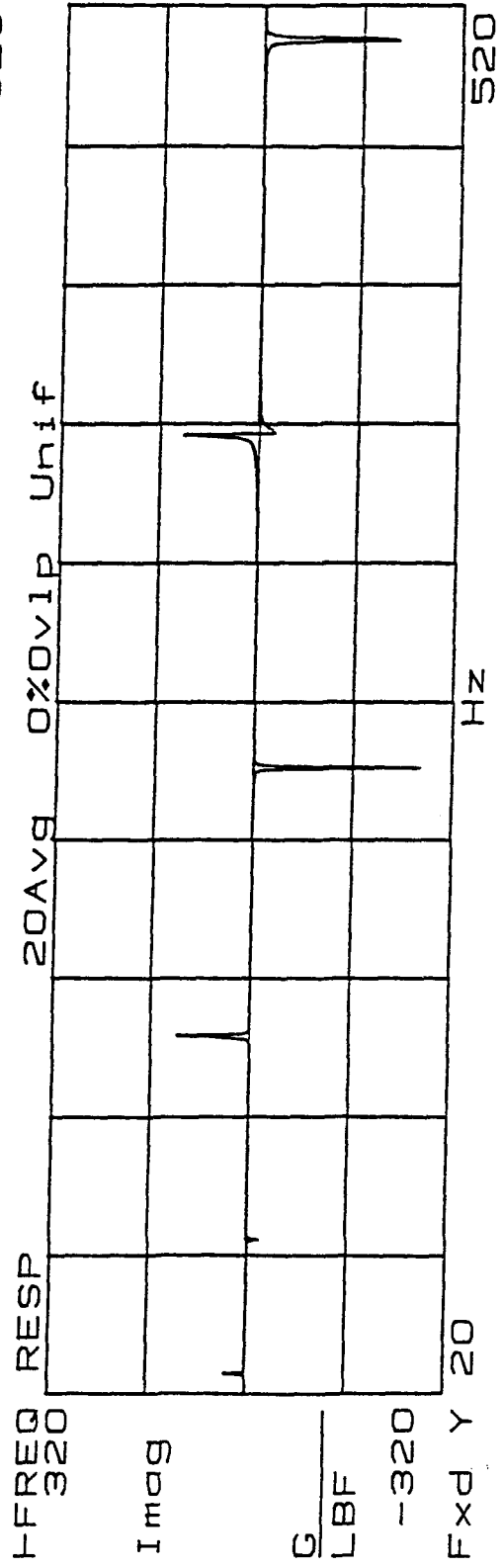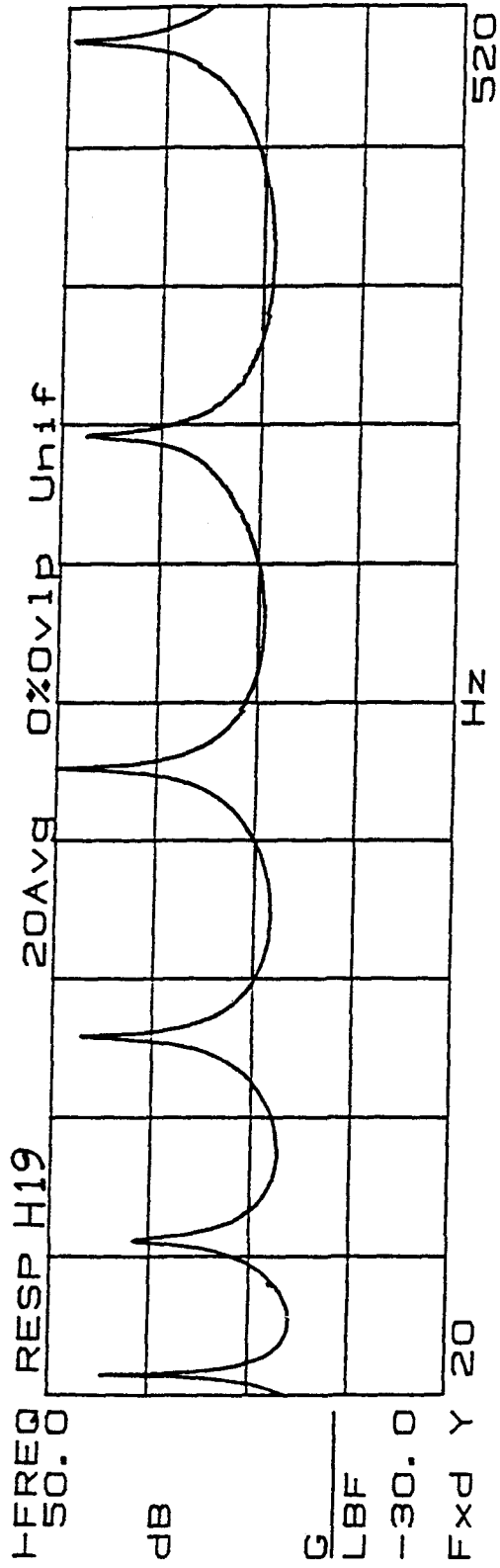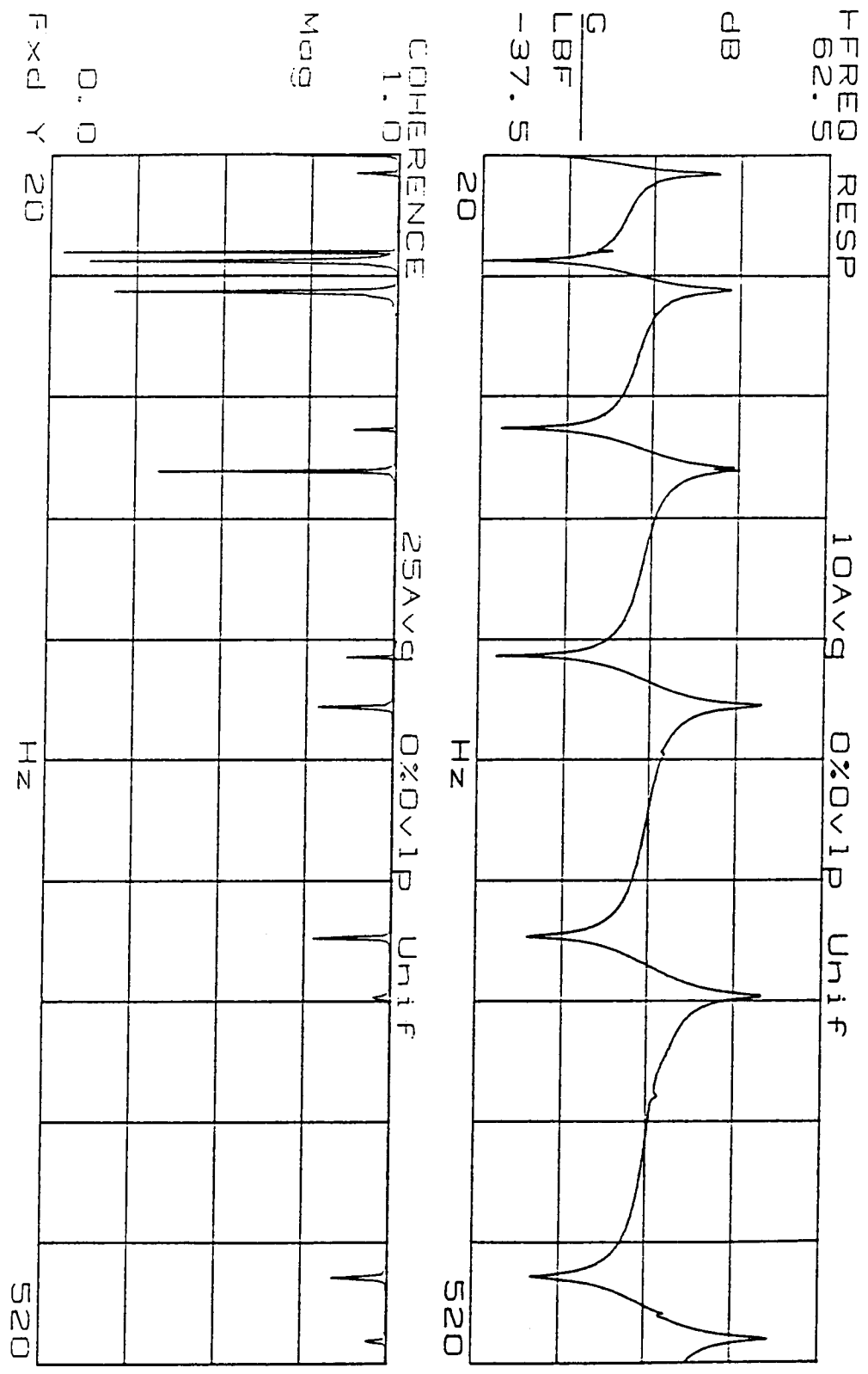
## APPENDIX D.  FE MODEL / COMPUTER CODES

The following is a brief description of MATLAB routines employed in this thesis:

- MODEL.M - Develops FE model FRF for composite beam.

- BUILD.M - Performs spatially incomplete localization by extraction reduction methods.

- BUILDIRS.M - Performs spatially incomplete localization by IRS reduction methods.

- FIRS_TAM.M - Routine which returns IRS reduced stiffness and mass matrices.

- FE_NOISE.M - Performs localization under simulated noise conditions.

- NOISEFILL.M - Routine which returns noisy FE FRF.

- LOADFRF.M - Builds experimental FRF matrix.  Converts analyzer output to units consistent with FE model.

- MAP.M - Ensures symmetry of test FRF matrix.

% __PURPOSE__ :   PROVIDE FINITE ELEMENT MODELING OF COMPOSITE BEAMS
% BACKGROUND: BERNOULLI-EULER THEORY IS EMPLOYED TO
% FORMULATE ELEMENTAL STIFFNESS AND MASS MATRICES.
% AXIAL DEFLECTION ASSUMED NEGLIGIBLE.  LUMPED MASSES INCLUDED.

%
% VARIABLES  USED IN THIS PROGRAM:
%
% conn - connectivity matrix
% ke/me -  elemental stiffness/mass matrices
% kglobal/mglobal - global stiffness/mass matrices
% matprops - matrix of EI, rho, area, length
% le - left end of element
% re - right end of element
% noel - # of elements
% nonodes - # of nodes
% ndof - # of degrees of freedom
% aset - retained coordinates (corresponding to measured coordinates)
% oset - omitted coordinates (coordinate set unavailable from test data)

```
format long
noel = 48;
span = 48;
nonodes=noel+1
ndof = nonodes*2
meas=ndof-1;
matprops = zeros(noel,4);
```

% ASSIGN ELEMENT MATERIAL PROPERTIES

```
for j=1:noel
matprops(j,1)= 0.05; % mass density [lbm/cu.in] each element
matprops(j,2)= 1.666; % cross sectional area [sq.in] each element
matprops(j,3) = 7.45e4;  % EI [lbf-in^2] each element
matprops(j,4) = span./noel;   % length [in] of each element
l(j)=matprops(j,4);
c1(j)=matprops(j,3)./(matprops(j,4).^3);
c2(j)=(matprops(j,1)./386.4)*matprops(j,2)*matprops(j,4)./420;
end;
```

% length=60.625"  width=1.5656"  thickness=0.5339"  density=0.284 lbf/cu.in.
% E=28e6psi

% INITIALIZE ELEMENTAL/GLOBAL MATRICES

```
ke = zeros(4,4);
me = zeros(4,4);
kglobal = zeros(ndof,ndof);
mglobal = zeros(ndof,ndof);
```

```
%  ASSEMBLE CONNECTIVITY MATRIX

for i = 1:noel;
   for j = 1:noel;
      conn(i,1) = i;
      conn(j,2) = j+1;
   end
end


%  ASSEMBLE GLOBAL STIFFNESS AND MASS MATRICES

for i = 1:noel;

le = conn(i,1).*2 - 1;   % le - refers to left end
re = conn(i,2).*2;       % re - refers to right end


kc = c1(i).*[12  6*l(i)  -12  6*l(i);...
             6*l(i)  4*(l(i).^2)  -6*l(i)  2*(l(i).^2);...
             -12  -6*l(i)  12  -6*l(i);...
             6*l(i)  2*(l(i).^2)  -6*l(i)  4*(l(i).^2)];

me = c2(i).*[156  22*l(i)  54  -13*l(i);...
             22*l(i)  4*(l(i).^2)  13*l(i)  -3*(l(i).^2);...
             54  13*l(i)  156  -22*l(i);...
             -13*l(i)  -3*(l(i).^2)  -22*l(i)  4*(l(i).^2)];

kglobal(le:(le+1),le:(le+1)) = kglobal(le:(le+1),le:(le+1))+ke(1:2,1:2);
kglobal(le:(le+1),(re-1):re) = kglobal(le:(le+1),(re-1):re)+ke(1:2,3:4);
kglobal((re-1):re,le:(le+1)) = kglobal((re-1):re,le:(le+1))+ke(3:4,1:2);
kglobal((re-1):re,(re-1):re) = kglobal((re-1):re,(re-1):re)+ke(3:4,3:4);

mglobal(le:(le+1),le:(le+1)) = mglobal(le:(le+1),le:(le+1))+me(1:2,1:2);
mglobal(le:(le+1),(re-1):re) = mglobal(le:(le+1),(re-1):re)+me(1:2,3:4);
mglobal((re-1):re,le:(le+1)) = mglobal((re-1):re,le:(le+1))+me(3:4,1:2);
mglobal((re-1):re,(re-1):re) = mglobal((re-1):re,(re-1):re)+me(3:4,3:4);

end

%  ADD LUMPED MASS/INERTIA TERMS

for disp = 1:12:ndof-1;
   rota = disp + 1;
   lump = 7.39e-5;  % mass of mounting disks [lbf-sec^2/in]
   inert = 8.083e-6;  % mass inertia of disks [lbf-sec^2-in]
   mglobal(disp,disp) = mglobal(disp,disp) + lump;
   mglobal(rota,rota) = mglobal(rota,rota) + inert;

end
```

```
%  COMPUTE NATURAL FREQUENCIES AND MODE SHAPES

   [psi,lambda] = eig(mglobal\kglobal);

   [lambda_diag,corrn] = sort(diag(lambda));

   for i = 1: length(lambda);
     lambda(i,i)= lambda_diag(i);
   end

   wn = sqrt(lambda);        % wn (rad/sec)
   freqs= diag(wn)/(2*pi);    % freqs (Hz)


%  IDENTIFY FREQUENCY RANGE OF ANALYSIS

   wcnt=0;
   mult1=o2i1x;
   range=(1:length(mult1));
   mult = mult1*2*pi;


%  ASSEMBLE REDUCTION ASET/OSET PARAMETERS FOR TRANSLATION AND
ROTATION

   aset=[1:noel/4:ndof-1];
   a1=aset(1,2);
   a2=aset(1,3);
   a3=aset(1,4);
   a4=aset(1,5);
   a5=aset(1,6);
   a6=aset(1,7);
   a7=aset(1,8);
   a8=aset(1,9);
   keep=length(aset);
   oset=[2:a1-1,a1+1:a2-1,a2+1:a3-1,a3+1:a4-1,a4+1:a5-1,a5+1:a6-1,...
       a6+1:a7-1,a7+1:a8-1,ndof];

   asetrot=[2:noel/4:ndof];


%  BUILD LOCALIZATION MATRIX

loc = zeros(ndof,length(mult));

crush=input('Choose analysis method: (1) Extraction  (2) IRS  => ');

if crush == 1
      build
    else
      buildirs
end
```

```
%*********************************************************************
% PURPOSE: CONSTRUCT USEFUL FRF MATRICES FROM EXPERIMENTAL DATA.
% ASSEMBLE LOCALIZATION MATRIX FROM EXPERIMENTAL FRF DATA.  THIS
% M-FILE PERFORMS LOCALIZATION BASED UPON EXTRACTION REDUCTION.
%*********************************************************************

  ndofr=18;          % Measured Degrees of Freedom
  nodes=9;           % Number of Measured Nodes

FRF0=FRF0(range,:);
FRF225=FRF225(range,:);
turn=[60 30];

wcnt=0;
for val = 1:length(range);

  h_fill=zeros(ndofr,nodes);
  h_fillx=zeros(ndofr,nodes);
  index=0;

  for ii=1:2:ndofr-1
    for jj=1:nodes
        index=index+1;
        h_fill(ii,jj)=FRF0(val,index);
        h_fillx(ii,jj)=FRF225(val,index);
    end
  end

  for ii=2:2:ndofr
    for jj=1:nodes
        index=index+1;
        h_fill(ii,jj)=FRF0(val,index);
        h_fillx(ii,jj)=FRF225(val,index);
    end
  end

  htrans_0=h_fill(1:2:ndofr-1,:);
  hrotat_0=h_fill(2:2:ndofr,:);

  htrans_225=h_fillx(1:2:ndofr-1,:);
  hrotat_225=h_fillx(2:2:ndofr,:);

% THIS LOOP ENSURES SYMMETRY OF THE EXPERIMENTALLY OBTAINED FRF.

for i = 1:nodes
 for j = i:nodes
      htrans_0(j,i)=htrans_0(i,j);
      htrans_225(i,j)=htrans_225(j,i);
      htrans_225(j,i)=htrans_225(i,j);
      hrotat_225(i,j)=hrotat_225(j,i);
 end
```

119

```
end
zt0 = inv(htrans_0);

zt225 = inv(htrans_225);

    z=kglobal-mult(val)^2*mglobal;
    ha= inv(z);    % Conversion to G's/lbf
    z=inv(ha);  map;
    haredt=ha(aset,aset);      % Reduced Analytical H (trans.)
    zredt=inv(haredt);
    wcnt=wcnt+1;
    hplot(wcnt)=ha(meas,meas);
    loc(:,val)=diag(z*deltah*z);
    locredt(:,val)=diag(zredt*deltaht*zredt);

diff_exp225=ha-ha_225;  % Full scale difference between FE and 2.25" beam

diff_exp0=ha-ha_0;  % Full scale difference between FE and No Crack beam

diffht_225=haredt-htrans_225;    % Diff FE/2.25" Crack H (trans.) 9x9

diffht_x=htrans_0-htrans_225;    % Diff No Crack/2.25" Crack H (trans.) 9x9

diffnocrackt=haredt-htrans_0;    % Diff FE/No Crack H (trans.)  9x9

loc225t(:,val)=diag(zredt*(diffht_225)*zredt);   % Localization Matrix FE/2.25" (trans.)

locexpt(:,val)=diag(abs(zt0)*(diffht_x)*abs(zt0));  % Localization Matrix Experimental
Matrices(trans.)

locfenocrackt(:,val)=diag(zredt*(diffnocrackt)*zredt); %  Localization Matrix FE/Nocrack (trans.)

locerrort=loc225t-locfenocrackt;   % Difference of FE/2.25" & FE/No Crack Localization Matrices
(trans.)

find225(:,val)= diag(za*(diff_exp225)*za);  %  Localization for FE/Experimental blend FRF

find0(:,val)= diag(za*(diff_exp0)*za);     %  Localization for FE/Experimental blend FRF

end

disp('***************** EXTRACTION REDUCTION EMPLOYED!!! *************')
```

```
%***********************************************************************
%  PURPOSE_ : CONSTRUCT USEFUL FRF MATRICES FROM EXPERIMENTAL
%  DATA. ASSEMBLE LOCALIZATION MATRIX FROM EXPERIMENTAL FRF
%  DATA.  IRS REDUCTION EMPLOYED.
%***********************************************************************

ndofr=18;          % Measured Degrees of Freedom
nodes=9;           % Number of Measured Nodes

FRF0=FRF0(range,:);
FRF225=FRF225(range,:);
turn=[60 30];

[kirs,mirs]=firs_tam(kglobal,mglobal,oset,aset);     % Calls function which returns kirs,
mirs
irslambda=eig(mirs\kirs);
irsfreqs=sort(sqrt(irslambda)/(2*pi))
wcnt=0;
for val = 1:length(range);

  h_fill=zeros(ndofr,nodes);
  h_fillx=zeros(ndofr,nodes);
  index=0;

  for ii=1:2:ndofr-1
    for jj=1:nodes
        index=index+1;
        h_fill(ii,jj)=FRF0(val,index);
        h_fillx(ii,jj)=FRF225(val,index);
    end
  end

  for ii=2:2:ndofr
    for jj=1:nodes
        index=index+1;
        h_fill(ii,jj)=FRF0(val,index);
        h_fillx(ii,jj)=FRF225(val,index);
    end
  end


htrans_0=h_fill(1:2:ndofr-1,:);
hrotat_0=h_fill(2:2:ndofr,:);

htrans_225=h_fillx(1:2:ndofr-1,:);
hrotat_225=h_fillx(2:2:ndofr,:);

% THIS LOOP ENSURES SYMMETRY OF THE EXPERIMENTALLY OBTAINED
FRF.

  for i = 1:nodes
```

```
for j = i:nodes
        htrans_0(i,j)=htrans_0(j,i);
        htrans_225(i,j)=htrans_225(j,i);

        hrotat_0(i,j)=hrotat_0(j,i);
        hrotat_225(i,j)=hrotat_225(j,i);
    end
end

zt0 = inv(htrans_0);

zt225 = inv(htrans_225);

    za=kglobal-mult(val)^2*mglobal;
    ha= inv(za);
    map;
    z=kirs-mult(val)^2*mirs;
    haredt=inv(z);      % Reduced Analytical H (trans.)
    zredt=inv(haredt);           % Reduced Analytical Z (trans.)
    wcnt=wcnt+1;
    hplot(wcnt)=ha(meas,meas);
    hplotrot(wcnt)=ha(ndof,meas);


  diff_exp225=ha-abs(ha_225);      % Full scale difference between FE and 2.25"
beam

  diff_exp0=ha-abs(ha_0);       % Full scale difference between FE and No Crack
beam

  diffht_225=haredt-abs(htrans_225);    % Diff FE/2.25" Crack H (trans.) 9x9

  diffht_x=htrans_0-abs(htrans_225);    % Diff No Crack/2.25" Crack H (trans.) 9x9

  diffnocrackt=haredt-abs(htrans_0);     % Diff FE/No Crack H (trans.) 9x9

  loc225t(:,val)=diag(zredt*(diffht_225)*zredt);   % Localization Matrix FE/2.25" (trans.)

  locexpt(:,val)=diag(abs(zt0)*(diffht_x)*abs(zt0));       % Localization Matrix
Experimental Matrices(trans.)

  locfenocrackt(:,val)=diag(zredt*(diffnocrackt)*zredt); %  Localization Matrix
FE/Nocrack (trans.)

  locerrort=loc225t-locfenocrackt;   % Difference of FE/2.25" & FE/No Crack
Localization Matrices (trans.)

  find225(:,val)= diag(za*(diff_exp225)*za); %  Localization for FE/Experimental blend
FRF

  find0(:,val)= diag(za*(diff_exp0)*za);      % Localization for FE/Experimental blend
FRF

end
```

```
disp('****************** IRS REDUCTION EMPLOYED!!! *************')



figure (1)
mesh(mult1,1:9,(abs(loc225t)))
title('FE vs CRACK')

 figure (2)
  subplot(211)
  mesh(mult1(1:10),1:9,abs(loc225t(:,1:10))), grid
  xlabel('Frequency (Hz)')
  ylabel('Measured Degrees of Freedom')
  title('FE vs Experimental Localization')


  subplot(212)
  mesh(mult1(18:75),1:9,abs(loc225t(:,18:75))), grid
  title('FE vs Experimental Localization')
  ylabel('Measured Degrees of Freedom')
  xlabel('Frequency (Hz)')

 figure (3)
  subplot(211)
  mesh(mult1(100:180),1:9,abs(loc225t(:,100:180))), grid
  xlabel('Frequency (Hz)')
  ylabel('Measured Degrees of Freedom')
  title('FE vs Experimental Localization')


  subplot(212)
  mesh(mult1(220:340),1:9,abs(loc225t(:,220:340))), grid
  title('FE vs Experimental Localization')
  ylabel('Measured Degrees of Freedom')
  xlabel('Frequency (Hz)')


figure (4)
mesh(mult1,1:9,(abs(locexpt)))
title('NO CRACK vs CRACK - Experimental')

 figure (5)
  subplot(211)
  mesh(mult1(1:10),1:9,abs(locexpt(:,1:10))), grid
  xlabel('Frequency (Hz)')
  ylabel('Measured Degrees of Freedom')
  title('Experimental vs Experimental Localization')


  subplot(212)
```

```
mesh(mult1(18:75),1:9,abs(locexpt(:,18:75))), grid
title('Experimental vs Experimental Localization')
ylabel('Measured Degrees of Freedom')
xlabel('Frequency (Hz)')


figure (6)
subplot(211)
mesh(mult1(100:180),1:9,abs(locexpt(:,100:180))), grid
xlabel('Frequency (Hz)')
ylabel('Measured Degrees of Freedom')
title('Experimental vs Experimental Localization')


subplot(212)
mesh(mult1(220:340),1:9,abs(locexpt(:,220:340))), grid
title('Experimental vs Experimental Localization')
ylabel('Measured Degrees of Freedom')
xlabel('Frequency (Hz)')




figure (7)
mesh(mult1,1:9,(abs(locfenocrackt)))
title('FE vs NO CRACK')
```

```
%
function [kirs,mirs]=firs_tam(k,m,oset,aset)
%
% THIS FUNCTION RETURNS THE IRS REDUCED STIFFNESS
% AND MASS MATRICES, GIVEN THE UNREDUCED COUTERPARTS.
% CARE MUST BE TAKEN THAT THE ASET AND OSET VECTORS CORRESPOND
% WITH THE EXISTING ARRANGEMENT OF K AND M.
% K AND M ARE UNPARTITIONED MATRICES.
%
aset_size=length(aset);
%
kaa=k(aset,aset);
kao=k(aset,oset);
koo=k(oset,oset);
koa=kao';
clear k;
k=[koo,koa;kao,kaa];
%
maa=m(aset,aset);
mao=m(aset,oset);
moo=m(oset,oset);
moa=mao';
clear m;
m=[moo,moa;mao,maa];
%
t_static=-koo\koa;
T_static = [t_static;eye(aset_size)];
%
kstat=T_static'*k*T_static;
mstat=T_static'*m*T_static;
%
tirs=t_static+inv(koo)*(moa+moo*t_static)*inv(mstat)*kstat;
T_irs=[tirs;eye(aset_size)];
%
kirs=T_irs'*k*T_irs;
mirs=T_irs'*m*T_irs;
%
% end function firs_tam
```

125

```
%
function [kirs,mirs]=firs_tam(k,m,oset,aset)
%
% this function returns the IRS reduced stiffness
% and mass matrices, given the unreduced couterparts.
% Care must be taken that the aset and oset vectors correspond
% with the existing arrangement of k and m.
% k and m are UNPARTITIONED matrices.
%
aset_size=length(aset);
%
kaa=k(aset,aset);
kao=k(aset,oset);
koo=k(oset,oset);
koa=kao';
clear k;
k=[koo,koa;kao,kaa];
%
maa=m(aset,aset);
mao=m(aset,oset);
moo=m(oset,oset);
moa=mao';
clear m;
m=[moo,moa;mao,maa];
%
t_static=-koo\koa;
T_static = [t_static;eye(aset_size)];
%
kstat=T_static'*k*T_static;
mstat=T_static'*m*T_static;
%
tirs=t_static+inv(koo)*(moa+moo*t_static)*inv(mstat)*kstat;
T_irs=[tirs;eye(aset_size)];
%
kirs=T_irs'*k*T_irs;
mirs=T_irs'*m*T_irs;
%
% end function firs_tam
```

```
%*****************************************************************
%  PURPOSE :   PROVIDE FINITE ELEMENT MODELING OF COMPOSITE BEAMS
%  BACKGROUND: BERNOULLI-EULER THEORY IS EMPLOYED TO
%  FORMULATE ELEMENTAL STIFFNESS AND MASS MATRICES.
%  AXIAL DEFLECTION ASSUMED NEGLIGIBLE.  LUMPED MASSES INCLUDED.
%  NOISE SIMULATION EMPLOYED DURING LOCALIZATION.
%*****************************************************************
%
%  VARIABLES  USED IN THIS PROGRAM:
%
%  conn -  connectivity matrix
%  ke/me -   elemental stiffness/mass matrices
%  kglobal/mglobal -  global stiffness/mass matrices
%  matprops - matrix of EI, rho, area, length
%  le - left end of element
%  re - right end of element
%  noel - # of elements
%  nonodes - # of nodes
%  ndof - # of degrees of freedom


    format long
    noel = 48;
    span = 48;
    nonodes=noel+1
    ndof = nonodes*2
    meas=ndof-1;
    matprops = zeros(noel,4);
```

%  ASSIGN ELEMENT MATERIAL PROPERTIES

```
    for j=1:noel
    matprops(j,1)= 0.05; % mass density [lbm/cu.in] each element
    matprops(j,2)= 1.666; % cross sectional area [sq.in] each element
    matprops(j,3) = 7.45e4;  % EI [lbf-in^2] each element
    matprops(j,4) = span./noel;  % length [in] of each element
    l(j)=matprops(j,4);
    c1(j)=matprops(j,3)./(matprops(j,4).^3);
    c2(j)=(matprops(j,1)./386.4)*matprops(j,2)*matprops(j,4)./420;
    end;
```

%  length=60.625"   width=1.5656"   thickness=0.5339"   density=0.284 lbf/cu.in.
E=28e6psi

```matlab
% BUILD IMPERFECT (EXPERIMENTAL) BEAM MODEL

  xprops = matprops;
  clx=cl;

  for j = 34:38
  xprops(j,3) = 6.703e4;  % .9EI=6.703e4,.95EI=7.076e4,.99EI=7.374e4 ,.67EI=5e4
  clx(j)=xprops(j,3)./(xprops(j,4).^3);
  end
  ei_reduction=.10;

% INITIALIZE ELEMENTAL MATRICES

 ke = zeros(4,4);
 me = zeros(4,4);

 kex = zeros(4,4);
 mex = zeros(4,4);


% INITIALIZE GLOBAL MATRICES

  kglobal = zeros(ndof,ndof);
  mglobal = zeros(ndof,ndof);

  kglobalx = zeros(ndof,ndof);
  mglobalx = zeros(ndof,ndof);

% ASSEMBLE CONNECTIVITY MATRIX

 for i = 1:noel;
    for j = 1:noel;
       conn(i,1) = i;
       conn(j,2) = j+1;
    end
 end


% ASSEMBLE GLOBAL STIFFNESS AND MASS MATRICES

 for i = 1:noel;

 le = conn(i,1).*2 - 1;   % le - refers to left end
 re = conn(i,2).*2;       % re - refers to right end

 ke = cl(i).*[12  6*l(i)  -12   6*l(i);...
         6*l(i)  4*(l(i).^2)  -6*l(i)  2*(l(i).^2);...
         -12 -6*l(i)  12   -6*l(i);...
         6*l(i)  2*(l(i).^2)  -6*l(i)  4*(l(i).^2)];

 kex = clx(i).*[12  6*l(i)  -12   6*l(i);...
         6*l(i)  4*(l(i).^2)  -6*l(i)  2*(l(i).^2);...
         -12 -6*l(i)  12   -6*l(i);...
         6*l(i)  2*(l(i).^2)  -6*l(i)  4*(l(i).^2)];
```

128

```
me = c2(i).*[156  22*l(i)  54  -13*l(i);...
            22*l(i)  4*(l(i).^2)  13*l(i)  -3*(l(i).^2);...
            54  13*l(i)  156  -22*l(i);...
            -13*l(i)  -3*(l(i).^2)  -22*l(i)  4*(l(i).^2)];

mex = me;

kglobal(le:(le+1),le:(le+1)) = kglobal(le:(le+1),le:(le+1))+ke(1:2,1:2);
kglobal(le:(le+1),(re-1):re) = kglobal(le:(le+1),(re-1):re)+ke(1:2,3:4);
kglobal((re-1):re,le:(le+1)) = kglobal((re-1):re,le:(le+1))+ke(3:4,1:2);
kglobal((re-1):re,(re-1):re) = kglobal((re-1):re,(re-1):re)+ke(3:4,3:4);

kglobalx(le:(le+1),le:(le+1)) = kglobalx(le:(le+1),le:(le+1))+kex(1:2,1:2);
kglobalx(le:(le+1),(re-1):re) = kglobalx(le:(le+1),(re-1):re)+kex(1:2,3:4);
kglobalx((re-1):re,le:(le+1)) = kglobalx((re-1):re,le:(le+1))+kex(3:4,1:2);
kglobalx((re-1):re,(re-1):re) = kglobalx((re-1):re,(re-1):re)+kex(3:4,3:4);

mglobal(le:(le+1),le:(le+1)) = mglobal(le:(le+1),le:(le+1))+me(1:2,1:2);
mglobal(le:(le+1),(re-1):re) = mglobal(le:(le+1),(re-1):re)+me(1:2,3:4);
mglobal((re-1):re,le:(le+1)) = mglobal((re-1):re,le:(le+1))+me(3:4,1:2);
mglobal((re-1):re,(re-1):re) = mglobal((re-1):re,(re-1):re)+me(3:4,3:4);

mglobalx(le:(le+1),le:(le+1)) = mglobalx(le:(le+1),le:(le+1))+mex(1:2,1:2);
mglobalx(le:(le+1),(re-1):re) = mglobalx(le:(le+1),(re-1):re)+mex(1:2,3:4);
mglobalx((re-1):re,le:(le+1)) = mglobalx((re-1):re,le:(le+1))+mex(3:4,1:2);
mglobalx((re-1):re,(re-1):re) = mglobalx((re-1):re,(re-1):re)+mex(3:4,3:4);

end

dampingfactor=0.01; kglobalx=kglobalx+sqrt(-1)*dampingfactor*kglobalx;

%  ADD LUMPED MASS/INERTIA TERMS


for disp = 1:12:ndof-1;
    rota = disp + 1;
    lump = 7.39e-5;  % mass of mounting disks [lbf-sec^2/in]
    inert = 8.083e-6;  % mass inertia of disks [lbf-sec^2-in]
    mglobal(disp,disp) = mglobal(disp,disp) + lump;
    mglobal(rota,rota) = mglobal(rota,rota) + inert;

    mglobalx(disp,disp) = mglobalx(disp,disp) + lump;
    mglobalx(rota,rota) = mglobalx(rota,rota) + inert;
end
```

% ASSEMBLE REDUCTION ASET/OSET PARAMETERS FOR TRANSLATION
AND ROTATION

```
    aset=[1:noel/4:ndof-1];
    a1=aset(1,2);
    a2=aset(1,3);
    a3=aset(1,4);
    a4=aset(1,5);
    a5=aset(1,6);
    a6=aset(1,7);
    a7=aset(1,8);
    a8=aset(1,9);
    keep=length(aset);
    oset=[2:a1-1,a1+1:a2-1,a2+1:a3-1,a3+1:a4-1,a4+1:a5-1,a5+1:a6-1,...
        a6+1:a7-1,a7+1:a8-1,ndof];
```

% COMPUTE NATURAL FREQUENCIES AND MODE SHAPES

```
    [psi,lambda] = eig(mglobal\kglobal);
    [psix,lambdax] = eig(mglobalx\kglobalx);

    [lambda_diag,corrn] = sort(diag(lambda));
    [lambda_diagx,corrnx] = sort(diag(lambdax));

    for i = 1: length(lambda);
      lambda(i,i)= lambda_diag(i);
      lambdax(i,i)= lambda_diagx(i);
    end

    wn = sqrt(lambda);        % wn (rad/sec)
    wnx = sqrt(lambdax);       % wnx (rad/sec)

    freqs= diag(wn)/(2*pi);    % freqs (Hz)
    xfreqs= diag(wnx)/(2*pi);  % xfreqs (Hz)
```

% IDENTIFY FREQUENCY RANGE OF ANALYSIS

```
    minfreq = 20;
    freqspan = 500;
    maxfreq = minfreq + freqspan;
    deltaf = freqspan/800;

    wcnt=0;
    mult1 = [minfreq:deltaf:maxfreq];
    mult = mult1*2*pi;

[kirs,mirs]=firs_tam(kglobal,mglobal,oset,aset);    % Calls function which returns kirs,
mirs
irslambda=eig(mirs\kirs);
irsfreqs=sort(sqrt(irslambda)/(2*pi))
```

```
%  BUILD LOCALIZATION MATRIX


for val=1:length(mult)

    za=kglobal-mult(val)^2*mglobal;
    zx=kglobalx-mult(val)^2*mglobalx;
    ha= inv(za);
    hx= inv(zx);

    [hx_noise1,hx_noise2,hx_noise5]=noisefill(hx);
    hx1=hx_noise1;hx2=hx_noise2;hx5=hx_noise5;

    haxredt=hx(aset,aset);
    haxredt1=hx1(aset,aset); % Reduced Experimental H (trans.)
    haxredt2=hx2(aset,aset);
    haxredt5=hx5(aset,aset);
    z=kirs-mult(val)^2*mirs;

    haredt=inv(z);       % Reduced Analytical H (trans.)
    zredt=inv(haredt);           % Reduced Analytical Z (trans.)

    deltah=(haredt-haxredt);
    deltah1=(haredt-haxredt1);
    deltah2=(haredt-haxredt2);
    deltah5=(haredt-haxredt5);

    wcnt=wcnt+1;
    hplot(wcnt)=ha(meas,meas);
    hplotrot(wcnt)=ha(ndof,ndof-1);
    hxplot(wcnt)=hx(meas,meas);

    locred(:,val)=diag(zredt*deltah*zredt);
    locred1(:,val)=diag(zredt*deltah1*zredt);
    locred2(:,val)=diag(zredt*deltah2*zredt);
    locred5(:,val)=diag(zredt*deltah5*zredt);


end
```

```
%****************************************************************
%   PURPOSE  : THIS M-FILE SIMULATES SIGNAL NOISE IN THE FREQUENCY
%   RESPONSE MATRIX TO DETERMINE THE EFFECTIVE DISTORTION OF
%   LOCALIZATION INFORMATION.
%****************************************************************

function [hx_noise1,hx_noise2,hx_noise5]=noisefill(hoax);


for icol = 1:length(hoax);
    alter=size(hoax(:,icol));
    nvec=rand(alter);           % Creates random noise matrix
    scale_nvec1=.01*norm(hoax(:,icol))/norm(nvec);
    hoax1(:,icol)=hoax(:,icol)+scale_nvec1*nvec;

    nvec=rand(alter);           % Creates random noise matrix
    scale_nvec2=.02*norm(hoax(:,icol))/norm(nvec);
    hoax2(:,icol)=hoax(:,icol)+scale_nvec2*nvec;

    nvec=rand(alter);           % Creates random noise matrix
    scale_nvec5=.05*norm(hoax(:,icol))/norm(nvec);
    hoax5(:,icol)=hoax(:,icol)+scale_nvec5*nvec;
end

hx_noise1=hoax1;
hx_noise2=hoax2;
hx_noise5=hoax5;
```

THIS M-FILE LOADS A SERIES OF .MAT FILES CONTAINING ANALYZER
FRF DATA. EACH FILE IS LOADED, AND THE FREQUENCY DATA ('O2I1X')
...IS CLEARED. EACH FRF IS STORED IN-A COLUMN OF THE MATRIX 'FRF'.
THE PROGRAM LOADS THE TRANSLATIONAL DATA, THEN THE
ROTATIONAL DATA.

```
%  INITIALIZE FRF MATRICES

FRF0 = zeros(801,162);        % No Crack Beam data
                     % 801 frequency points
                     % 162 responses {81 trans / 81 rot.}
                     % excited at 9 locations
FRF225 = zeros(801,162);      % 2.25" Crack Beam data
                     % 801 frequency points
                     % 162 responses {81 trans / 81 rot.}
                     % excited at 9 locations
fill_col = 0;              % initializes FRF matrix column counter

%  LOAD TRANSLATIONAL RESPONSES

for row = 1:9
   for col=1:9
      fill_col = fill_col + 1;

      eval(['load ','/users/mcamp/nocrack/H',num2str(row),num2str(col),'A.MAT'])
      FRF0(:,fill_col) = o2i1;
      clear o2i1x,clear o2i1;

      eval(['load ','/users/mcamp/crack225/H',num2str(row),num2str(col),'A.MAT'])
      FRF225(:,fill_col) = o2i1;
      clear o2i1x, clear o2i1;
   end
end

%  LOAD ROTATIONAL RESPONSES

for row = 1:9
   for col=1:9
      fill_col = fill_col + 1;

      eval(['load ','/users/mcamp/nocrack/HO',num2str(row),num2str(col),'A.MAT']);
      FRF0(:,fill_col) = o2i1;
      clear o2i1x, clear o2i1;

      eval(['load ','/users/mcamp/crack225/HO',num2str(row),num2str(col),'A.MAT']);
      FRF225(:,fill_col) = o2i1;
      clear o2i1;
   end
end
```

133

```
expwn= 2*pi*o2ilx;
for i=1:length(expwn)
    FRF0(i,1:81)=(-386.4*(FRF0(i,1:81)))/expwn(i)^2;
    FRF0(i,82:162)=(1024/.483)*(FRF0(i,82:162))/expwn(i)^2;
    FRF225(i,1:81)=(-386.4*(FRF225(i,1:81)))/expwn(i)^2;
    FRF225(i,82:162)=(1024/.483)*(FRF225(i,82:162))/expwn(i)^2;
end
```

## MAP.M

```
%  PURPOSE : THIS M-FILE ENSURES SYMMETRY OF EXPERIMENTAL
%  MATRICES
ha_225=ha;
ha_0=ha;
maptrans=[1 13 25 37 49 61 73 85 97];
maprotat=maptrans+1;

 for i=1:9
   for j=1:9

    transrow=maptrans(i);

    transcol=maptrans(j);

    rotatrow=maprotat(i);

    rotatcol=transcol;

    ha_225(transrow,transcol)=htrans_225(i,j);
    ha_225(rotatrow,rotatcol)=hrotat_225(i,j);
    ha_0(transrow,transcol)=htrans_0(i,j);
    ha_0(rotatrow,rotatcol)=hrotat_225(i,j);

  end
 end


for i=1:9
  for j=1:9
     ha_225(i,j)=ha_225(j,i); ha_0(i,j)=ha_0(j,i);
  end
end
```

# LIST OF REFERENCES

1. Keyser, C.A., Materials of Engineering: Properties, Fabrication, Uses, and Testing, pp. 79-90, Prentice-Hall, Inc., 1964.

2. Ewins, D.J., Modal Testing Theory and Practice, pp.3-21, Research Studies Press, LTD, 1992.

3. Ewins, D.J., Lieven, N.A.J., "Effect of Incompleteness and Noise on Error Matrix Calculations," 10th International Modal Analysis Conference, 1992.

4. Ewins, D.J., Lieven, N.A.J., "Error Location and Updating of Finite Element Models Using Singular Value Decomposition," 8th International Modal Analysis Conference, 1990.

5. Sidhu, J., Ewins, D.J., "Correlation of Finite Element and Modal Tests - Study of a Practical Structure," 2nd International Modal Analysis Conference, Orlando, FL 1984.

6. Gordis, J.H., "Spatial, Frequency Domain Updating of Linear, Structural Dynamic Models," AIAA-93-1652-CP, 1993, pp. 3050-3058.

7. Craig, R.R., Structural Dynamics, An Introduction to Computer Methods, pp. 383-387, John Wiley and Sons, Inc., 1981.

8. Guyan, R.J., "Reduction of Stiffness and Mass Matrices," Journal of the American Institute of Aeronautics and Astronautics, Vol. 3, Feb 1965, p. 380.

9. O'Callahan, J. "A Procedure for an Improved Reduction System (IRS) Model," 7th International Modal Analysis Conference, Las Vegas, NV 1989.

10. Gordis, J.H., Bielwa, R.L., and Flannery, W.G., "A General Theory for Frequency Domain Structure Synthesis," Journal of Sound and Vibration, 150(1), Sep 1989, pp.139-158.

11. Brillhart, R.D., Hunt, D.L., and St. Pierre, M., "Advantages of Excitation Using Plastic Stinger Rods," 11th International Modal Analysis Conference, Kissimmee, FL, 1993.

12. Good, M., Rost, R., "Summary of Excitation Signals for Structural Testing," pp.566-571.

13. Park, Y., "Improved Estimation of Frequency Response Function," 11th International Modal Analysis Conference, Kissimmee, FL, 1993

14. PCB Piezotronics, Inc., General Guide to ICP Instrumentation.

15. Kistler Instrument Corporation, Operating Instructions Model 8832 TAP System, March 1990.

16. Hewlett-Packard Company, HP3562A Operator Introduction to the HP3562A Dynamic Signal Analyzer, Product Note 3562A1.

# INITIAL DISTRIBUTION LIST

|  |  | No. Copies |
|---|---|---|
| 1. | Defense Technical Information Center<br>Cameron Station<br>Alexandria, Virginia 22304-6145 | 2 |
| 2. | Library, Code 52<br>Naval Postrgaduate School<br>Monterey, California 93943-5101 | 2 |
| 3. | Professor J.H. Gordis, Code ME/GO<br>Department of Mechanical Engineering<br>Naval Postgraduate School<br>Monterey, California 93943 | 3 |
| 4. | Professor Y. Kwon, Code ME/KW<br>Department of Mechanical Engineering<br>Naval Postgraduate School<br>Monterey, California 93943 | 2 |
| 5. | Naval Engineering Curricular Office<br>Code 34<br>Naval Postgraduate School<br>Monterey, California 93943-5000 | 1 |
| 6. | LT Marvin G. Campbell, USN<br>3606 Clark's Lane<br>Baltimore, Maryland 21215 | 2 |